

إقرار

أنا الموقع أدناه مقدم الرسالة التي تحمل العنوان:

**The Influence of Copper-phthalocyanine Layer, Heat Treatment, and Electric
Field on the Performance of Poly (9-Vinylcarbazole)/Rhodamine B/Pb
Organic Light Emitting Diodes**

تأثير طبقة Copper-phthalocyanine و المعالجة بالحرارة والمعالجة باستخدام المجال الكهربائي على
ثنائي عضوي باعث للضوء ذو التركيب Poly (9-Vinylcarbazole)/Rhodamine B/Pb

أقر بأن ما اشتملت عليه هذه الرسالة إنما هي نتاج جهدي الخاص، باستثناء ما تمت الإشارة
إليه حيثما ورد، وإن هذه الرسالة ككل، أو أي جزء منها لم يقدم من قبل لنيل درجة أو لقب
علمي أو بحثي لدى أية مؤسسة تعليمية أو بحثية أخرى.

DECLARATION

The work provided in this thesis, unless otherwise referenced, is the
researcher's own work, and has not been submitted elsewhere for any
other degree or qualification

Student's name:

اسم الطالب: محمد صلاح القرندوي

Signature

التوقيع: 

Date:

التاريخ: 20/05/2015

Islamic University of Gaza
Deanery of Graduate Studies
Faculty of Science
Physics Department



**The Influence of Copper-phthalocyanine Layer, Heat Treatment, and Electric
Field on the Performance of Poly (9-Vinylcarbazole)/Rhodamine B/Pb
Organic Light Emitting Diodes**

تأثير طبقة Copper-phthalocyanine و المعالجة بالحرارة والمعالجة باستخدام المجال الكهربائي على
ثنائي عضوي باعث للضوء ذو التركيب Poly (9-Vinylcarbazole)/Rhodamine B/Pb

By

Mohammed Salah Al-Qrinawi

B.Sc. in Physics, Islamic University of Gaza

Supervised By

Dr. Taher El-Agez
Associate Professor of Physics

Dr Sofyan A. Taya
Associate Prof. of Physics

Thesis

**Submitted to the Faculty of Science as Partial Fulfillment of the Master of
Science (M.Sc.) in Physics**

Palestine, Gaza

1436 – 2015



نتيجة الحكم على أطروحة ماجستير

بناءً على موافقة شئون البحث العلمي والدراسات العليا بالجامعة الإسلامية بغزة على تشكيل لجنة الحكم على أطروحة الباحث/ محمد صلاح صالح القريناوي لنيل درجة الماجستير في كلية العلوم قسم الفيزياء وموضوعها:

تأثير طبقة copper-phthalocyanine والمعالجة بالحرارة والمعالجة باستخدام المجال الكهربائي على ثنائي عضوي باعث للضوء ذو التركيب Poly (9-Vinylcarbazole)/Rhodamine B/Pb

The influence of copper-phthalocyanine layer, heat treatment, and Electric field on the performance of Poly (9-Vinylcarbazole)/Rhodamine B/Pb Organic Light Emitting Diodes

وبعد المناقشة العلنية التي تمت اليوم الأربعاء 10 رجب 1436هـ، الموافق 2015/04/29 الساعة الواحدة والنصف ظهراً بمبنى القدس، اجتمعت لجنة الحكم على الأطروحة والمكونة من:

Tahir M. E. Agor

عبد

عبد

عبد

مشرفاً ورئيساً

مشرفاً

مناقشاً داخلياً

مناقشاً خارجياً

د. طاهر محمد العاجز

د. سفيان عبد الرحمن تايه

أ.د. ناصر إسماعيل فرحات

د. أحمد أسعد التيان

وبعد المداولة أوصت اللجنة بمنح الباحث درجة الماجستير في كلية العلوم/ قسم الفيزياء.

واللجنة إذ تمنحه هذه الدرجة فإنها توصيه بتقوى الله ونزوم طاعته وأن يسخر علمه في خدمة دينه ووطنه.

والله والتوفيق،،،

مساعد نائب الرئيس للبحث العلمي والدراسات العليا

أ.د. فؤاد علي العاجز



CONTENTS

CONTENTS.....	II
<i>إهداء</i>	VI
ACKNOWLEDGMENTS	VII
ABSTRACT.....	VIII
ABSTRACT IN ARABIC.....	IX
LIST OF SYMBOLES AND ABBREVIATIONS	X
LIST OF TABLES	XIV
LIST OF FIGURS.....	XVI
CAPTER 1	1
INTRODUCTION TO POLYMER	1
1.1 INTRODUCTION	1
1.2 LITERATURE REVIEW	1
1.3. ADVANTAGES AND DISADVANTAGES OF OLEDs	3
1.4 BASIC CONSEPTS OF POLYMER SCIENCES.....	4
1.5 TYPES OF POLYMER MOLECULAR STRUCTURES	5
1.5.1 Homopolymers	5
1.5.2 Copolymers.....	6
1.6 CONJUGATED POLYMER.....	9

1.7 MATERIALS USED	12
1.8 THESIS ORGANIZATION.....	13
CHAPTER 2.....	14
ELECTRICAL CONDUCTION MECHANISMS	14
2.1 INTRODUCTION	14
2.2 ELECTRICAL CONTACTS AND POTENTIAL BARRIERS.....	14
2.3 METAL AND NON-METAL CONTACT	17
2.4 BASIC OLED STRUCTURE AND ENERGY LEVEL ALIGNMENT	22
<i>2.4.1 Basic OLED Structure</i>	<i>23</i>
<i>2.4.2 Energy Levels of Electroluminescence Materials</i>	<i>23</i>
2.5 MECHANISMS OF CHARGE CARRIER INJECTION THROUGH A METAL / NON-METAL INTERFACE	25
<i>2.5.1 Thermionic Emission.....</i>	<i>25</i>
<i>2.5.2 Field Emission.....</i>	<i>27</i>
2.6 CARRIER TRANSPORT IN OLEDs.....	28
2.7 OHMIC CONTACT.....	29
2.8 SPACE-CHARGE EFFECT	30
2.9 CHARGE RECOMBINATION	30
2.10 LUMINESCENCE.....	32
CHAPTER 3.....	34
EXPERIMENTAL TECHNIQUES	34
3.1 INTRODUCTION	34
3.2 EXPERIMENTAL TECHNIQUES.....	34
<i>3.2.1 Inclined Casting Coating</i>	<i>34</i>

3.2.2 Thickness and Optical Constants Measurements.....	35
3.2.3 Thermal Vacuum Evaporation	38
3.2.4 Measurement of J-V characteristic Curves.....	39
3.2.5 Electrochemical Impedance Spectroscopy.....	40
3.2.6 Capacitance-Voltage Measurements	41
CHAPTER 4.....	42
THE CURRENT DENSITY-VOLTAGE-ELECTROLUMINESCENCE	
CHARACTERISTIC CURVES	42
4.1 INTRODUCTION	42
4.2 DEVICE FABRICATION	42
4.2.1 Substrate Cleaning	42
4.2.2 Depositing the Device Layers	43
4.2.3 Post Processing Treatment	44
4.3 THICKNESS AND REFRACTIVE INDEX MEASUREMENT	46
.....	47
4.4 RESULTS AND DISCUSSIONS.....	47
4.4.1 The Influence of CuPc Hole-injection Layer.....	48
4.4.2 Post-treatment	56
CHAPTER 5.....	65
IMPEDANCE SPECTROSCOPY OF OLEDs	65
5.1 INTRODUCTION	65
5.2 IMPEDANCE SPECTROSCOPY	65
5.3 CAPACITANCE-VOLTAGE CHARACTERIZATION	67
5.3.1 Influence of CuPc thin layer on C-V curves.....	68

5.3.2 Heat treatment	71
5.3.3 External electric field-heat treatment	73
5.3.4 Comparison between heat treatment with and without an electric field.....	74
5.3.5 Comparison between (J-V) and (C-V).....	76
5.4 BODE PLOTS.....	84
5.4.1 Bode modulus for OLEDs with CuPc layer	85
5.4.2 Bode modulus for OLEDs treated by heat	90
5.4.3 Bode modulus for OLEDs treated by an electric field during heating.....	94
CONCLUSION	99
REFERANCES	102

إهداء

إلى من زرع في نفسي حب العلم والدي الحبيب حفظه الله تعالى.
إلى من كان رضاها سر نجاحي والدتي الغالية حفظها الله تعالى.
إلى من ساندني وصبر لإتمام دراستي زوجتي الفاضلة إكراماً و عرفاناً.
إلى من بهم تحلوا الحياة إخواني وأخواتي حفظهم الله.
إلى من تميزون بالعطاء أصدقائي الأعزاء جزاهم الله خير الجزاء.
إلى كل من آمن بالله رباً، وبالإسلام ديناً، وبالقرآن دستوراً وبمحمد نبياً ورسولاً.
أهدي هذا الجهد المتواضع راجي المولى أن يجعله خالصاً لوجهه الكريم وأن ينفع به ويجعله مقارباً للصواب.

ACKNOWLEDGMENTS

All gratitude and thanks to Allah to help me in my life, and I thank the prophet mohammed, who guided me to the path of guidance.

I wish to express my deep gratitude and thanks to my supervisor Dr. Taher El-Agez, Dr. Sofyan Taya, and prof. Monzir Abdel-Latif for suggesting the problems discussed in the thesis, for their continuous encouragement and invaluable help during my research.

Special thanks to my colleagues and staff in the Physics Department at the Islamic University of Gaza, for their encouragement and assistance during the time of writing this thesis.

Finally, I must thank my family, my mother and father who pushed me to the end my studies. Lastly, and most especially, I have to thank my wife who loved and stood by me in my difficult time.

ABSTRACT

In this work, two groups of samples have been prepared and their characterizations have been studied. The first group is a double layer device with the structure of ITO/PVK/Rhodamine B dye/Pb. Some of the samples were thermally annealed without any external electric field while others were treated by an external electric field during heating. The annealing process occurs after depositing the Rhodamine B dye layer on the PVK film, and before depositing Pb as a cathode. It is found that the annealing temperature of PVK/Rhodamine B layer increases the threshold voltage of the device except at 90°C. On the other hand, in the electric field-heat treatment, the threshold voltage is observed to decrease as the annealing temperature is increased and the maximum current density of the device is dramatically enhanced except at 110°C.

The second group is a multilayer device with the structure ITO/CuPc with different thicknesses/PVK/ Rhodamine B/Pb. The influence of copper-phthalocyanine (CuPc) hole-injection layer on the current voltage characteristic and the electroluminescence have been measured and studied. The results showed that the threshold voltage of the devices can be dramatically lowered by inserting the CuPc layer.

ABSTRACT IN ARABIC

تم تحضير ودراسة مجموعتين من عينات ثنائي عضوي باعث للضوء. المجموعة الأولى مكونة من طبقتين الطبقة الأولى عبارة عن طبقة PVK و الثانية طبقة Rhodamine B dye ، التركيب العام لهذه المجموعة هو: ITO/PVK/Rhodamine B dye/Pb .

قد أجريت على OLED device ذو التركيب السابق، بعض عمليات المعالجة مثل المعالجة بالحرارة و المعالجة بالحرارة في وجود مجال كهربائي خارجي لدراسة مدى تأثير هذه العمليات على أداء و كفاءة العينات. وقد وجد من خلال دراسة منحنيات التيار مع الجهد للعينات التي عولجت باستخدام الحرارة فقط ، أنه كلما زادت درجة الحرارة زادت بذلك قيم جهد العتبة للعينات باستثناء عند درجة حرارة 90°C . بينما العينات التي عولجت باستخدام الحرارة بوجود مجال كهربائي خارجي كانت النتيجة أنه كلما زادت الحرارة قلت قيمة جهد العتبة و زادت قيمة التيار باستثناء عند درجة حرارة 110°C .

المجموعة الثانية من العينات تتكون من ثلاث طبقات وهي PVK و Rhodamine B dye و طبقة CuPc ، التركيب العام لهذه المجموعة هو: ITO/CuPc/PVK/ Rhodamine B dye/ Pb . عملت على تقليل من قيمة جهد العتبة. OLED device كطبقة ثالثة ل CuPc وتظهر النتائج أن إضافة طبقة

LIST OF SYMBOLES AND ABBREVIATIONS

Alq_3	8-hydroxyquinoline aluminum
σ^*	Anti-bonding orbitals
π^*	Anti-bonding orbitals
AC	Alternative current
Φ_A	Anode work function
A^*	Effective Richardson constant
Σ	Bonding orbitals
Π	Bonding orbitals
\hbar	Blank constant
Φ_B	Barrier height
ΔE_h	Barriers to hole injection at the anode
C-f	Capacitance-frequency
C-V	Capacitance-voltage
CuPc	Copper-phthalocyanine
Φ_C	Cathode work function
σ_s	Charge per unit area
DC	Direct current
ζ	Difference in potential energy of the electron between the inside and outside of the metal
EL	Electroluminescence
E_C	Conductive band
E_F	Fermi level
E_V	Valence band

E_{Fm}	Fermi level for metal
E_g	Energy gap
ETM	Electron-transfer material
ELM	Emitting light material
EBL	Electron bloke layer
ETL	Electron transport layer
EL-V	Electroluminescence-voltage curves
EA	Electron affinity
ΔE_c	Electron injection at the cathode
EIS	Electrochemical Impedance Spectroscopy
ϵ_k	Permittivity of the material
FRA	Frequency response analyzer
GHS	Guest hopping side
Hg	Mercury
HTM	Hole-transfer material
HBL	Hole block layer
HTL	Hole transport layer
HOMO	Highest Occupied Molecular Orbital
ITO	Indium tin oxide
IP	Ionization potential
IS	Impedance Spectroscopy
J-V	Current density-voltage characteristics
k	Extinction coefficient
K_B	Boltzmann constant
LCD	Liquid crystal display

LUMO	Lowest unoccupied Molecular Orbital
LED	Light emitting diode
Mg:Ag	Magnesium:Silver
NDR	Negative differential resistance
OLED	Organic light emitting diode
PPV	Poly (Parapheny-lenevinylene)
PLEDs	Polymer Light Emitting Diodes
P_z	Unhybridized orbital
p-	A negatively charged polaron
p+	A positively charged polaron
PVK	Poly (9-Vinylcarbazole)
Pb	Lead
Si	Silicon
S_n^*	Number of excited singlet state
S_1	First excited singlet state
S_0	Ground state
TPD	Diamine
TFT	Thin film transistor
t	Thickness of the layer
T	Absolute temperature
T_1	First triplet excited state
T_n^*	Number of a triplet excited state
THF	Tetrahydrofuran
V_d	Contact potential
V_{th}	Threshold voltage

V_T	Transition voltage
V_{bi}	Built-in voltage
V_{on}	The voltage at which the device starts emission
φ	Phase shift between voltage and current
ω_f	Angular frequency for fluorescent emitter
ω_p	Phosphorescent emitters angular frequency
W	Width of the barrier
Φ_S	Work function for a semiconductor material
χ	Electron affinity
Φ_m	Work function of the metal
Φ	Work function for a nonmetallic material
Z	Total impedance
Z_R	Impedances of a resistor
Z_C	Impedances of a capacitor
Z_L	Impedances of an inductor
Z'	Real parts of the impedance
Z''	Imaginary parts of the impedance
$Z-f$	Modulus-frequency

LIST OF TABLES

Table 1.1 . Molecular formula, molecular weight, and molecular structure of the three materials.....	12
Table 4. 1. V_{th} and maximum current densities for OLED devices with different CuPc layer thickness.....	52
Table 4. 2. Experimental values of slope for each region of lnJ-lnV characteristic curves.....	55
Table 4. 3. Threshold voltages and maximum current densities of the devices after heat treatment.....	57
Table 4. 4. Experimental values of slope for each region of lnJ-lnV characteristic curves.....	58
Table 4. 5. Threshold voltages and maximum current densities of devices treated by an external electric field during annealing.....	60
Table 4. 6. Experimental values of slope for each region of lnJ-lnV characteristic curves.....	61
Table 4. 7. Threshold voltages and maximum current densities for OLEDs treated by heating with and without an electric field.....	64
Table 5. 1. The transition and build-in voltages for different CuPc layer thickness. ..	71
Table 5. 2. The transition and build-in voltages for different annealing temperature.	72
Table 5. 3.The transition and build-in voltages for the devices treated by an external electric field during thermal annealing.....	74
Table 5. 4. Values of series and parallel resistances.....	90

Table 5. 5. Values of series and parallel resistances for devices treated by heating at different temperatures.94

Table 5. 6. Values of series and parallel resistances for devices treated by E-field at different temperatures.98

LIST OF FIGURS

Fig. 1. 1. Some applications of OLEDs and PLEDs.....	4
Fig. 1. 2. The general shape of linear homopolymer.	5
Fig. 1. 3. The general shape of branched homopolymer.....	6
Fig. 1. 4. The general shape of crosslinked homopolymer.	6
Fig. 1. 5. General Structure of linear random copolymer.	7
Fig. 1. 6. General structure of alternating copolymer.	7
Fig. 1. 7. General structure of block copolymer.	7
Fig. 1. 8. General structure of branched copolymer.	8
Fig. 1. 9. Structure of a crosslinked copolymer phenolic.	9
Fig. 1. 10. Scheme of orbitals (above) involved in the bonding between carbons in a conjugated backbone (below).	10
Fig. 1. 11. (a) Classification of molecular orbitals with respect to electron occupancy, (b) Comparasion between bonding and antibonding states of (σ , π).	11
Fig. 2. 1. The energy diagram of the metal and semiconductor before (a) and after contact (b).	15
Fig. 2. 2. Formation of the depletion region due to the contact between two different materials.....	16
Fig. 2. 3. Energy band diagram showing the work function of metal, Φ_m [9].....	18
Fig. 2. 4. Energy band diagram showing the work function of (a) n-type semiconductor and (b) p-type semiconductor [9].	19
Fig. 2. 5. Energy level diagram for a contact between a metal and an n-type semiconductor for $\Phi_m > \Phi_s$ before contact [9].	20

Fig. 2. 6. Energy level diagram for a contact between a metal and an n-type semiconductor for $\Phi_m > \Phi_S$ in thermal equilibrium [9].	21
Fig. 2. 7. Energy levels diagram for a contact between a metal and an n-type semiconductor for $\Phi_m > \Phi_S$ in intimate contact [9].	21
Fig. 2. 8. Energy level diagrams at contact between a metal and an intrinsic semiconductor with applied different voltage $V_4 > V_3 > V_2 > V_1 > 0$ [9].	22
Fig. 2. 9. Energy level diagram of an organic light-emitting diode with a hole-transport material(HTM), an electron-transport material (ETM),the electron affinity (EA),the ionization potential (IP),cathode work function (Φ_C), and the anode work function (Φ_A) [11].	24
Fig. 2. 10. Multilayer OLED device with a hole-transport layer (HTL), electron transport layer (ETL), electron block layer (EBL), hole block layer (HBL) and emitting material layer (EML).	25
Fig. 2. 11. Energy band diagram showing thermionic emission of electrons over the barrier [13].	26
Fig. 2. 12. Wave functions showing electron tunneling through a rectangular barrier where W is the width and ϕ_B is the barrier height [13].	28
Fig. 2. 13. Schematic diagram illustrating an electron hopping across and an electron tunneling through a square potential barrier [12].	29
Fig. 2. 14. Schematic illustration of (a) the Frenkel exciton and (b) Wannier exciton [9].	32
Fig. 2. 15. Jablonski diagram and illustration of the relative positions of absorption, fluorescence and phosphorescence spectra.	33

Fig. 3. 1. Single interface reflection occurs whenever light crosses the interface between different materials [15].35

Fig. 3. 2. Multiple interface reflection occurs whenever light crosses the interface between different materials [15].36

Fig. 3. 3. (a) Schematic diagram of Filmetrics F20 Thin-Film Analyzer component [15], (b) Photograph of real instrument.37

Fig. 3. 4. (a) Photograph of Minilab 080, (b) Schematic diagram of the evaporating system.38

Fig. 3. 5. A SQM-160 quartz crystal monitor that used to know the thickness of film deposition.....39

Fig. 3. 7. Photo image of J-Vmeasuring setup.....40

Fig. 3. 8. Autolab instrument in combination with the frequency response analyzer (FRA) that is used in Electrochemical Impedance Spectroscopy (EIS) measurements.41

Fig. 3. 9. LCR-821 instrument that is used in C-V measurments.....41

Fig. 4. 1. The picture in the left hand appeared the schematic drawing of a multilayer ITO/CuPc/PVK/Rhodamine B dye/Pb, and the picture in the right hand appeared the device fabrication.....44

Fig. 4.2. The picture in the left hand appeared the schematic drawing of a double-layer ITO/PVK/Rhodamine B/Pb OLED, and the picture in the right hand appeared the device fabrication.45

Fig. 4. 3. The electric field treatment setup.45

Fig. 4. 4. Reflectance of light (a) and optical constants (n and k) for the PVK film deposited on silicon wafer in the spectral range 400 nm to 1600 nm.....47

Fig. 4. 5. Current density- voltage characteristic curve of the control device consisting of ITO/~44.88nm PVK/ 30nm Rhodamine B dye/ 35nm Pb.....	48
Fig. 4. 6. Relative light intensity-voltage characteristic curve of the control device consisting of ITO/ ~ 44.8nm PVK/ 30nm Rhodamine B/ 35nm Pb.	49
Fig. 4. 7. Energy level diagram for the device consisting of ITO/PVK/ Rhodamine B dye/ Pb.	50
Fig. 4. 8. Energy level diagram for device consisting of ITO/CuPc/Rhodamine B dye/Pb.	50
Fig. 4. 9. The threshold voltage versus thickness of CuPc layer.	52
Fig. 4. 10. Current density- voltage characteristic curves of the device consisting of ITO/ (0, 5, 10, 30, and 50nm) CuPc / 44.8nm PVK/ 30nm Rhodamine B/ 35nm Pb..	53
Fig. 4. 11. Current density-voltage characteristic curves of devices consisting of ITO/ (0, 5, 10, 30, and 50 nm) CuPc/44 nm PVK/30 nm Rhodamine B dye/35nm Pb in logarithmic scale.	55
Fig. 4. 12. Current density-voltage characteristic curves of the heat-treated devices consisting of ITO/~44.88nmPVK/30nm Rhodamine B/35nm Pb at different annealing temperatures.	57
Fig. 4. 13. Current density-voltage characteristic curves of the heat-treated devices consisting of ITO/44.8nmPVK/30nm Rhodamine B/35nm Pb at different annealing temperatures in logarithmic scale.	58
Fig. 4. 14. Current density-voltage characteristic curves of the OLEDs consisting of ITO/~44.8nmPVK/30nm Rhodamine B dye/35nm Pb treated with an external electric field during heating.	60

Fig. 4. 15. Current density-voltage characteristic curves of the OLEDs consisting of ITO/~44.88nmPVK/30nm Rhodamine B dye/35nm Pb treated with an external electric field during heating in logarithmic scale.....61

Fig. 4. 16. Photos of the samples treated by electric field at temperature 90 °C, 100 °C, 110 °C and 120 °C.62

Fig. 4. 17. Current density-voltage characteristic curves of the OLEDs thermally treated with and without an electric field.....63

Fig. 5. 1. A typical C-V curve for an OLED device under forward applied bias [27].68

Fig. 5. 2. Capacitance- voltage characteristic curve of the standard device consisting of ITO/ ~44.88nm PVK/ 30nm Rhodamine B/ 35nm Pb.70

Fig. 5. 3. Capacitance- voltage characteristic curves of the device consisting of ITO/(5, 10, 30, and 50 nm) CuPc/ ~44.88nm PVK/ 30nm Rhodamine B/ 35nm Pb. .70

Fig. 5. 4. Capacitance-voltage curves for the devices consisting of ITO/~44.88nm PVK/30nm Rhodamine B dye/35nm Pb at different annealing temperatures.72

Fig. 5. 5. Capacitance-voltage curves for the devices consisting of ITO /~44.88nm PVK /30nm Rhodamine B dye/35nm Pb which were treated by external electric field at different temperatures.73

Fig. 5. 6. Capacitance-voltage curves for devices consisting of ITO/~44.88nm PVK/30nm Rhodamine B dye/Pb treated by heat and electric field.....75

Fig. 5. 7. The reflected beam received from the sample center and the two edges which was treated at temperature 110 °C as a function of wavelength.75

Fig. 5. 8. Current density-capacitance curve (a) and relative light intensity-capacitance curve (b) as a function of the applied forward bias for ITO/~44.88nm PVK/30nm Rhodamine B/35nm Pb device.....77

Fig. 5. 9. Current density-capacitance curves as a function of the applied forward bias for the device consisting of ITO/ 5nm CuPc/ ~44.88nm PVK/ 30nm Rhodamine B dye/ 35nm Pb.	78
Fig. 5. 10. Current density-capacitance curves as a function of the applied forward bias for the device consisting of ITO/ 10nm CuPc/ ~44.88nm PVK/ 30nm Rhodamine B dye/ 35nm Pb.....	78
Fig. 5. 11. Current density-capacitance curves as a function of the applied forward bias for the device consisting of ITO/ 30nm CuPc/ ~44.88nm PVK/ 30nm Rhodamine B dye/ 35nm Pb.....	79
Fig. 5. 12. Current density-capacitance curves as a function of the applied forward bias for the device consisting of ITO/ 50nm CuPc/ 44.8nm PVK/ 30nm Rhodamine B/ 35nm Pb.	79
Fig. 5. 13. Current density-capacitance curves as a function of the applied forward bias for the device consisting of ITO/ ~44.88nm PVK/ 30nm Rhodamine B dye/35nm Pb, was treated at 90 °C.....	80
Fig. 5. 14. Current density-capacitance curves as a function of the applied forward bias for the device consisting of ITO/ ~44.88nm PVK/ 30nm Rhodamine B dye/35nm Pb was treated at 100 °C.....	81
Fig. 5. 15. Current density-capacitance curves as a function of the applied forward bias for the device consisting of ITO/ ~44.88nm PVK/ 30nm Rhodamine B dye/35nm Pb was treated at 110°C.....	81
Fig. 5. 16. Current density-capacitance curves as a function of the applied forward bias for the device consisting of ITO/ ~44.88nm PVK/ 30nm Rhodamine B dye/35nm Pb was treated at 120°C.....	82

Fig. 5. 17. Current density-capacitance curves as a function of the applied forward bias for the device consisting of ITO/ ~44.88nm PVK/ 30nm Rhodamine B dye/35nm Pb which was treated by external electric field at 90°C.	82
Fig. 5. 18. Current density-capacitance curves as a function of the applied forward bias for the device consisting of ITO/ ~44.88nm PVK/ 30nm Rhodamine B dye/35nm Pb which was treated by external electric field at 100°C.	83
Fig. 5. 19. Current density-capacitance curves as a function of the applied forward bias for the device consisting of ITO/ ~44.88nm PVK/ 30nm Rhodamine B dye/35nm Pb which was treated by external electric field at 110°C.	83
Fig. 5. 20. Current density-capacitance curves as a function of the applied forward bias for the device consisting of ITO/ ~44.88nm PVK/ 30nm Rhodamine B dye/35nm Pb which was treated by external electric field at 120°C.	84
Fig. 5. 21. Equivalent Circuit of OLED devices.	85
Fig. 5. 22. Deducing equivalent circuit from impedance plots.	85
Fig. 5. 23. Bode modulus and phase for the OLED device consisting of ITO/PVK/Rhodamine B dye/Pb.	86
Fig. 5. 24. Bode modulus and phase for the OLED device consisting of ITO/50nmCuPc/PVK/Rhodamine B dye/Pb.	87
Fig. 5. 25. Bode modulus and phase for the OLED device consisting of ITO/30nmCuPc/PVK/Rhodamine B dye/Pb.	87
Fig. 5. 26. Bode modulus and phase for the OLED device consisting of ITO/10nmCuPc/PVK/Rhodamine B dye/Pb.	88
Fig. 5. 27. Bode modulus and phase for the OLED device consisting of ITO/5nmCuPc/PVK/Rhodamine B dye/Pb.	88

Fig. 5. 28. Bode modulus for the OLED devices consisting of ITO/CuPc/PVK/Rhodamine B dye with different thicknesses of CuPc layer.	89
Fig. 5. 29. Phase modulus for the OLED devices consisting of ITO/CuPc/PVK/Rhodamine B dye with different thicknesses of CuPc layer.	89
Fig. 5. 30. Bode modulus and phase for the OLED device consisting of ITO /PVK/Rhodamine B dye/Pb which was treated at 90°C.....	91
Fig. 5. 31. Bode modulus and phase for the OLED device consisting of ITO /PVK/Rhodamine B dye/Pb which was treated at 100°C.....	91
Fig. 5. 32. Bode modulus and phase for the OLED device consisting of ITO /PVK/Rhodamine B dye/Pb which was treated at 110°C.....	92
Fig. 5. 33. Bode modulus and phase for the OLED device consisting of ITO /PVK/Rhodamine B dye/Pb which was treated at 120°C.....	92
Fig. 5. 34. Bode modulus of OLEDs devices treated by heating at different temperatures.....	93
Fig. 5. 35. Phase modulus of OLEDs devices treated by heating at different temperatures.....	93
Fig. 5. 36. Bode modulus and phase for the OLED device consisting of ITO /PVK/Rhodamine B dye/Pb which was treated by an E-field at 90°C.....	95
Fig. 5. 37. Bode modulus and phase for the OLED device consisting of ITO /PVK/Rhodamine B dye/Pb which was treated by an E-field at 100°C.....	95
Fig. 5. 38. Bode modulus and phase for the OLED device consisting of ITO /PVK/Rhodamine B dye/Pb which was treated by an E-field at 110°C.....	96
Fig. 5. 39. Bode modulus and phase for the OLED device consisting of ITO /PVK/Rhodamine B dye/Pb which was treated by E-field at 120°C.	96

Fig. 5. 40. Phase modulus of OLEDs devices treated by E-field at different temperatures.....97

Fig. 5. 41. Bode modulus of OLEDs devices treated by E-field at different temperatures.....97

CAPTER 1

INTRODUCTION TO POLYMER

1.1 INTRODUCTION

Generally, lighting is an area in which large amount of electrical energy is spent. If we consider the most common light sources like incandescent filament lamps, we find that a large amount of energy is consumed to produce light. Incandescent filament lamp is a deficient technology and a big part of its operating energy is converted to heat. Other technologies as gas filled electrical discharge lamps are more efficient but they cause pollution.

Researchers are now working hard to create lighting sources that have better performance and higher efficiency and are clean for the environment. Organic light emitting diode (OLED) is one of the most recent development in this field. Based on electroluminescence (EL) effect OLEDs are found to be more active and friendly for the environment.

EL is a phenomenon in which light can be generated by an electric current flowing in non-incandescent materials. EL from inorganic materials has been studied since 1904 and multi devices have been built using materials of ZnS, CaS and SrS as Luminescent centers [1].

1.2 LITERATURE REVIEW

The introduction of organic semiconductors in EL applications has started in 1953s by Faculte de la Pharmacie de Nancy [2]. In 1963, Prop et.al studied EL in anthracene using very thick fabricated devices (up to 5 mm) and very high voltages (400 – 2000V). Their devices were not commercialized due to the high voltage [2].

Tang and Van Slyke (1987) [3] created the first multilayer organic device using small 8-hydroxyquinoline aluminum (Alq_3) molecule as a green emitter and diamine (TPD) as a hole transport layer (HTL). In this device, they used a transparent indium thin oxide (ITO) as an anode and Mg: Ag as a cathode. This device was the first accepted one in OLED industry due to its low threshold-voltage, quantum efficiency of 1% photon /electron and luminance of about 1000 cd/m^2 [1,3].

In 1990, the first EL from a conjugated polymer was reported [2]. Braun and Heeger confirmed this result and reported improvements, the first conjugated polymer used in EL was poly (Parapheny-lenevinylene) PPV [4]. Researchers faced a problem in applying conjugated polymers in multilayer organic devices. They found that different polymers were soluble in the same organic solvent. When one layer deposited on top of the other, the underlying layer was removed leading to a device that only consists of one layer with low performance. The development in science allowed different polymers to be dissolved in different solvents which improved the construction of multilayer polymer devices [5].

Both academic institutions and commercial companies have exhibited extensive interests to improve the characteristics of OLEDs and Polymer Light Emitting Diodes (PLEDs). These include the following advantages: (1) molecular design can be produced to emit various colors, (2) low power consumption and high display intensity,(3) very thin thickness of display device (thinner than film transistor-liquid crystal display ,TFT-LCD) and (4) light weight and a large area display [1].

1.3. ADVANTAGES AND DISADVANTAGES OF OLEDs

Currently OLEDs are used in low information displays with limited size such as mobile phones, car radios, and digital cameras. Fig. 1.1 displays some applications of OLEDs and PLEDs in our life.

OLEDs have many advantages over other technologies such as

- **Self-luminous:** The efficiency of OLEDs displays is better than that of other display technologies.
- **Low cost and easy fabrication.**
- **Color selectivity:** There are abundant organic materials to produce blue to red light.
- **Lightweight and thin devices:** OLEDs are generally very thin, measuring only about 100nm, and have very small weight.
- **Flexibility:** OLEDs can be easily fabricated on plastic substrates paving the way for flexible electronic.
- **High brightness and high resolution:** OLEDs are very bright at low operating voltages.
- **Wide viewing angle:** OLED emission is lambertian and so the viewing angle is as high as 160 degrees.

OLEDs have few disadvantages that can be summarized as follows :

- Organic materials are very sensitive to oxygen and water molecules, which can degrade the device very, fast [3]. Therefore, the main disadvantage of an OLED is its the lifetime.
- Low mobility due to amorphous nature of organic molecules.



Fig. 1. 1. Some applications of OLEDs and PLEDs.

1.4 BASIC CONCEPTS OF POLYMER SCIENCES

A polymer is a large molecule in which repeated units linked together to form a long chain. The repeating unit is called a monomers.

The name of a polymer is derived by adding the prefix poly before the monomer's name, like poly acetylene. The number of repeated units in the chain is called the degree of polymerization "n". The molecular mass of the polymer is given by multiplying n with the molecular mass M of a monomeric unit.

$$M_{\text{pol}} = nM$$

The Polymer with high degree of polymerization are called high polymer but the polymer, which has low degree of polymerization is called oligomers [6]. Polymers can be classified a according to their source, method of synthesis, thermal processing behavior, structural shape, and end use.

1.5 TYPES OF POLYMER MOLECULAR STRUCTURES

One of the most common classification of polymer is according to molecular structure. There are two main types of molecular structures homopolymer and copolymer.

1.5.1 Homopolymers

Homopolymer constructed from repeated units of the same type. The molecular structure of homopolymers can be classified to three major types: linear, branched, and crosslinked (three-dimensional) structure.

a) Linear Homopolymer

Linear polymer consists of a long chain with high degree of symmetry, which can be described as beads on a string. The length of these strings is huge, and the beads represent the repeating unit, as shown in Fig. 1.2.

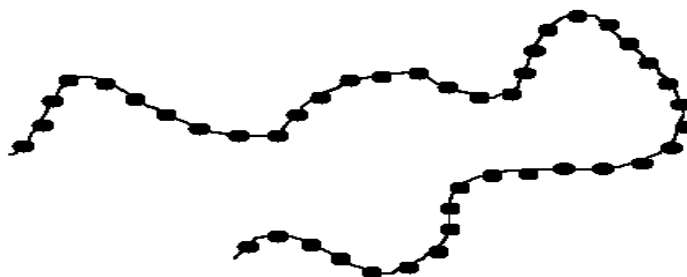


Fig. 1. 2. The general shape of linear homopolymer.

b) Branched Polymer

A branched polymer is a long chain with side branches (side chains), the number and length of which may be very large. This type is also know a two dimensional polymer, the monomers of this type can react with more than two molecules, so the monomer must be at least trifunctional, as show in Fig. 1.3

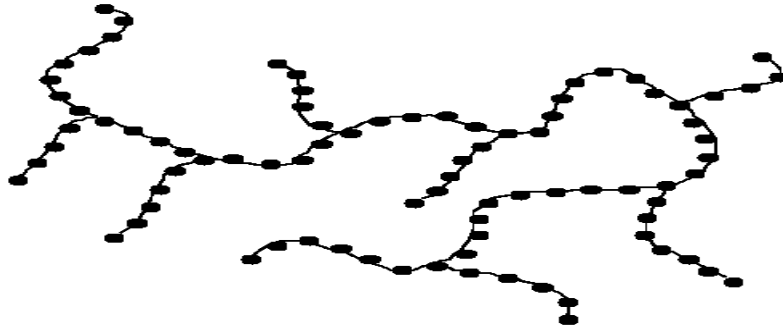


Fig. 1. 3. The general shape of branched homopolymer.

c) Crosslinked Polymers

A long chain connected into a three-dimensional network by chemical crosslinks is called crosslinked polymer and the individual molecular chains within a crosslinked polymer are themselves linked together by covalent bonds. Figure. 1.4 shows the general structure of crosslinked polymer.

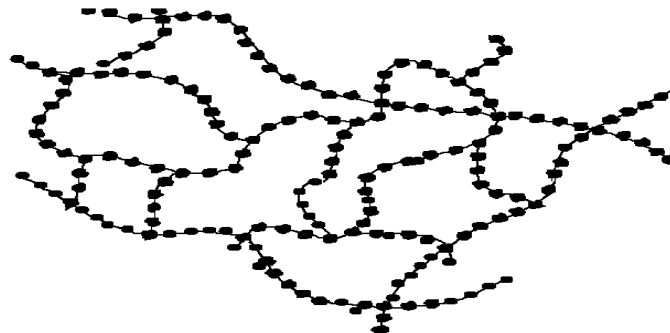


Fig. 1. 4. The general shape of crosslinked homopolymer.

1.5.2 Copolymers

When two different monomers are used in the polymerization process as A and B, the result is called a copolymer. Copolymer are classified into linear, branched, and cross-linked polymers.

a) Linear Copolymer

Linear copolymer appears in three different forms: random, alternating, and block copolymer. When the distribution of repeated units is irregular in its structure, this is referred to as a random copolymer as shown in Fig. 1.5.

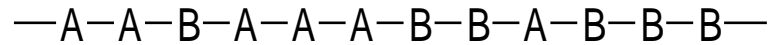


Fig. 1. 5. General Structure of linear random copolymer.

In the alternating copolymer, the two mers alternate in a regular shape along the polymer chain as show in Fig. 1.6.

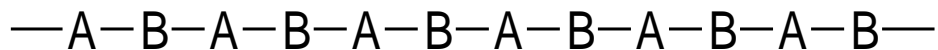


Fig. 1. 6. General structure of alternating copolymer.

A block copolymer comprises two or more homopolymer subunits linked by covalent bonds as shown in Fig. 1.7. The union of homopolymer subunits may require intermediate non-repeating subunits, known as a junction block. Block copolymers with two or three distinct blocks are called diblock copolymer and triblock copolymer.

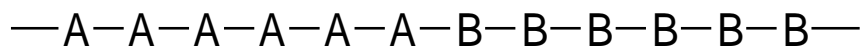


Fig. 1. 7. General structure of block copolymer.

b) Branched (Graft) Copolymers

Branched copolymers has a long chain of monomers of one kind in their main backbone and a chain of monomers of another type in their side branches. The structures of branched copolymers are shown in Fig. 1.8.

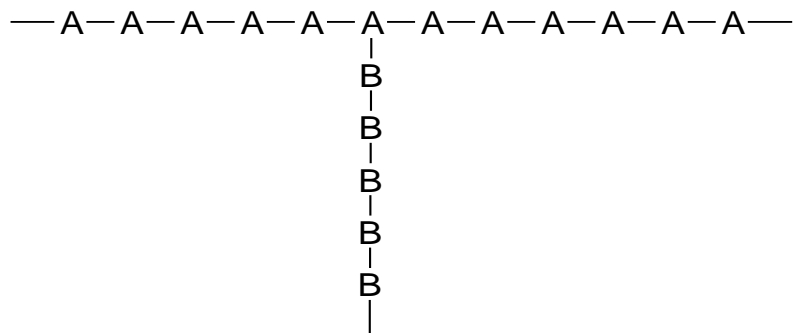


Fig. 1. 8. General structure of branched copolymer.

c) Crosslinked Copolymer

The monomer that form crosslinked polymers must be at least trifunctional. During polymerization of each polymer, acrosslink (i.e., a covalent bond) is formed between individual molecular chains. An example of the crosslinked copolymer is phenolics as shown in Fig. 1.9. It should be noted that the structure of phenolics is much more random than that shown in Fig. 1.9. The figure is simplified in order to clarify the three-dimensional network.

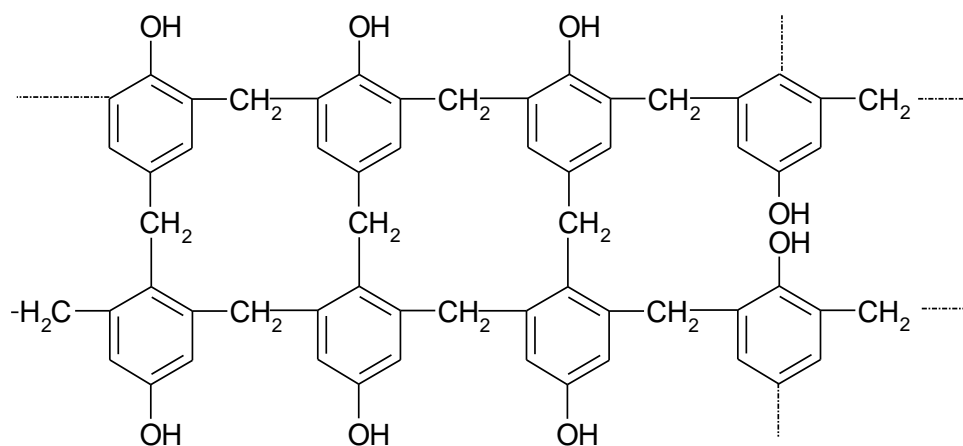


Fig. 1. 9. Structure of a crosslinked copolymer phenolic.

1.6 CONJUGATED POLYMER

Conjugated polymers are organic macromolecules, which have a system of alternating single and double carbon-carbon bonds. Single bonds are referred to as σ -bonds and are associated with a highly localized electron density in the plane of molecule, and double bonds consist of a σ -bond and a π -bond, where π -bond is an overlap between P_z orbitals of neighboring atoms along the conjugate path.

The structure of conjugated bonds (single and double bonds) establishes a delocalization of the electrons situated above and below the plane of molecule, π -band are either empty (called the lowest unoccupied Molecular Orbital-LUMO) which is formed by overlap between anti-bonding π orbitals (π^*), or filled with electrons (called the Highest Occupied Molecular Orbital-HOMO) which is formed by overlapping molecular π -orbitals. Figure 1.10 illustrates the main structure of a conjugated polymer.

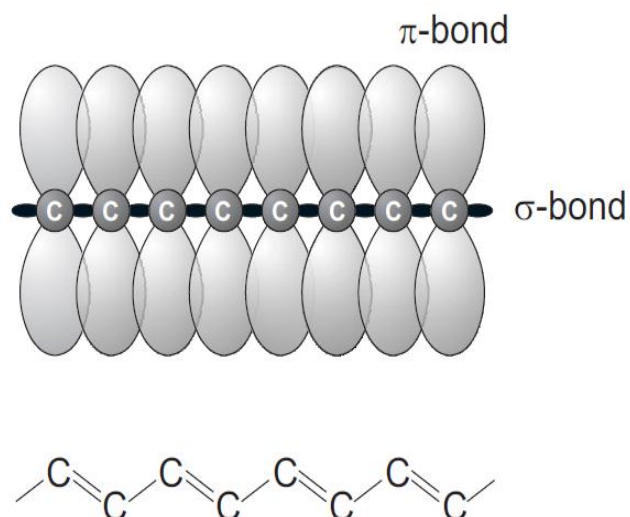
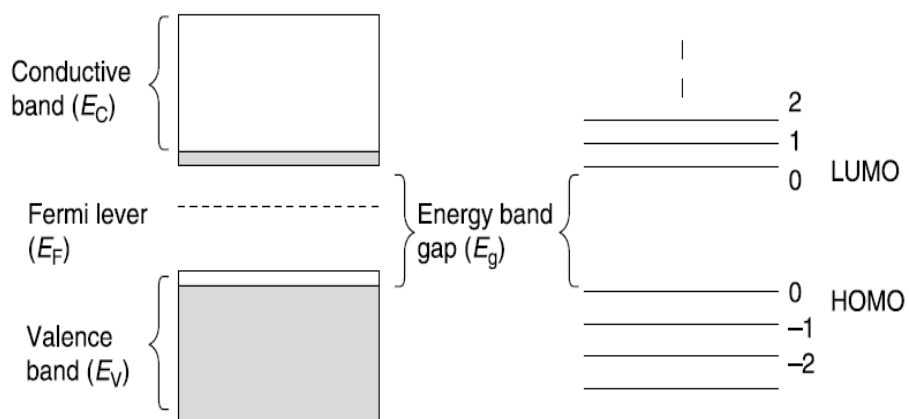
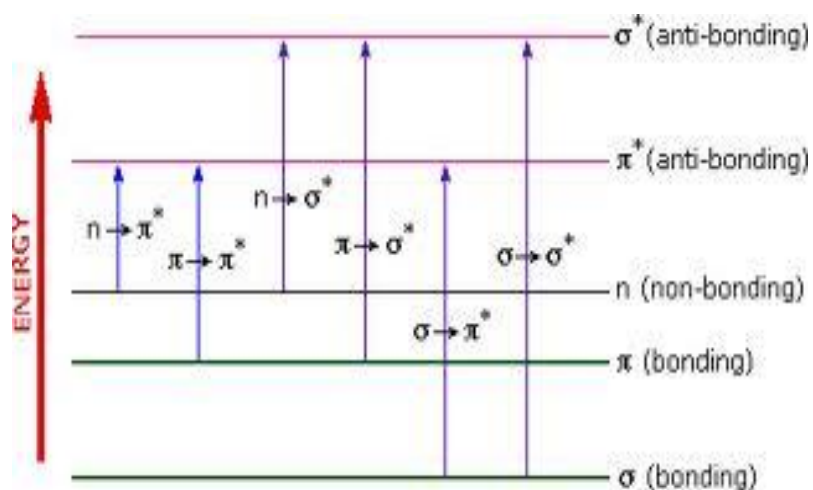


Fig. 1. 10. Scheme of orbitals (above) involved in the bonding between carbons in a conjugated backbone (below).

The band gap of these materials is denoted as the difference between HOMO and LUMO as shown in Fig 1.11 (a) [7]. In this material we look after π -bond not σ -bond, because the energy gap between bonding and anti-bonding states (σ - σ^* gap) in a conjugate organics σ bond is > 5 eV. This gap is too large to play a direct role in the electrical properties of conjugated system, but the (π - π^* gap) is between 1.5 and 3.5 eV [5] as shown Fig 1.11 (b). This is the best band gap for semiconductor used in application of LED and photovoltaic.



(a)



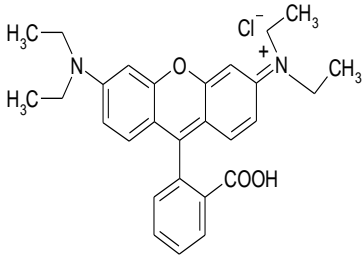
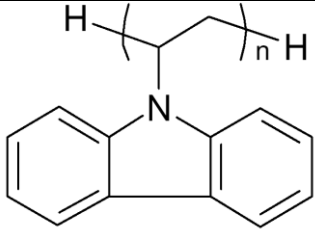
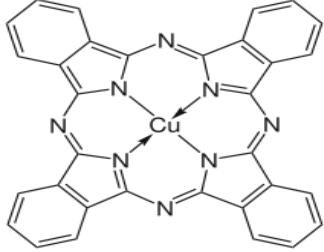
(b)

Fig. 1. 11. (a) Classification of molecular orbitals with respect to electron occupancy, (b) Comparison between bonding and antibonding states of (σ , π).

1.7 MATERIALS USED

In this research, three materials were used namely CuPc, PVK, and Rhodamine B dye. Table 1.1 shows molecular formula, molecular weight, and molecular structure of each materials.

Table 1.1 . Molecular formula, molecular weight, and molecular structure of the three materials.

Materials	Molecular formula	Molecular weight	Molecular structures
Rhodamine B dye	$C_{28}H_{31}ClN_2O_3$	479.01034 g/mol	
Poly (9-Vinylcarbazole).	$C_{14}H_{11}N$	193.24384 g/mol	
Copper-phthalocyanine	$C_{32}H_{16}N_8Cu$	576.06904 g/mol	

1.8 THESIS ORGANIZATION

The goal of the research presented in this thesis is to improve the OLED efficiency by develop new method fabrication. The organization of the thesis is as follows.

Chapter 1 contains an introduction to the history of organic devices and their development from 1953 to present along with the device structures used and the basic concepts of polymer materials used. Chapter 2 will look at the theoretical workings of organic light emitting systems. Chapter 3 focuses on the experimental techniques used for data collection and analysis. Chapter 4 discusses the DC measurement, including important results of all studies in this research. Finally, Chapter 5 does the same, but for small signal AC measurement.

CHAPTER 2

ELECTRICAL CONDUCTION MECHANISMS

2.1 INTRODUCTION

In this chapter, we will discuss what happens when two materials are brought into contact with each other, how a Schottky barrier is formed, the factors influencing about improving the performance of OLED, and an overview of emission mechanism of light from an OLED.

2.2 ELECTRICAL CONTACTS AND POTENTIAL BARRIERS

When two materials with different Fermi levels (Fermi level is the highest energy level of the electron in a material at zero Kelvin, and sometimes called the electrochemical potential or simply the chemical potential) are brought into contact, a state of energy equal to E_F will have the same probability ($f = 50\%$) for being occupied or not. This means that the probability for a state at the level ΔE above E_F to be occupied is equal to that at the level ΔE below E_F to be vacant.

Free charge carriers (electrons and holes) will flow from one material into the other until an equilibrium condition is established, that is until the Fermi levels of both materials are aligned (Fermi levels for electrons in both materials are equal at the contact). Figure 2.1 shows the energy diagram of the metal and semiconductor before (2.1a) and after contact (2.1b). The barrier to charge injection from the metal to the semiconductor, ϕ_B , is given by,

$$\phi_B = \phi_M - \chi_s \quad (2.1)$$

where ϕ_M is called the work function of metal, and χ_s is called electron affinity which is defined as the energy required for an electron to be removed from the bottom edge of the conduction band to the surface to vacuum level.

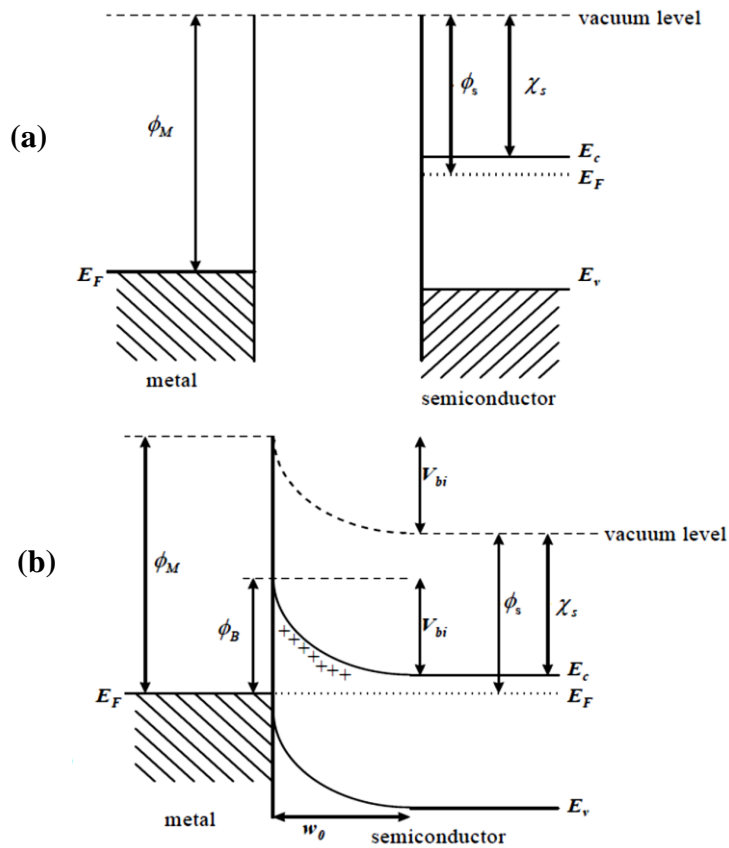


Fig. 2. 1. The energy diagram of the metal and semiconductor before (a) and after contact (b).

This net charge carrier flow will establish a positive space charge on one side and a negative space charge on the other side of the interface forming an electric double layer. This double layer is generally called the potential barrier. The function of this double layer is to set up an electric field to stop any further net flow of free carriers from one material to the other [5,8]. This phenomenon happens in p-n junction when two types of a semiconductor are brought in contact to make a junction.

Before the p-n junction is formed, there are as many electrons as protons in the n-type material making the material neutral in terms of net charge. The same is true for the p-type. After the p-n junction is formed, the n-region loses free electrons as

they diffuse across the junction creating a layer of positive charge near the junction in the n-region. The same process occurs in the p-region when holes diffuse across the junction creating a layer of negative charge near the junction in p-region as shown in Fig. 2.2. the depletion region is found between the two layers due to combination of electrons and holes through moving process. These two layers of positive and negative charges form the depletion region.

The force between opposite charges form a "field of force" E-field which is given by

$$\mathbf{F} = q \mathbf{E} \quad (2.2)$$

This E-field represents a barrier to the free electron flow across the p-n-junction [9]. The voltage required to move an electron through the E-field is equal to the potential barrier value expressed in volts. The potential barrier of p-n junction depends on the type of semiconductor material, the amount of doping and the temperature.

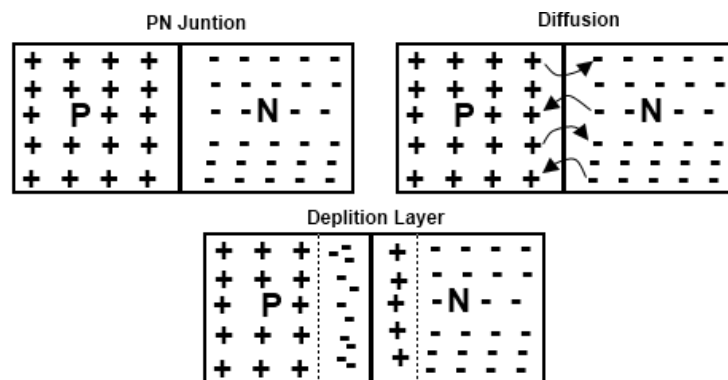


Fig. 2. 2. Formation of the depletion region due to the contact between two different materials.

when an external voltage is applied on p-n junction used the positive terminal is connected to the n-type and the negative terminal with p-type (reverse bias). The depletion region in reverse bias will increase and the charge carriers need more energy to cross the barrier. On the other hand, in a forward bias condition,

a negative voltage is applied to the n-type material and a positive voltage is applied to the p-type material, the negative voltage pushes or repels electrons towards the junction giving them the energy to cross over and combine with the holes being pushed in the opposite direction towards the junction by the positive voltage, then the depletion region will decrease. The forward bias imparts sufficient energy to free electrons to overcome the barrier potential of the depletion region and move into the p-region.

2.3 METAL AND NON-METAL CONTACT

The simplest contact between a metal and a nonmetallic material is the contact between a metal and a vacuum. When two metallic plates are placed in parallel in a vacuum with a small separation, the current flow is negligible if the applied voltage across the two plates is small. This is not because there are no free electrons in the metal, but any electrons present in the vacuum are not mobile in the vacuum. Rather, it is because the electrons in the metal must surmount a potential barrier before they can leave the metal and enter the vacuum [9]. This potential barrier between the highest energy level of the electrons in the metal (termed the Fermi level of metal) and the lowest energy level of the electrons in the vacuum (termed the vacuum level) is called the work function of the metal Φ_m , as show in Fig. 2.3.

It is given by

$$\Phi_m = \zeta - E_{Fm}, \quad (2.3)$$

where ζ is the difference in potential energy of the electron between the inside and outside of the metal, and depends on the structure of the crystal and the condition of the surface, and E_{Fm} is Fermi level for the metal.

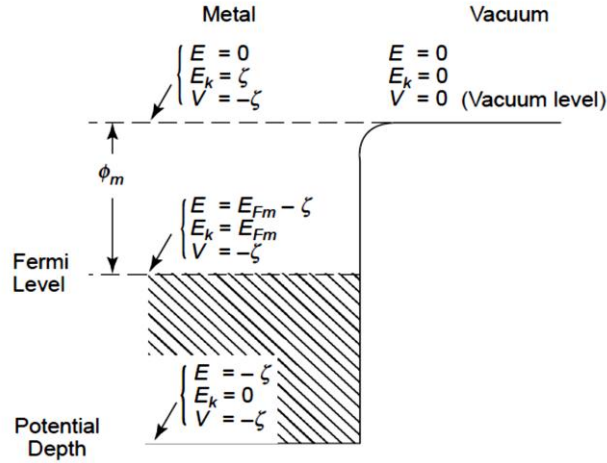


Fig. 2. 3. Energy band diagram showing the work function of metal, Φ_m [9].

From Eqn (2.3), the work function consists of two parts: the energy of binding the electron and the energy required to move the electron through an electrostatic double layer at the surface ζ . This implies that ζ must depend partly on the structure of the surface and partly on the dipole moment of such a double layer. The dipole moment per unit area is $\sigma_s t$ where σ_s is the charge per unit area, and t is the thickness of the layer. So cleaning the metal surfaces is very important to have a good result in practice, because when the metal surface is not clean, the surface potential barrier changes and there may raise or lower to the work function of the metal by more than 2 eV.

The work function of a metal surface is therefore mainly determined by the top few layers of atoms and not by the metal as a whole. However, different ways for cleaning the substrate lead to change in work function. For example, when using gas treatment in cleaning, like oxygen that has electronegative gas adsorbed on the surface will capture electrons from the metal and form a layer of negative ions. This layer will in turn induce a layer of positive image charge in the metal. A double layer will be formed in this case with the negative potential that tends to raise the

work function. On the other hand when using atoms of an electropositive like cesium gas that tends to lower the work function [9].

In general, all the fundamental principles outlined above for metal can also be applied to nonmetallic materials. In nonmetallic material the Fermi level is always located within the energy band gap E_g , and the work function of this material depends on the location of E_F which is a function of temperature, impurity concentration, external pressure, etc. For example, in n-type semiconductor the E_F located near E_C , but for p-type E_F located near E_V as shown in Fig. 2.4 (a) and (b), respectively.

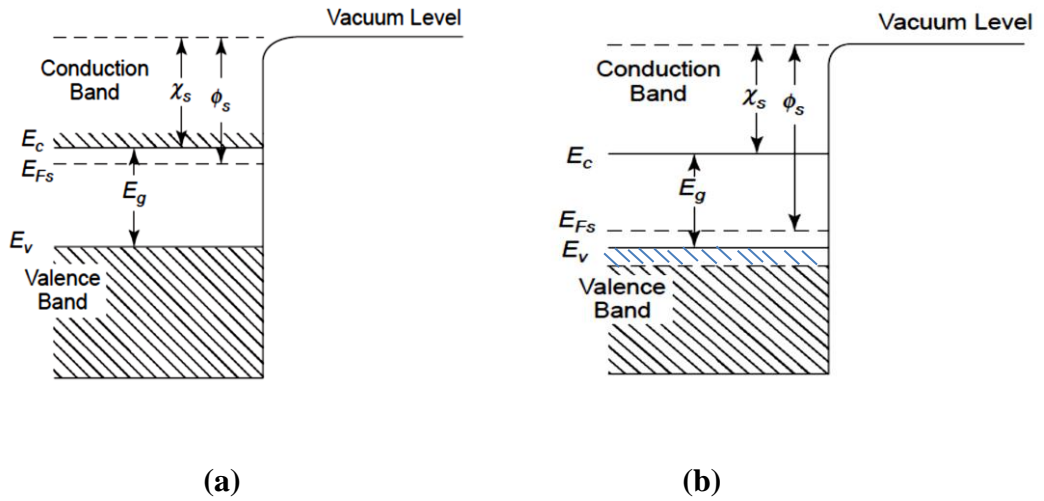


Fig. 2. 4. Energy band diagram showing the work function of (a) n-type semiconductor and (b) p-type semiconductor [9].

We can express the work function for a nonmetallic material as

$$\Phi = \chi_s + (E_C - E_F), \quad (2.4)$$

when two materials (metal- n-type semiconductor) with different work functions are brought into contact the contact potential is given by

$$V_d = \frac{1}{q} (\Phi_m - \Phi_s) = \frac{1}{q} [\Phi_m - \chi_s - (E_C - E_F)], \quad (2.5)$$

Since $E_C - E_F$ is sensitive to temperature and impurity concentration, V_d depends strongly on temperature and impurity concentration. Depending on their relative Fermi levels, either schottky or ohmic junction may form when a metal and a semiconductor are brought into intimate contact. Charges will flow between them until the semiconductor's Fermi level is brought in line with that of the metal. The system will be in thermal equilibrium at this point [6].

Fig. 2.5 shows a metal and n-type semiconductor before contact. The electrons are not able to move from the metal to the semiconductor because are not mobile in vacuum. If the electrons are allowed to flow from one solid to the other (by contacting the back faces of the solids by a metal wire), leaving the front faces not in contact as shown in Fig. 2.6, there will be a net flow of electrons from the n-type semiconductor to the metal because ($\Phi_S < \Phi_m$), but the width of potential barrier is large because the separation between two surface. when we reduce the separation gap between the two surfaces, the width of barrier also decreases as shown in Fig. 2.7 and the electrons can move by two ways: thermionic emission and field emission [9].

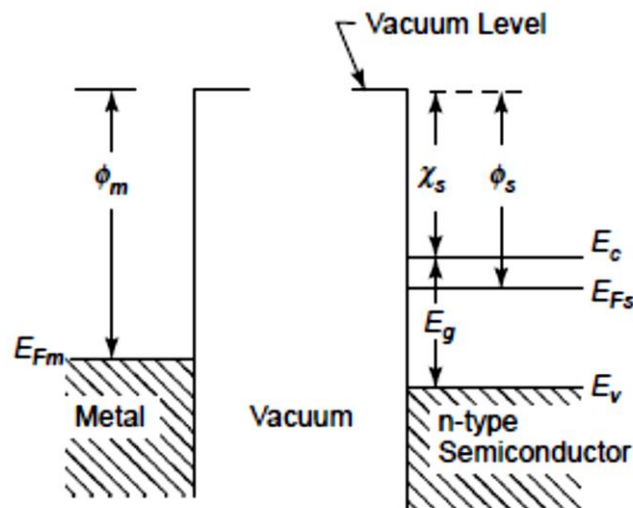


Fig. 2. 5. Energy level diagram for a contact between a metal and an n-type semiconductor for $\Phi_m > \Phi_S$ before contact [9].

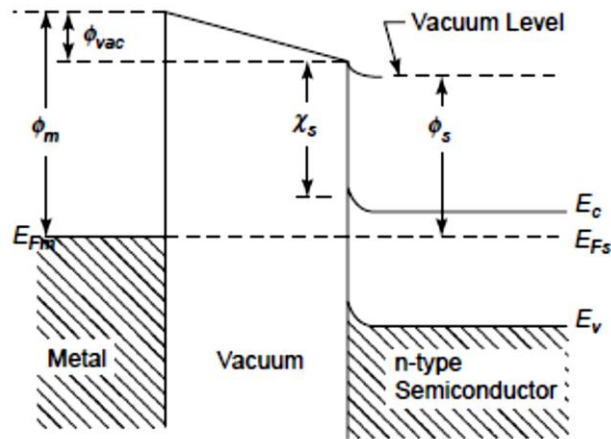


Fig. 2. 6. Energy level diagram for a contact between a metal and an n-type semiconductor for $\Phi_m > \Phi_s$ in thermal equilibrium [9].

The potential barrier after thermal equilibrium will be built due to the creation of the double layer or the space charge region. This barrier has width and height. The electrons at the bottom of the conduction band of the semiconductor must have energy equal to or larger than the height of the potential barrier (qV_d) to move from the semiconductor to the metal.

Similarly, the electrons at the Fermi level of the metal must have energy equal to or larger than the height of the potential barrier ($\Phi_m - \chi_s$) before they can be injected from the metal into the semiconductor as shown in Fig. 2.7.

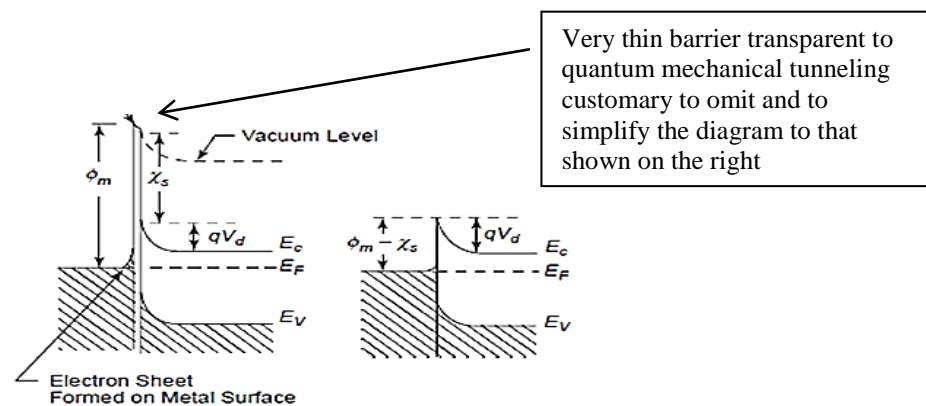


Fig. 2. 7. Energy levels diagram for a contact between a metal and an n-type semiconductor for $\Phi_m > \Phi_s$ in intimate contact [9].

The height and width of the potential barrier can be controlled by adjusting the applied potential, doping process, and selecting a material with proper work function [4, 9]. when increasing the applied forward voltage, the width of the barrier W decreases as shown in Fig. 2.8.

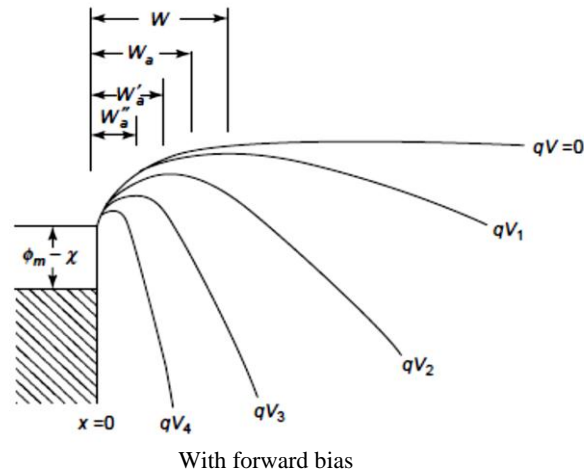


Fig. 2. 8. Energy level diagrams at contact between a metal and an intrinsic semiconductor with applied different voltage $V_4 > V_3 > V_2 > V_1 > 0$ [9].

On the other hand W depends on the energy separation between the Fermi level and the bottom edge of the conduction band, i.e., it depends on the free carrier density, so that when the amount of free carrier density are large by increasing doping process the W decreases [10].

2.4 BASIC OLED STRUCTURE AND ENERGY LEVEL ALIGNMENT

In organic light emitting diodes (OLEDs), three major physical processes exist: (i) charge injection and transport, (ii) charge recombination and exctions energy transfer, and (iii) light emission. Each of these processes plays an important role in such factors as the threshold voltage, external quantum efficiency and luminance of OLEDs.

In last decades, large development in OLEDs industry has been conducted. These development not only involve the improvement of processing technology, but also understanding of the device physics and synthesis of new organic material.

2.4.1 Basic OLED Structure

The basic current structure of an OLED has a high work function conducting transparent anode, one or more organic layer, and low work function of cathode. Most OLEDs use ITO as the anode due to its relatively high work function and high transparency (90%) to visible light. The band gap of ITO is in the range ($E_g = 3.5 - 4.3$ eV) and it consists of indium oxide (In_2O_3) and small amount of tin oxide (SnO_2). Another very important parameter is its work function (Φ_0) or Fermi energy level (E_F) relative to the organic materials, because the (HOMO) energies of organic materials that inject holes to organic layer are typically $E_{\text{HOMO}} = 5 - 6$ eV. A high Φ_0 is needed for anode to have more efficient OLEDs [3]. On the other hand, the work function of cathode materials are chosen to have a low work function, to allow a lot of electrons inject into organic layer and have more efficiently of OLEDs.

2.4.2 Energy Levels of Electroluminescence Materials

The light-emitting wavelength for emitting material is mainly determined by E_g , but is also affected by another condition like the associations of molecules, self-absorption, and alignment of energy levels of the material [11].

There are three main types of materials that used in OLEDs: hole-transport materials (HTM), electron- transport material (ETM), and emitting light material (ELM). In the fabrication of OLEDs these materials (HTM, ETM, and ELM) are chosen carefully according to the energy levels of these materials, especially the HOMO and LUMO energy levels which considered as key parameters for OLEDs as shown in Fig. 2.9. The energy-level diagram defines some of the electronic structure

parameters relevant in designing organic materials for OLEDs. The electron affinity (EA) or LUMO level and the ionization potential (IP) or HOMO level relative to the cathode work function (Φ_C) and anode work function (Φ_A) respectively, determine the charge injection into the diode.

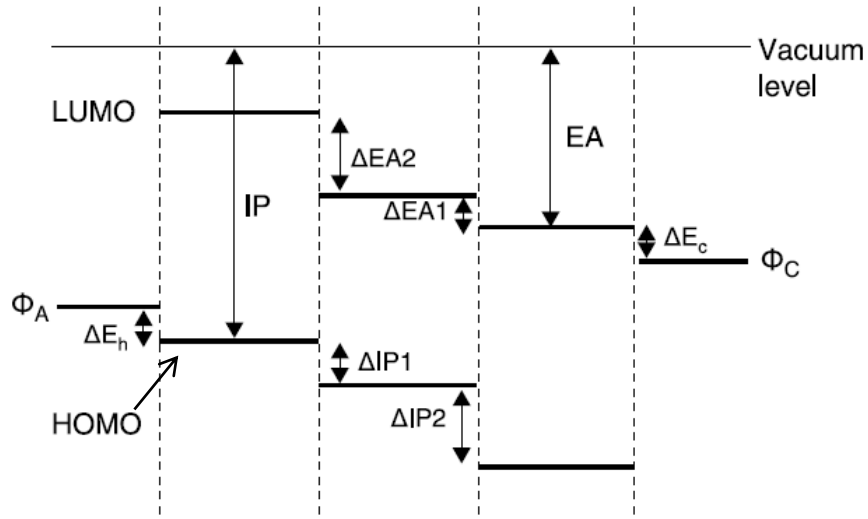


Fig. 2. 9. Energy level diagram of an organic light-emitting diode with a hole-transport material (HTM), an electron-transport material (ETM), the electron affinity (EA), the ionization potential (IP), cathode work function (Φ_C), and the anode work function (Φ_A) [11].

Any mismatches in OLED layers lead to creating large barriers to hole injection at the anode ($\Delta E_h = \Phi_A - IP$) and electron injection at the cathode ($\Delta E_e = \Phi_C - EA$), resulting in poor OLED performance [11].

In order to have an efficient OLED, $\Delta EA1$ barrier between ETM and ELM must be small to allow electron transport through, but $\Delta EA2$ barrier between ELM and HTM must be large enough to avoid electrons for go to the anode and catch it in ELM to recombine with holes to have high efficiency.

Similarly, for holes $\Delta IP1$ must be small but $\Delta IP2$ must be large. In some cases, adding multilayer like electron block layer (EBL), and hole block layer (HBL) to increase the efficiency of OLED as show in Fig. 2.9

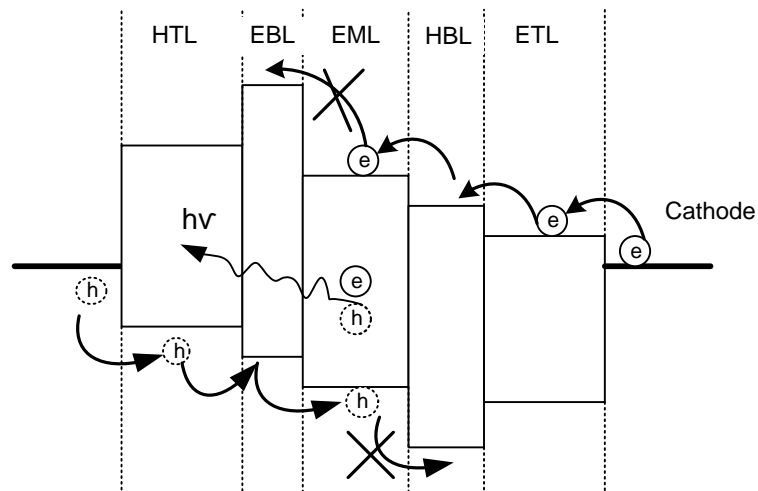


Fig. 2. 10. Multilayer OLED device with a hole-transport layer (HTL), electron transport layer (ETL), electron block layer (EBL), hole block layer (HBL) and emitting material layer (EML).

2.5 MECHANISMS OF CHARGE CARRIER INJECTION THROUGH A METAL / NON-METAL INTERFACE

2.5.1 Thermionic Emission

At any finite (non-zero kelven) temperature, the charge carrier density at any energy is not zero. They have thermal energy denoted by $(K_B T)$ [12, 13]. When the charge carriers have thermal energy larger than the height of the potential barrier (ϕ_B), they can overcome the potential barrier as shown in Fig. 2.11. This process is called thermionic emission.

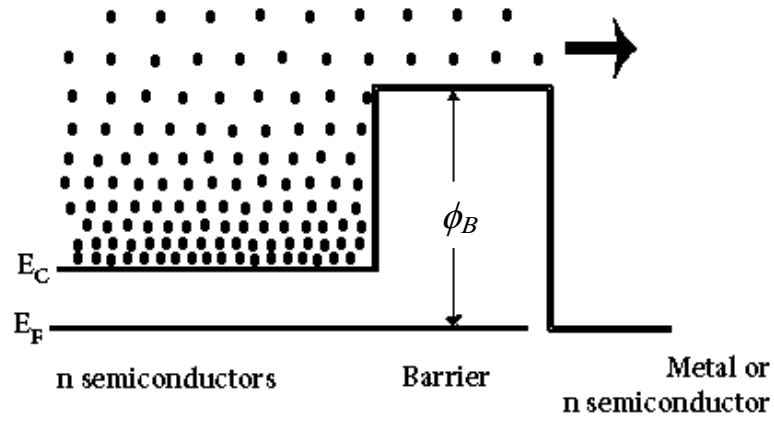


Fig. 2. 11. Energy band diagram showing thermionic emission of electrons over the barrier [13].

In the current density-voltage characteristic of OLEDs, charge injection at low applied bias is due to thermal emission of charge. For example: the intimate contact between n-type semiconductor and metal creates a barrier with height ϕ_B and width W . The total electron current density over the barrier is given by [9].

$$J = A^* T^2 \exp\left(-\frac{q\phi_B}{k_B T}\right), \quad (2.6)$$

$$A^* = \frac{4\pi q m^* k^2}{h^3}, \quad (2.7)$$

where ϕ_B is the barrier height, A^* is called the effective Richardson constant, and m^* is the effective mass of the electron.

2.5.2 Field Emission

Field emission is the tunneling of electrons through the potential barrier from metal to insulator or semiconductor in the presence of a strong electric field and low temperature. Tunneling is a quantum - mechanical phenomenon.

In classical mechanics, carriers are completely confined by the potential walls. Only those carriers having energy higher than the barriers can escape (thermionic emission). In quantum mechanics, an electron can be represented by its wave function. Then it can penetrate through the barrier even if its energy is less than that of the barrier as shown in Fig. 2.12.. when the field emission dominates, the J-V characteristics are described by

$$J = AE^2 \exp\left(-\frac{8\pi\sqrt{2m^*}\phi_B^{3/2}}{3hqE}\right), \quad (2.8)$$

where m^* is the effective charge carrier mass, E is the applied electric field, and A (in A/V^2) is the rate coefficient that contains a tunneling prefatory and the rate of current back-flow [9,10,13]. It can be deduced from the treatment by Kao and Huang [10] that A is given by

$$A = \frac{q^3}{8\pi\hbar\phi_B}, \quad (2.9)$$

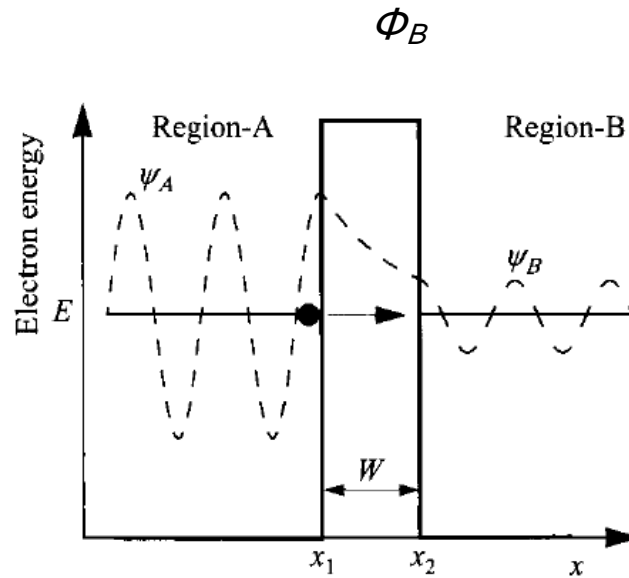


Fig. 2. 12. Wave functions showing electron tunneling through a rectangular barrier where W is the width and ϕ_B is the barrier height [13].

2.6 CARRIER TRANSPORT IN OLEDs

Transport of charge carriers between two layers like (organic-organic), or (polymer-polymer) materials inside the OLED device can be described by two ways, transport by tunneling or hopping processes.

1. Electrical transport by tunneling process

An electron in a molecule, when excited to a higher energy level, can tunnel through a potential barrier to an unoccupied state in a neighboring molecule with energy conserved. If the width of the barrier (i.e., the distance between the two sites) is smaller than 10 \AA , transport occurs by tunneling process [9, 13].

2. Electrical transport by hopping

A charge carrier can move from one molecule to another by hopping process if it has energy higher than the height of potential barrier. The probability of hopping process may be determined by both the distance

between two sites (width of barrier) and the potential barrier that must be overcome, if the potential barrier width is larger than 10 \AA , charge carrier hop rather than tunnel from one molecule to another [9,13] as show Fig. 2.13.

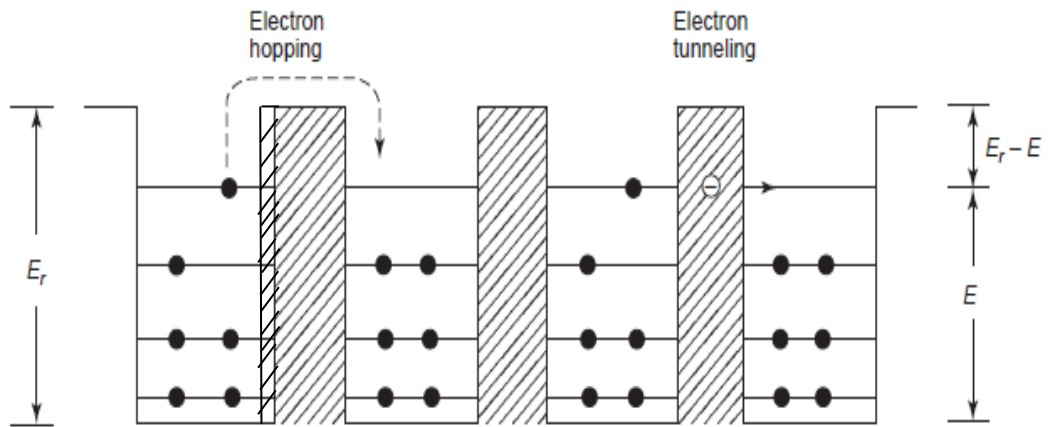


Fig. 2. 13. Schematic diagram illustrating an electron hopping across and an electron tunneling through a square potential barrier [12].

2.7 OHMIC CONTACT

The ohmic contact refers to metal-semiconductor contact with very low junction resistance and is independent of applied voltage. It has a linear J - V characteristic curve in both directions. The charge carrier density at and near the contact is too high. To obtain an ohmic contact, the semiconductor surface has to be doped to create a Sckottky barrier at the interface between the metal and the semiconductor. This barrier is so thin and the charge carriers can tunnel through it. Ohm's law can be written as [12].

$$J_{ohm} = qn\mu \frac{V}{d}, \quad (2.10)$$

where q is the electronic charge, n is the charge carrier density, μ the carrier mobility, V is the applied voltage, and d is the thickness of the sample.

2.8 SPACE-CHARGE EFFECT

Space charge effect occurs when the charge carriers injected under bias are larger than their value in equilibrium before charge injection. This will form space charge cloud near electrodes. In general, the DC current of a device can be divided into two main regimes, ohmic regime and space charge regime. In the ohmic regime, the current is linearly proportional to the electric field according to the following relation

$$J \propto E. \quad (2.11)$$

In the second regime, the current density is proportional to the square of the electric field

$$J \propto E^2 \quad (2.12)$$

This regime is called space charge limited current (SCLC). The space-charge effect is more common in lightly doped materials and it can occur outside the depletion region [12].

If the injected charge changes the electric field configuration inside the semiconductor that screens the source-drain field, the transport becomes space-charge limited. The screening due to these “space charges” produces nonlinear J-V characteristics. The space charge effect emerges in a material such as an organic semiconductor, where the mobility of the charge carrier is poor.

2.9 CHARGE RECOMBINATION

In OLEDs, when an electron is injected into the higher energy polaron level, a negatively charged polaron (p-) is formed (charge -1/2, spin 1/2). Likewise, when a hole injected from the anode removes an electron from the lower energy polaron level, it forms a positively charged polaron (p+) (charge 1/2, spin 1/2). These charged polarons can then move through the organic layer by hopping from state to state.

When two oppositely charged polarons get close enough to each other they begin to affect each other through the coulomb attraction. The two particles may then start to act as a new species of particle called an exciton. An exciton is a neutrally charged particle that can transmit energy but not charge [4].

There are three primary types of excitons: Frenkel, Wannier-mott, and charge-transfer excitons. The Wannier-Mott exciton is large and weakly bound. The electron and hole do not reside on the same atom as shown in Fig. 2.14. Moreover, the radius is approximately 4-10 nm. Wannier-Mott excitons are commonly found in inorganic semiconductors. Frenkel excitons have a small radius ($<0.5\text{nm}$) and usually reside on a single molecule. The charge-transfer exciton is an intermediate state between the Frenkel and Wannier-mott excitons. Frenkel excitons are common in organic system [4, 9].

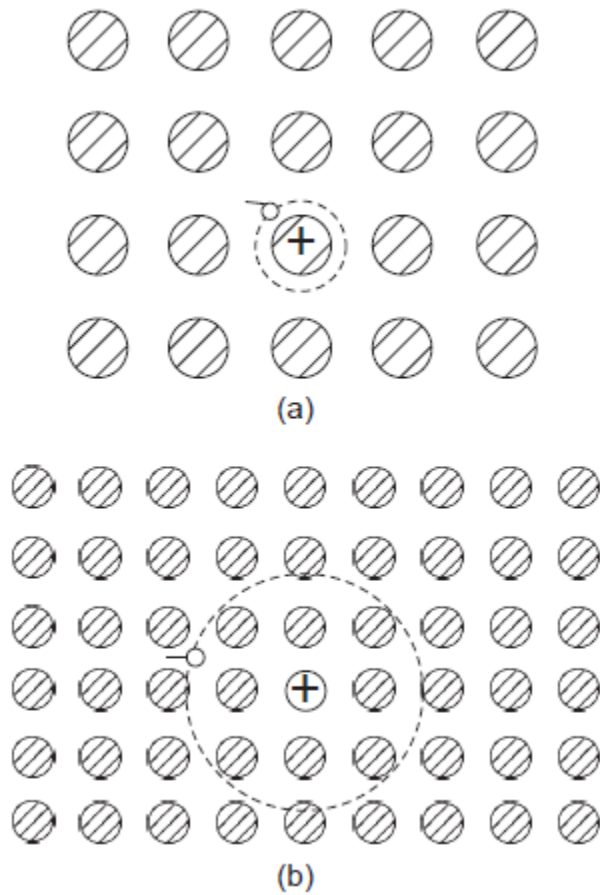
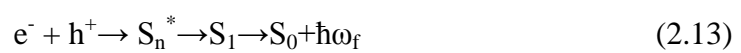


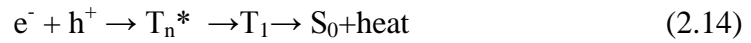
Fig. 2. 14. Schematic illustration of (a) the Frenkel exciton and (b) Wannier exciton [9].

2.10 LUMINESCENCE

Luminescence is the emission of light that occurs from electronically excited state. Luminescence is divided into two types: Fluorescence and Phosphorescence. Fig. 2.15, shows Jablonski diagram and illustration of the relative positions of absorption, fluorescence and phosphorescence spectra. For fluorescent emitter molecules, electrons and holes form either a singlet state S_n^* that relaxes to S_1 and then to S_0 under emission of light with angular frequency ω_f



or a triplet state T_n^* that relaxes non-radiatively to S_0 , generating heat,



The situation is similar for phosphorescent emitters, however, electrons and holes can form a triplet T_n^* that relaxes to T_1 and then to S_0 under emission of light with angular frequency ω_p [4, 9, 14].

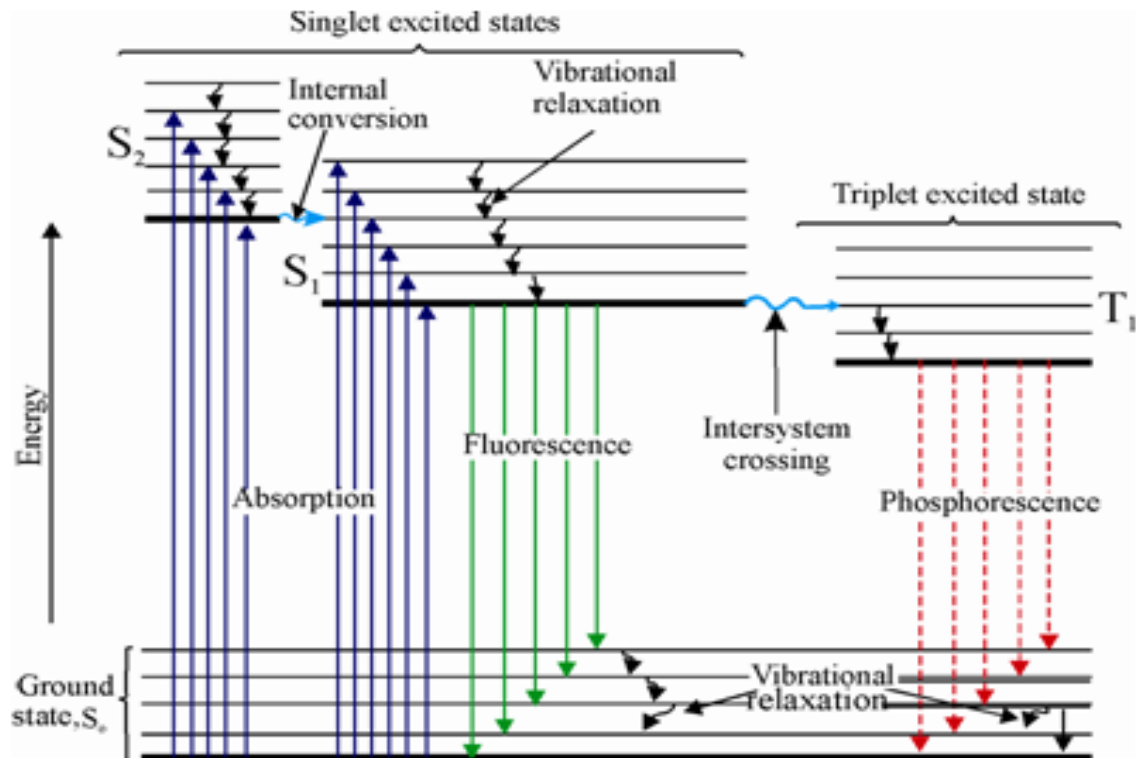
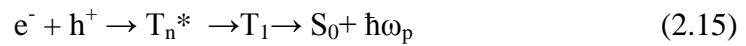


Fig. 2. 15. Jablonski diagram and illustration of the relative positions of absorption, fluorescence and phosphorescence spectra.

CHAPTER 3

EXPERIMENTAL TECHNIQUES

3.1 INTRODUCTION

In this chapter, the equipments and techniques used in this work are described. These equipments were used for preparation and characterization of double layer and multilayer films by inclined casting coating and thermal vacuum evaporation techniques. Filmetrics F20-UVX Thin-Film Analyzer, Keithley 2602A, LCR-821, and Autolab instrument are presented and described here. Moreover, Filmetrics F20 Thin-Film Analyzer used to measure the thickness and the refractive index of the organic film will be presented. The voltage-current signals were applied and recorded through a Keithley 2602A. Finally, Impedance Spectroscopy (IS) is used. Two instruments were used to measure IS. LCR-821, and Autolab.

3.2 EXPERIMENTAL TECHNIQUES

3.2.1 Inclined Casting Coating

Thin film of soluble polymer can be prepared by a simple technique. A small amount of the desired solution is placed on the substrate and the substrate is then inclined at different angles for several minutes to have a good film. The best inclination angle depends on the polymer concentration. The sample is then placed in an oven at 60°C for 24 hours in order to remove the residual solvents. The thickness can be increased by increasing the concentration of polymer in solution. This process is sensitive to the variations in temperature due to different evaporation rates [12].

3.2.2 Thickness and Optical Constants Measurements

Filmetrics F20 Thin-Film Analyzer is used to measure thickness and optical constants (n and k) of dielectric and semiconductor thin films where n and k are the film's refractive index and extinction coefficient, respectively.

The refractive index is defined as ratio of speed of light in a vacuum to the speed of light in material, and the extinction coefficient is a measure of how much light is absorbed in the material. The principle of operation of Filmetrics F20 depends on the interaction of light with the film surface. When a ray of light traveling through a transparent medium encounters a boundary leading into another transparent medium, as shown in Fig. 3.1, part of light is reflected and the other enters the second medium. The ray that enters the second medium is said to be refracted.

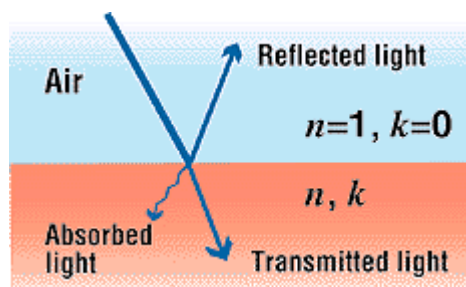


Fig. 3. 1. Single interface reflection occurs whenever light crosses the interface between different materials [15].

The fraction of light that is reflected by an interface is determined by discontinuity in n and k. For light reflected off of a material in air

$$R = \frac{(n-1)^2 + k^2}{(n+1)^2 + k^2} \quad (3.1)$$

For the simple case, when the light reflected by a single nonabsorption material (k=0) as shown in Fig. 3.1, then

$$R = \left(\frac{n-1}{n+1} \right)^2 \quad (3.2)$$

at this case the refraction index of material can be determined from measurement of R.

When a thin film is deposited on the top of substrate, at this moment both the top and the bottom of the film reflect light. The total amount of reflected light is the sum of these two individual reflections. According to the nature of light, the reflections from two interfaces may add together either constructively or destructively, depending upon their phase relationship as shown in Fig. 3.2 [15]. The difference in optical path lengths of the two reflections from two different materials can be measured from which the film thickness can be measured [15].

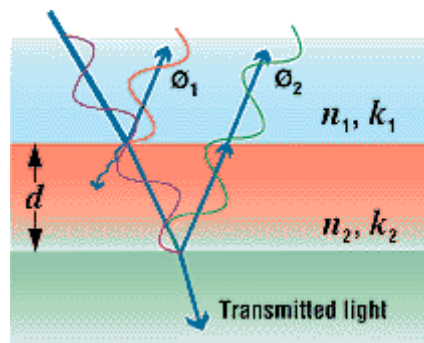


Fig. 3. 2. Multiple interface reflection occurs whenever light crosses the interface between different materials [15].

Reflections are in-phase and therefore add constructively when the light path is equal to one integral multiple of the wavelength of light

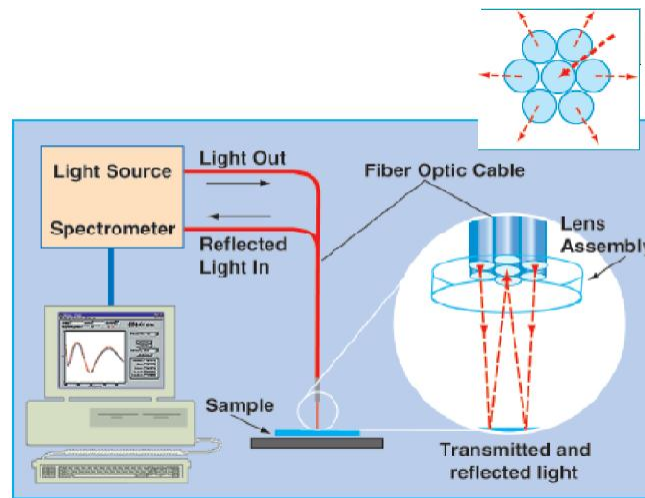
$$2nd = m\lambda, \quad (3.3)$$

where d is the thickness of the film, m is an integer, n is refractive index, and λ is the wavelength of the reflected light. On the other hand, reflections are out of phase and add destructively when the light path is one half of wavelength different from the in-phase condition, that is

$$2nd = (m+1/2)\lambda, \quad (3.4)$$

The Filmetrics F20 is able to determine thin-film characteristics by measuring the amount of light reflected from the thin film over range of wavelengths. Light is supplied by a tungsten-halogen bulb and UV light

source as shown in Fig. 3.3 (a) and (b). This light is delivered to the sample and collected from it through a fiber-optic cable bundle and a lens. The intensity of the reflected light is measured at different wavelengths with a spectrometer. The Filmetrics F20 spectrometer uses a diffraction grating to disperse the light and a linear photodiode array to measure the light at the different wavelengths.



(a)



(b)

Fig. 3. 3. (a) Schematic diagram of Filmetrics F20 Thin-Film Analyzer component [15], (b) Photograph of real instrument.

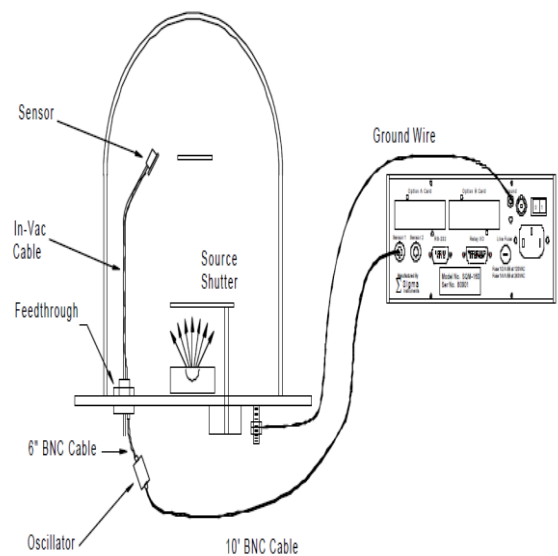
3.2.3 Thermal Vacuum Evaporation

Vacuum deposition is a technique used to deposit materials by heating a source material under vacuum until it evaporates into a gaseous vapor or sublimates. The vapors condense on a substrate surface to form a film. Evaporation takes place in vacuum where the mean free path of atoms (molecules) of the evaporated material is longer than the distance from source to substrate [2].

Film thickness can be controlled by the quantity or rate of generated vapor material as well as the distance from the source to substrate. Deposition rates depend significantly upon the substrate and source geometry. Film thickness is inversely proportional to the square of the distance to the source. The components of the evaporating system (Moorfield, Minilab 080) are shown in Fig. 3.4 (a) and(b).



(a)



(b)

Fig. 3. 4. (a) Photograph of Minilab 080, (b) Schematic diagram of the evaporating system.

The thickness of deposited film can be determined using a quartz crystal monitor as shown in Fig. 3.5. A quartz crystal monitor in the deposition chamber monitors the deposition rate of the films and their thicknesses. It has a resonant quartz crystal with one surface exposed to the deposition source. As the material is deposited onto the surface of the device, the resonant frequency changes because of the added mass of the deposited film. The monitor then uses the known parameters of density and acoustic impedance of the source material to determine the deposition rate and thickness [2].



Fig. 3. 5. A SQM-160 quartz crystal monitor that used to know the thickness of film deposition.

3.2.4 Measurement of J-V characteristic Curves

Current density-voltage (J-V) characteristics were measured using a Keithley 2602A source meter. The source meter was used to apply a DC voltage to the device then measure the resulting current. The voltage output to the device and the current output were both controlled by TSP program and were recorded by a computer as shown in Fig. 3.6. The program allowed the user to specify the voltage range to be scanned, the step size of the voltage, and the amount of time each voltage was applied to the device. Data was saved as an excel file and plotted by Origin 8.5 program.



Fig. 3. 6. Photo image of J-Vmeasuring setup.

3.2.5 Electrochemical Impedance Spectroscopy

Electrochemical Impedance Spectroscopy (EIS) measurements were performed by Autolab AUT 85276 Potentiostat- Galvanostat with frequency response analyzer FRA 32 Module as shown in Fig 3.7.

In a typical electrochemical impedance measurement, the FRA module generates a sine wave with a user-defined frequency and small amplitude. This signal is superimposed on the applied DC potential or current on the device. The AC voltage and current components are analyzed by the two FRA channels and the transfer function, the total impedance Z , is calculated, together with the phase angle shift and the real and imaginary components of the total impedance. In the current work, the AC amplitude was set to 10 mV for all measurements. All measurements were carried out with the NOVA software. The impedance was measured and plotted to obtain Bode plots.

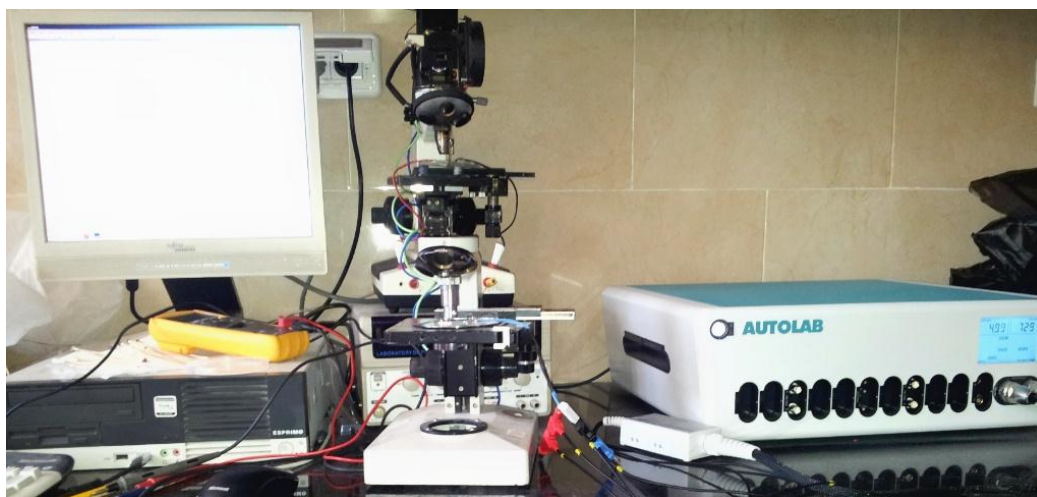


Fig. 3. 7. Autolab instrument in combination with the frequency response analyzer (FRA) that is used in Electrochemical Impedance Spectroscopy (EIS) measurements.

3.2.6 Capacitance-Voltage Measurements

The Capacitance-Voltage (C-V) characteristics curves of OLEDs can be used to know and determine the onset of majority and minority charge carrier injection into the active organic layer from the electrodes. The (C-V) curves were measured and recorded by GW 821 LCR meter from the range of 0V up to 30V. Fig. 3.8 shows a photo of GW 821 LCR meter setup.



Fig. 3. 8. LCR-821 instrument that is used in C-V measurements.

CHAPTER 4

THE CURRENT DENSITY-VOLTAGE-ELECTROLUMINESCENCE CHARACTERISTIC CURVES

4.1 INTRODUCTION

In this chapter, three studies will be presented in details, including the post-fabrication heat treatment, a combined external electric field and heat post-fabrication for organic layer before metal cathode deposition, and the influence of copper-phthalocyanine (CuPc) as hole-injection layer on the current density-voltage characteristic and the device electroluminescence. The devices were fabricated in the same run together with a control device without annealing and without CuPc layer deposition for comparison. The control device has an identical structure of ITO/PVK/Rhodamine B dye/Pb. All of the characteristic curves were measured at room temperature and without glove box, and the results were plotted using origin 8.5 program.

4.2 DEVICE FABRICATION

4.2.1 Substrate Cleaning

ITO-coated glass substrates (Delta Technologies, USA) were cut into pieces of dimension 2.5cm × 2.5cm and used as anodes. The substrates were chemically cleaned using acetone, isopropanol and aqua regia solution with concentration of 3:1 at 60°C for 5 min. The substrates were then cleaned by distilled water in an ultrasonic cleaner for 20 min and placed in an oven at 60°C for 24 hours in order to remove the residual water.

4.2.2 Depositing the Device Layers

The influence of copper-phthalocyanine (CuPc) hole-injection layer on the current density-voltage characteristic and the electroluminescence performance of ITO/CuPc/PVK/Rhodamine B dye/Pb devices were investigated. A schematic of the fabricated device is shown in Fig. 4.1. After cleaning the ITO surface, CuPc layer was deposited on ITO by thermal vacuum evaporation at 1.0×10^{-5} torr using MiniLab 080 system (Moorfield Associates, UK) with various thicknesses.

The next step was the deposition of PVK layer, an amount of 15mg of PVK powder with an average molecular weight of 11×10^5 , were weighed using a sensitive electrical balance (ESJ182-4) with a resolution of 10^{-4} gm. The PVK was dissolved in mixed solvents consisting of 5ml tetrahydrofuran (THF) and 1ml toluene. A homogenous solution was then deposited on the CuPc layer to form a thin film with thickness of about 44.88 nm. The thin film of PVK was obtained by placing a small amount of desired solution on the substrate. The substrate was inclined at an angle of 45° for several minutes. The solution spreads on the surface of the substrate due to gravity forming a thin film on the surface. This process is sensitive to the variation in temperature due to different evaporation rates of solvents [12]. The thickness was measured using FILMETRICS F20-UVX thin-film analyzer.

A 30nm Rhodamine B dye layer is then deposited on the PVK layer by thermal vacuum deposition at 1.0×10^{-5} torr. Finally, 35nm thick and 3.5 mm diameter Pb layer was deposited as a cathode electrode on Rhodamine B dye layer. The negative terminal of the applied voltage was connected to the Pb electrode through a drop of Hg. whereas the positive terminal was connected to ITO substrate by silver paste.

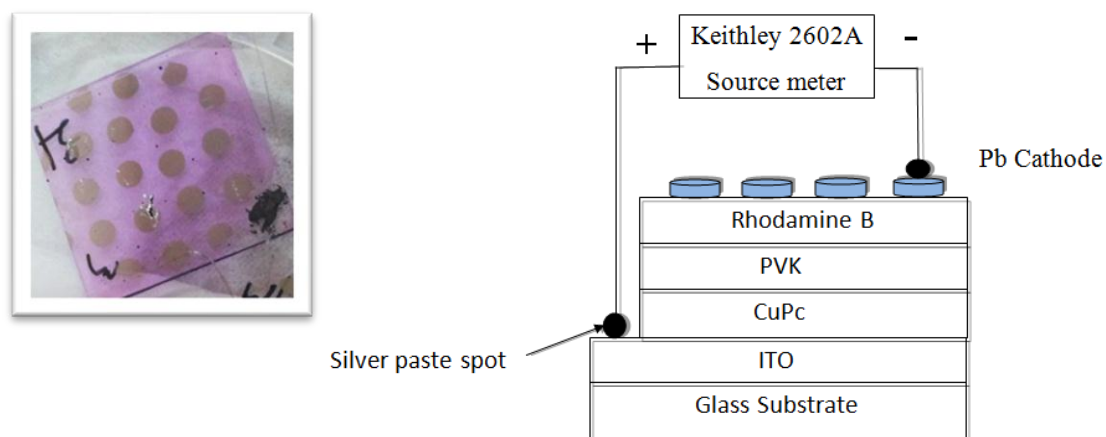


Fig. 4. 1. The picture in the right hand appeared the schematic drawing of a multilayer ITO/CuPc/PVK/Rhodamine B dye/Pb, and the picture in the left hand appeared the device fabrication.

4.2.3 Post Processing Treatment

After depositing the Rhodamine B dye layer on the PVK film as explained in section 4.2.2, the samples were thermally annealed at different temperatures (90°C, 100°C, 110°C and 120°C) using a hot plate for 15 min under the atmosphere environment.

After annealing, the Pb film was thermally vacuum evaporated on top of the Rhodamine B dye layer as the second electrode. Some of the samples were thermally annealed without any applied external electric field while other samples were annealed under an external electric field. The fabricated OLEDs have the structure ITO/PVK/Rhodamine B dye/Pb as shown in Fig. 4.2.

During the thermal annealing, these samples were exposed to high voltage of +10 KV applied to Cu disc with radius of 2.5 cm located 2 cm above the organic surface while the ITO electrode was grounded. The heater was turned off while the applied voltage is still on for another 15 min, then the electric field was turned off.

The electric field setup is depicted in Fig. 4.3. Finally, a 35 nm Pb film was thermally vacuum evaporated on top of the organic layer as a second electrode.

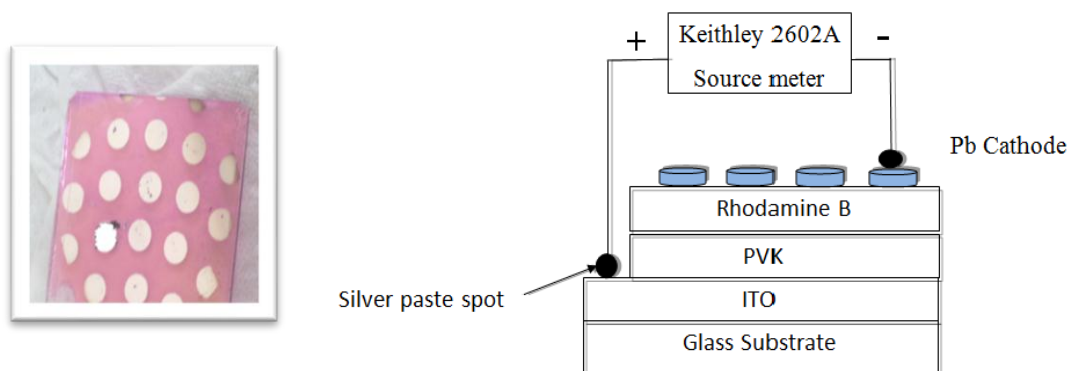


Fig. 4.2. The picture in the right hand appeared the schematic drawing of a double-layer ITO/PVK/Rhodamine B/Pb OLED, and the picture in the left hand appeared the device fabrication.

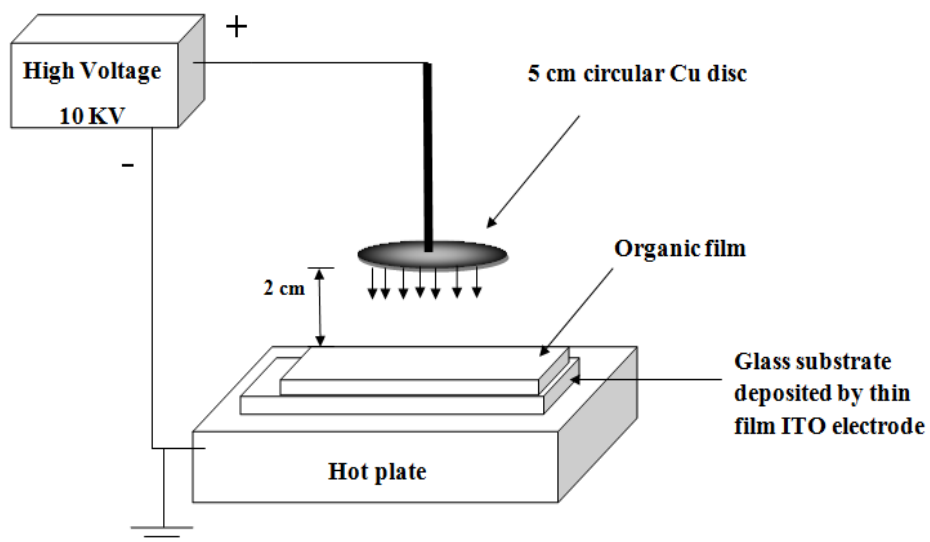
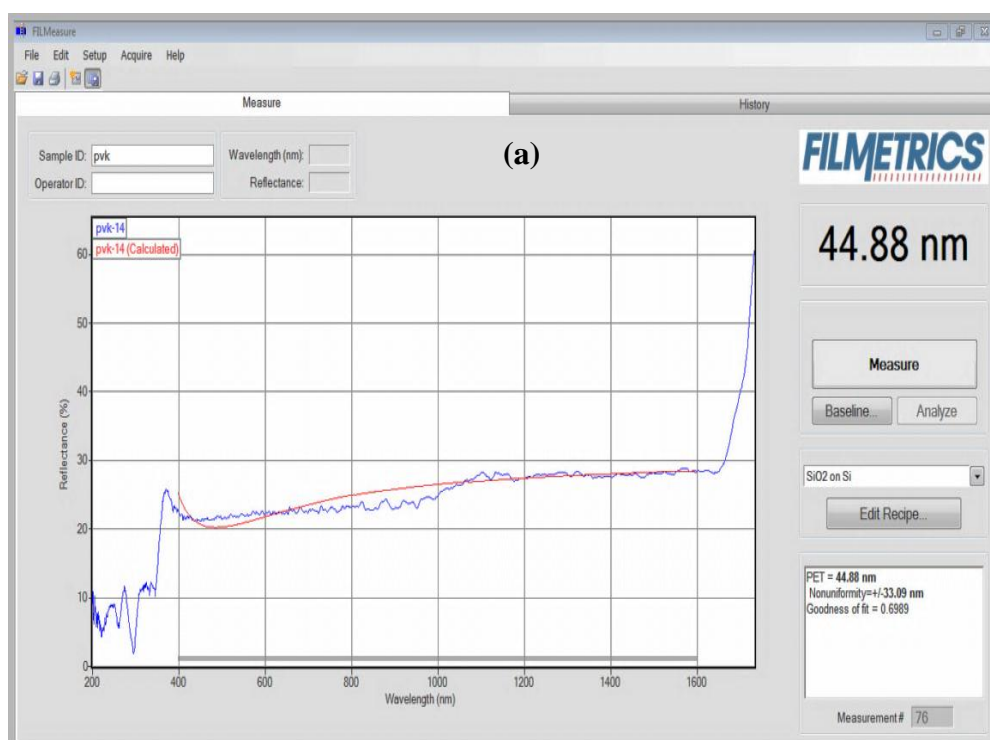


Fig. 4. 3. The electric field treatment setup.

4.3 THICKNESS AND REFRACTIVE INDEX MEASUREMENT

The thickness and refractive index of the PVK film can be measured on Silicon (Si) substrate using Filmetrics F20 UVX thin film analyzer. The measurements of thickness and refractive index of the PVK film in the spectral range from 400 nm to 1600 nm are shown in Fig. 4.4 (a) and (b).

The thicknesses of other layers "CuPc, Rhodamine B dye, and Pb" were measured during the thermal vacuum evaporation process through a SQM-160 quartz crystal monitor. The measured thicknesses were 44.88 nm for PVK, 30 nm for Rhodamine B dye, different thicknesses for CuPc layer (5 nm, 10 nm, 30 nm, and 50 nm), and 35 nm for Pb as cathode electrode.



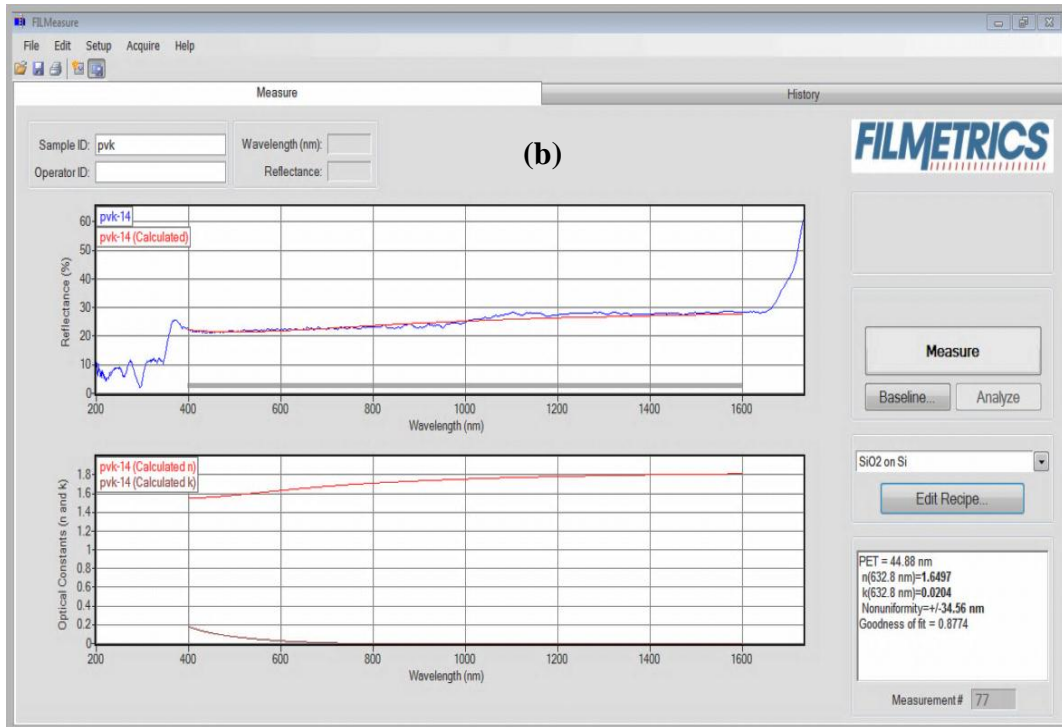


Fig. 4. 4. Reflectance of light (a) and optical constants (n and k) for the PVK film deposited on silicon wafer in the spectral range 400 nm to 1600 nm.

4.4 RESULTS AND DISCUSSIONS

In this section, the experimental results obtained for all fabricated devices are presented. These results include the current density-voltage characteristics, and relative light intensity with the applied voltage. The Pb electrode was negatively biased whereas the ITO electrode was positively biased.

Electrical measurements were carried out at room temperature in ambient and the driving voltage and the resulting current were obtained and measured using a kithely 2602A source meter. The relative intensity was measured using a photodiode. The output of the photodiode was amplified and collected by a kithely 2602A.

4.4.1 The Influence of CuPc Hole-injection Layer

Figures 4.5 and 4.6 show the current density-voltage (J-V) and electroluminescence-voltage (EL-V) characteristics of the control OLED device with the structure of ITO/~44.8 nm PVK/30 nm Rhodamine B dye/ 35 nm Pb. The currents flowing through the samples are attributed to the injection of charges from the metallic electrode. The threshold voltage (V_{th}) of this device is about 7.8 volt from the J-V curve. As can be seen from Fig. 4.6, the voltage at which the light is detected is ~ 14 volt due to recombination of electrons and holes.

Sometime the threshold voltage does not correspond to the same voltage at which brightness is detected [16].

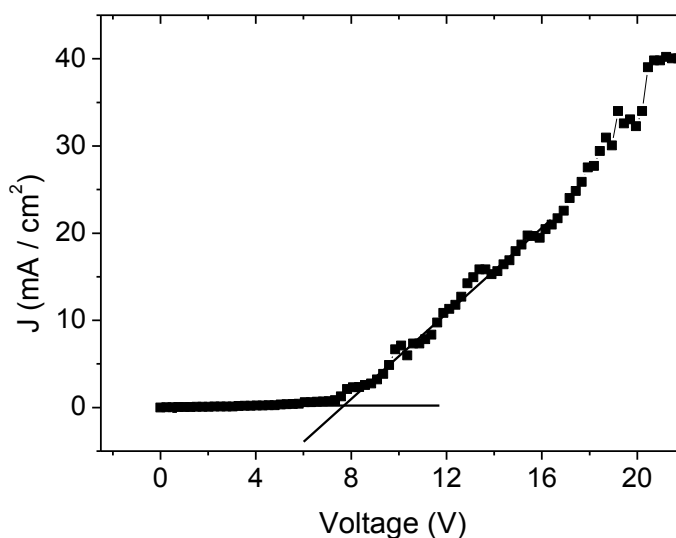


Fig. 4. 5. Current density- voltage characteristic curve of the control device consisting of ITO/~44.88nm PVK/ 30nm Rhodamine B dye/ 35nm Pb.

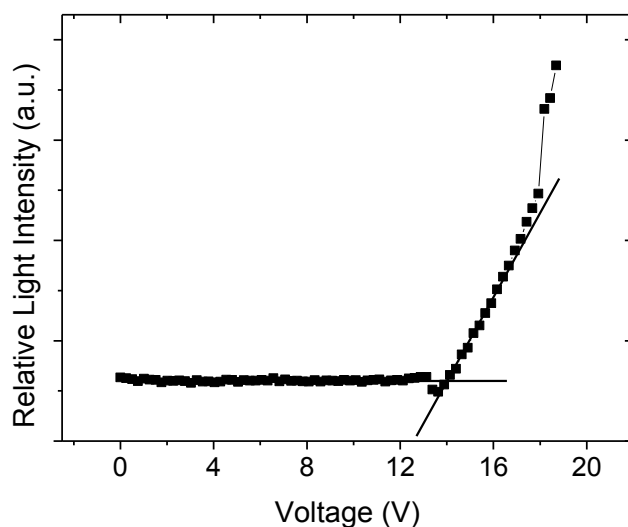


Fig. 4. 6. Relative light intensity-voltage characteristic curve of the control device consisting of ITO/ ~ 44.8nm PVK/ 30nm Rhodamine B/ 35nm Pb.

The energy level diagram of the control device is shown in Fig. 4.7. The barrier to hole injection at the anode is obtained from the equation $\Delta E_h = \Phi_A - IP$ where Φ_A is work function of anode and IP is the ionization potential or HOMO level relative to the anode. We find that $\Delta E_h = 4.8 \text{ eV (ITO)} - 5.8 \text{ eV (PVK)} = -1 \text{ eV}$.

The aim of this work is to reduce the hole injection barrier (ΔE_h) of the device by adding a CuPc layer as a hole injection layer (HIL) with different thicknesses (5nm, 10nm, 30nm and 50nm). As shown in Fig. 4.8 the hole injection barrier (ΔE_h) of the device in the presence of the CuPc layer is about $\Delta E_h = 4.8 \text{ eV (ITO)} - 5.2 \text{ eV (CuPc)} = -0.4 \text{ eV}$.

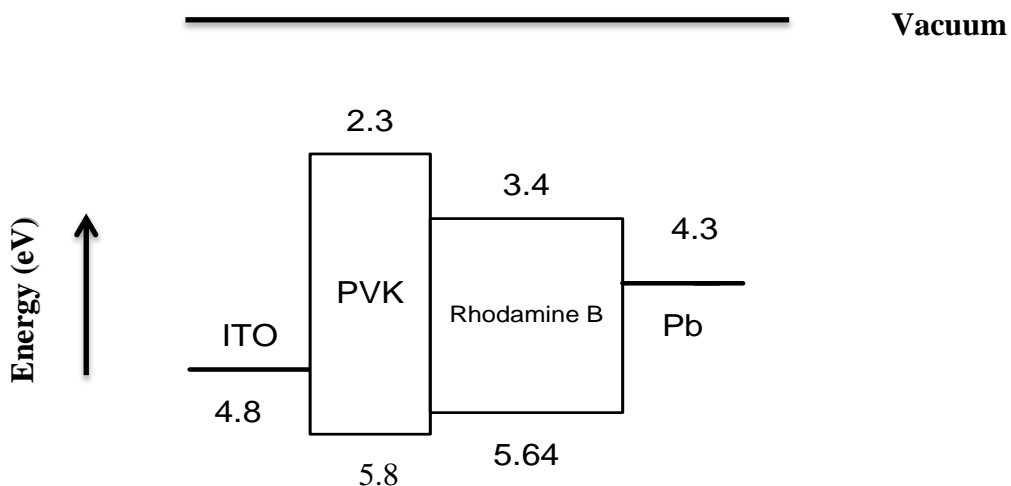


Fig. 4. 7. Energy level diagram for the device consisting of ITO/PVK/ Rhodamine B dye/ Pb.

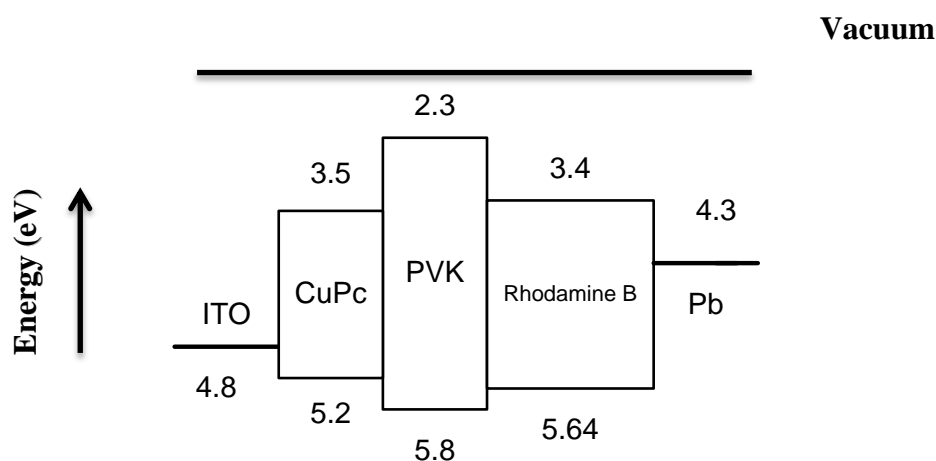


Fig. 4. 8. Energy level diagram for device consisting of ITO/CuPc/Rhodamine B dye/Pb.

As can be seen in Fig. 4.9, the threshold voltage decreases as the CuPc film thickness decreases. The reduction in threshold voltage can be attributed to a decrease in the hole-injection barriers (ΔE_h) between CuPc and anode. This is because the HOMO level of CuPc is near to the work function of the ITO anode. When the CuPc film is sandwiched between the PVK layer and ITO anode, a ladder effect makes it easier for holes to inject into the organic material which in turn leads to enhanced hole

injection. It was reported that the decrease in the overall barrier height to hole injection depends weakly on the CuPc film thickness, this result is agreement with referance [17].

Figures 4.10 illustrate the J-V characteristic curves for OLED devices with different CuPc layer thicknesses under forward bias. All figures show almost the same behavior of J as a function of V. The forward J-V curves have two regions, a low-current region with weak voltage dependence and a high-current region with a steeper current rise as a function of the voltage. Compared to the control device in which the threshold voltage was 7.8 V, it is obvious that the insertion of the CuPc layer reduces significantly the threshold voltage. For a thickness of 50 nm of the CuPc layer the threshold voltage is 7.4 V. The threshold voltages are 5.5 V and 1.4 V for devices with a CuPc layer thickness of 30 nm and 10 nm whereas it is about 1 volt for device with the 5 nm CuPc layer thickness.

On the other hand, it seems that the injected holes are the dominant charge carriers because the hole injection barrier is smaller than the electron injection barrier. Injection of electrons from the cathode into the organic layer is smaller compared to injection of holes from the anode into the organic layer (figure 4.8). This makes the device increasingly single carrier " hole-only". The current in the device is controlled, almost exclusively, by the holes [18].

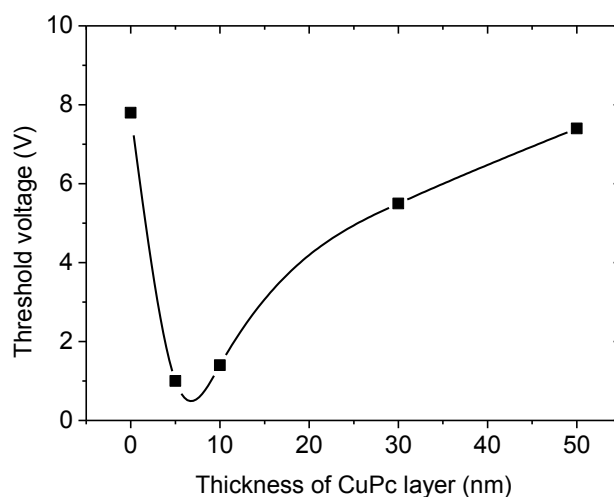


Fig. 4. 9. The threshold voltage versus thickness of CuPc layer.

The threshold voltages and maximum current densities for different CuPc film thickness devices are listed in Table 4.1. The maximum current density was recorded just before the device damage occurred.

It should be mentioned that no luminescence was detected in the devices containing CuPc as HIL layer. This may suggest that there is an easier route for electron injection other than that for the LUMO level of Rhodamine B dye. It is expected that using a polymer, with a low-lying LUMO, instead of the organic material could cause light emission because the threshold voltage of such a polymer light emitting diode should be smaller than that of OLED device.

Table 4. 1. V_{th} and maximum current densities for OLED devices with different CuPc layer thickness.

Thickness of CuPc(nm) layer	0	5	10	30	50
V_{th} (Volt)	7.80	1.00	1.40	5.50	7.40
J_{max} (mA/cm ²)	39.92	0.69	29.87	40.39	0.87

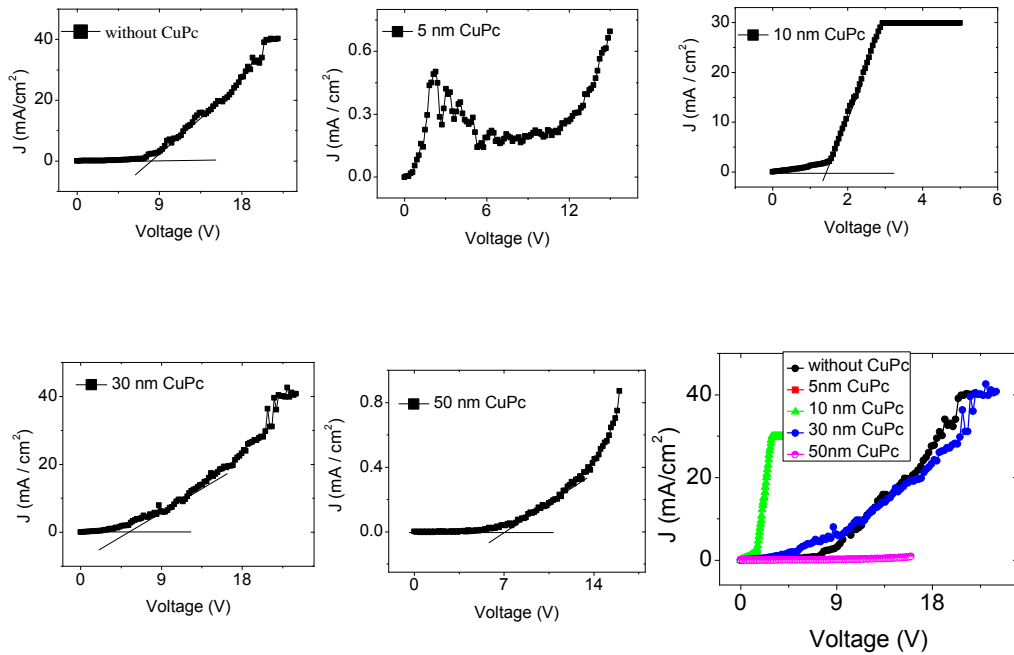


Fig. 4. 10. Current density- voltage characteristic curves of the device consisting of ITO/ (0, 5, 10, 30, and 50nm) CuPc / ~44.8nm PVK/ 30nm Rhodamine B/ 35nm Pb.

Moreover, it is worth mentioning that when the thickness of CuPc film is 5 nm, negative differential resistance (NDR) characteristics can be observed at a low voltage region as can be seen in Fig. 4.10. This phenomenon may be attributed to the diffusion of the PVK layer with the small thickness of CuPc.

Present understanding of NDR in molecular systems is not definitely clear. Several models have been found in the literature [19-24]. The mechanism proposed to explain the NDR behavior for the generation of guest hopping side (GHS) and phonon scattering phenomenon, as shown in Fig. 4.10. The applied voltage on the device is increased but the current through it decreases so that there is a negative resistance region between about 1.5-5.0 V. It is postulated that the generation of GHS is an important feature that causes the reduction in the effective barrier height where injection mechanism is enhanced.

On the other hand, the carrier mobility is rapidly reduced due to high intensity of phonon emission at high voltage, similar to the results of [24].

Figure 4.11 shows the dependence of the current density J on the voltage V in the natural logarithmic scale for OLED devices with different CuPc film thickness. These curves exhibit non-linear relationship and can be divided into two to four regions. These different regions have different slopes which referred the J-V relation (in the natural logarithmic scale) in the form $J \propto V^s$ where s is the slope of the curve. The region where the slope of $\ln J$ - $\ln V$ curves is equal about 1, the conduction is said to be ohmic mechanism. At the region where the slope equal 2, the conduction is space charge limited (SCL) mechanism [12]. Table 4.2 shows the experimental values of slopes for each region of these curves.

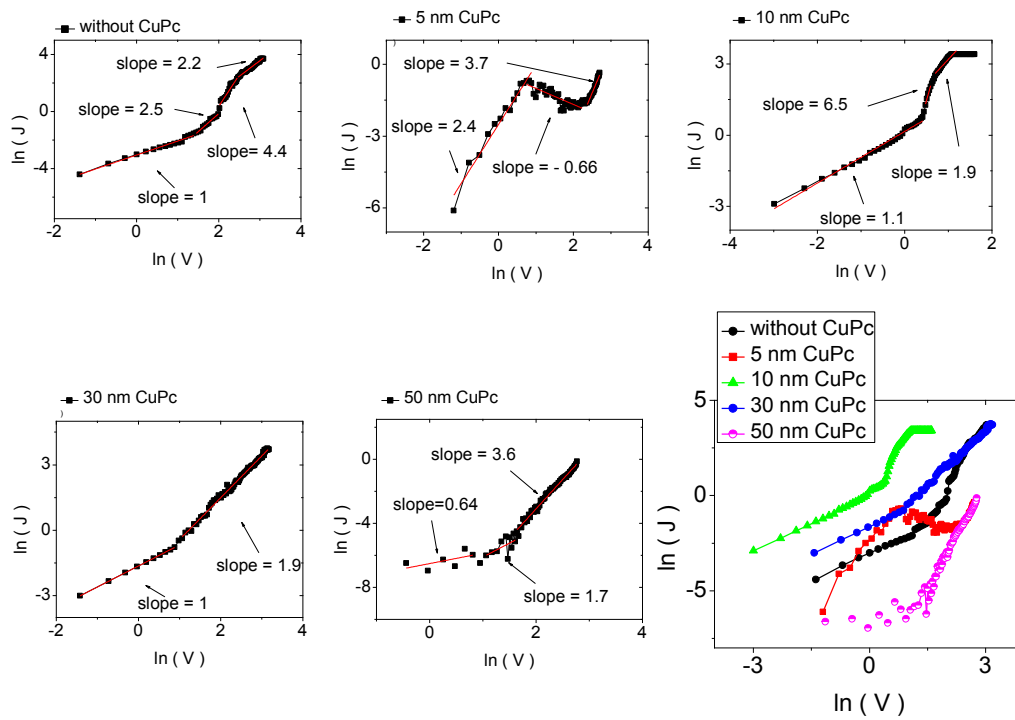


Fig. 4. 11. Current density-voltage characteristic curves of devices consisting of ITO/ (0, 5, 10, 30, and 50 nm) CuPc/44 nm PVK/30 nm Rhodamine B dye/35nm Pb in logarithmic scale.

Table 4. 2. Experimental values of slope for each region of $\ln J$ - $\ln V$ characteristic curves.

Thickness of CuPc (nm)	Slope(1)	Slope(2)	Slope(3)	Slope(4)
0	1.0	2.5	4.4	2.2
5	2.4	-0.66	3.7
10	1.1	6.5	1.9
30	1.0	1.9
50	0.64	1.7	3.6

4.4.2 Post-treatment

4.4.2.1 Heat treatment Only

The J-V and EL-V characteristics curves for OLEDs after thermal annealing at different temperatures of (90°C, 100°C, 110°C, and 120°C) were investigated. The heat treatment process was described in section 4.2.3. The J-V characteristic curves of the treated devices were recorded by Keithely 2602A source meter and are shown in Fig. 4.12 that represents the J-V characteristic curves for the heat treated OLEDs consisting of ITO/~44.88nm PVK/30nm Rhodamine B dye/35nm Pb. As can be seen from the figure, as the annealing temperature of PVK/Rhodamine B dye layer increases the threshold voltage increases except at 90°C, this result is similar to the result appeared in the reference [25, 26].

On the other hand, all devices treated by heating didn't emit light compared to the control device without any annealing. The annealing process may cause dye aggregation for this reason the luminance disappeared, this result is agreement with the reference [27]. Table 4.3 presents the threshold voltages and the maximum current densities of the treated devices at the different annealing temperatures.

The best annealing temperature was 110°C which corresponds to the highest current density. The maximum current density was measured just before the device damage.

Figure 4.13 shows the dependence of the current density J on the voltage V in the natural logarithmic scale for OLED devices treated at different temperatures.

These curves exhibit non-linear relationship and can be divided into two to five regions. These different regions have different slopes depending on different conduction mechanisms. The region where the slope of $\ln J$ - $\ln V$ curves is equal about 1, the region is called ohmic. At the region where the slope equal 2, the conduction is called space charge limited (SCL) mechanism [12].

Table 4.4 shows the experimental values of slopes for each region of current density-voltage for OLED devices treated at different temperatures.

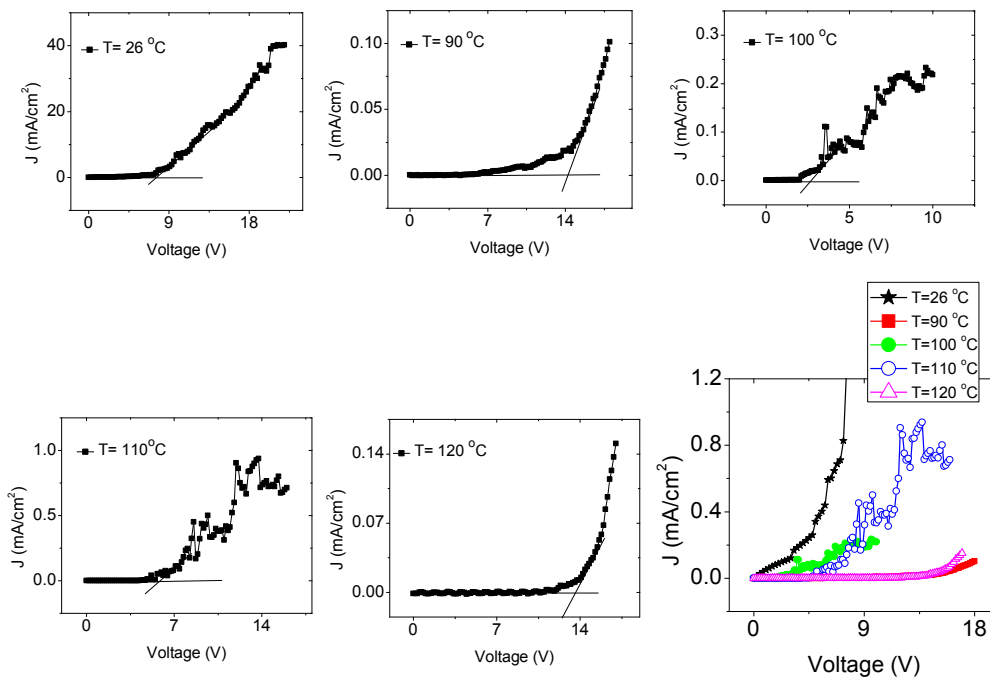


Fig. 4. 12. Current density-voltage characteristic curves of the heat-treated devices consisting of ITO/ \sim 44.88nmPVK/30nm Rhodamine B/35nm Pb at different annealing temperatures.

Table 4. 3. Threshold voltages and maximum current densities of the devices after heat treatment.

Temperatures	90°C	100°C	110°C	120°C	Control device
V_{th} (Volt)	14.26	2.53	5.53	13.60	7.80
J_{max} (mA/cm ²)	0.10	0.23	0.93	0.15	39.92

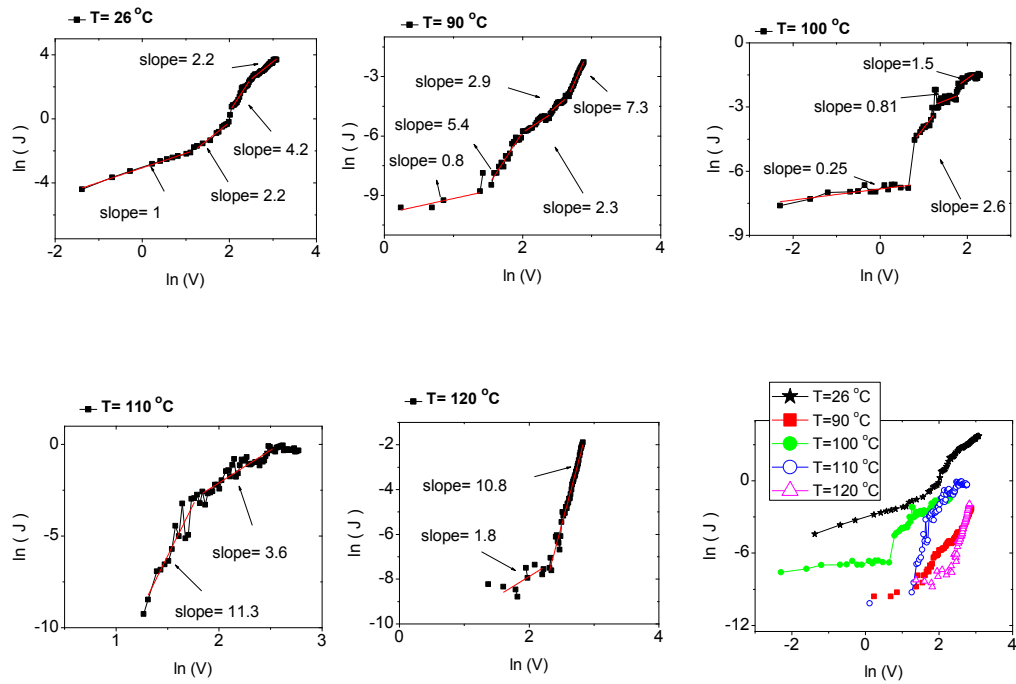


Fig. 4. 13. Current density-voltage characteristic curves of the heat-treated devices consisting of ITO/ $\sim 44.88\text{nm}$ PVK/ 30nm Rhodamine B/ 35nm Pb at different annealing temperatures in logarithmic scale.

Table 4. 4. Experimental values of slope for each region of $\ln J$ - $\ln V$ characteristic curves.

Temperatures	Slope(1)	Slope(2)	Slope(3)	Slope(4)	Slope (5)
26°C	1.00	2.50	4.40	2.20
90°C	0.80	5.40	2.30	2.90	7.30
100°C	0.25	2.60	0.81	1.50
110°C	11.30	3.60
120°C	1.80	10.80

4.4.2.2 Heat and Electric Field treatment

A set of samples were treated by applying an external field during heating as described earlier in section 4.2.3. The same voltage of 10 KV was applied at different annealing temperatures (90°C, 100°C, 110°C and 120°C).

The J-V characteristic curves of these samples are shown in Fig. 4.14. As can be seen from the figure, when the annealing temperature increases the threshold voltage decreases and the current flowing in the device is enhanced except at 110°C. For devices treated at temperatures of 90°C, 100°C, 110°C and 120°C, the threshold voltages were 11.87 V, 6.26 V, 5.38 V and 4.73 V, respectively. Table 4.5 presents the threshold voltages and maximum current densities of the devices treated by applying an electric field during the annealing process.

The improved threshold voltages of OLEDs with organic layers annealed at elevated temperature could be attributed to the reduced defects and improved the interface structures of organic and organic/ITO interfaces, similar to the results of [27].

Figure 4.15 shows the dependence of the current density J on the voltage V in the natural logarithmic scale for OLED devices treated at different temperatures. These curves exhibit non-linear relationship and can be divided into three to five regions. These different regions have different slopes which referred to the J-V relation (in the natural logarithmic scale) in type $J \propto V^s$ where s is the slope of the line segment. The experimental values of slopes for each region are recorded in Table 4.6.

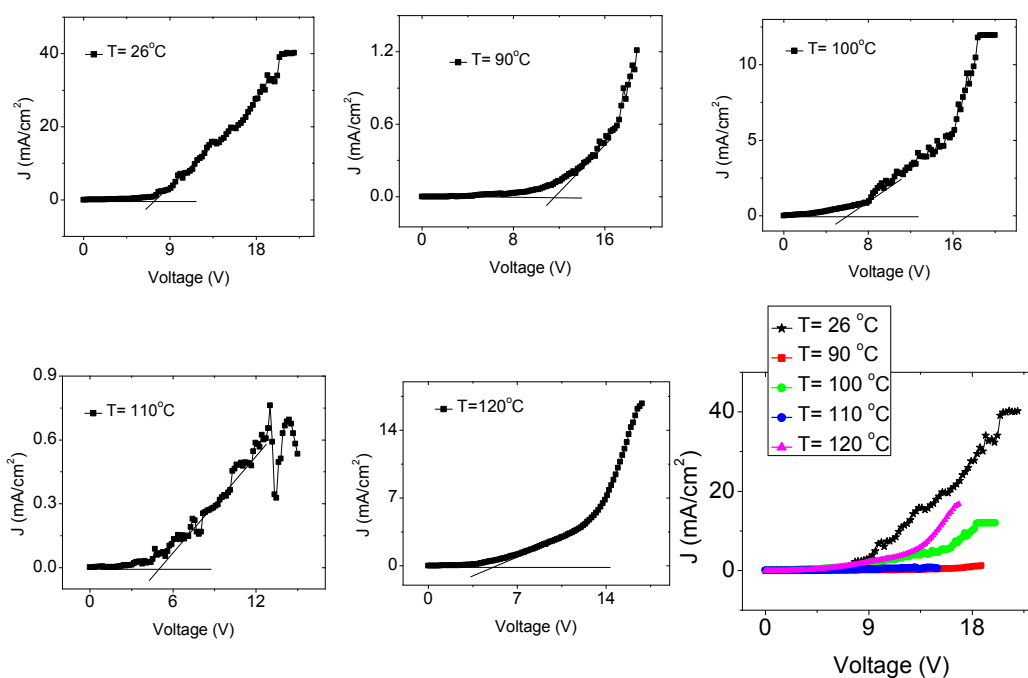


Fig. 4. 14. Current density-voltage characteristic curves of the OLEDs consisting of ITO/ \sim 44.8nmPVK/30nm Rhodamine B dye/35nm Pb treated with an external electric field during heating.

Table 4. 5. Threshold voltages and maximum current densities of devices treated by an external electric field during annealing.

Temperature	90 °C	100 °C	110 °C	120 °C	Control device
V_{th} (Volt)	11.87	6.26	5.38	4.73	7.80
J_{max} (mA/cm ²)	1.20	11.94	0.76	16.74	39.92

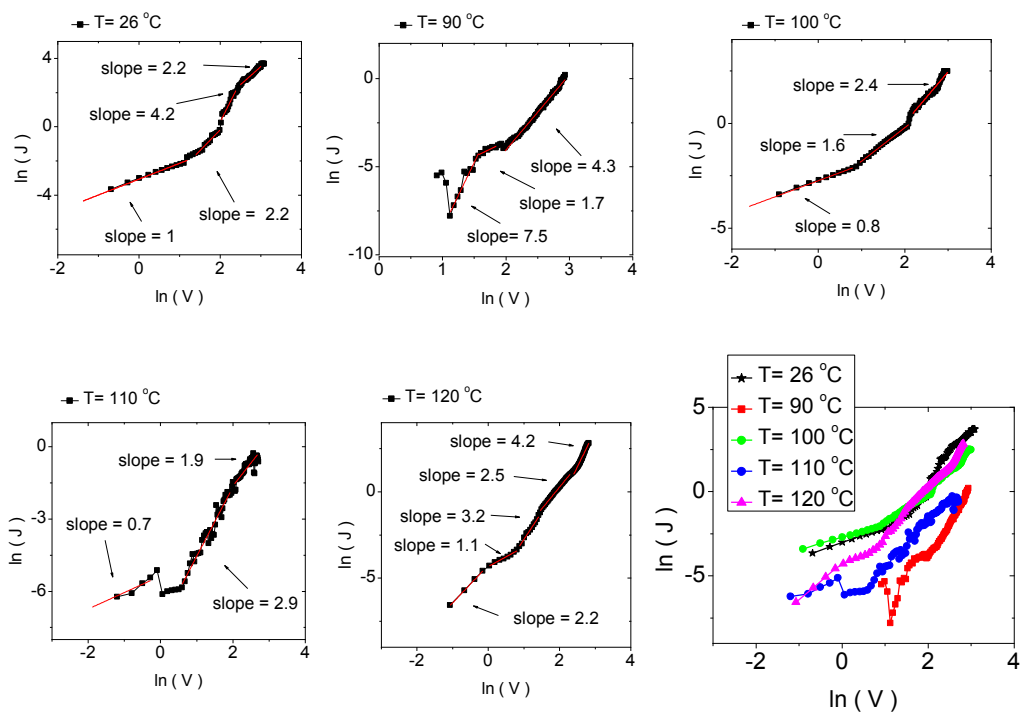


Fig. 4. 15. Current density-voltage characteristic curves of the OLEDs consisting of ITO/ \sim 44.88nmPVK/30nm Rhodamine B dye/35nm Pb treated with an external electric field during heating in logarithmic scale.

Table 4. 6. Experimental values of slope for each region of $\ln J$ - $\ln V$ characteristic curves.

Temperatures	Slope(1)	Slope(2)	Slope(3)	Slope(4)	Slope (5)
26 °C	1.00	2.50	4.40	2.20
90 °C	7.50	1.70	4.30
100 °C	0.80	1.60	2.40
110 °C	0.70	2.90	1.90
120 °C	2.20	1.10	3.20	2.50	4.20

On the other hand, all devices treated by applying an external field during heating didn't emit light compared to the control device without any annealing. This can be attributed to the dye aggregation caused by the field-heat treatment as shown in Fig. 4.16.

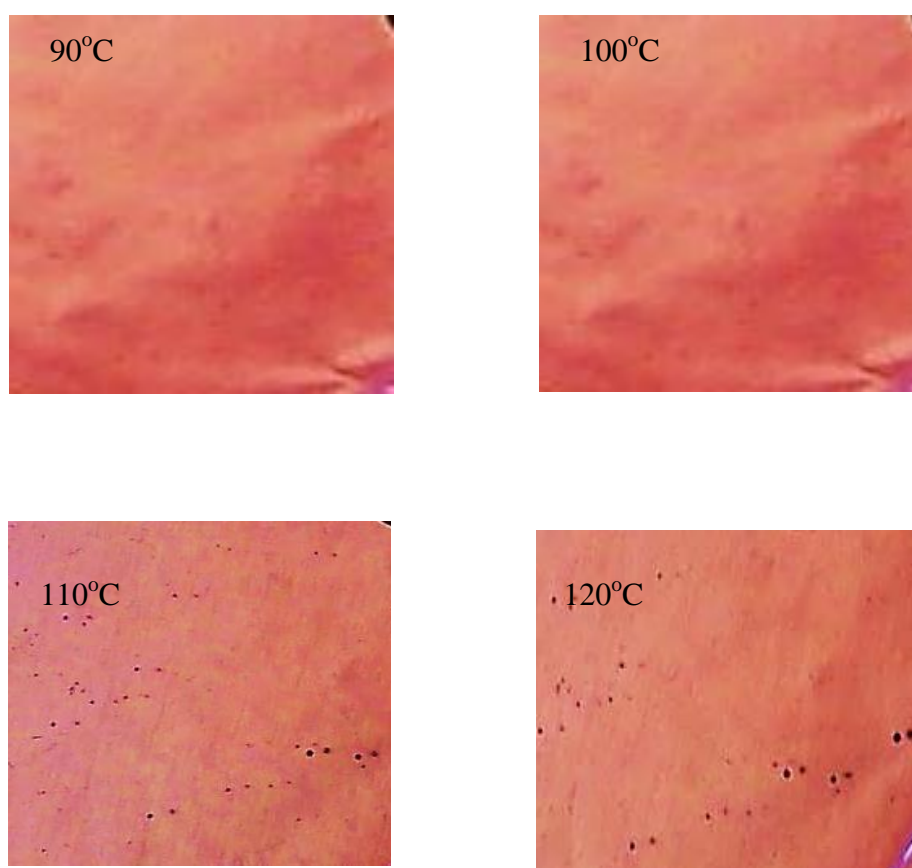


Fig. 4. 16. Photos of the samples treated by electric field at temperature 90°C, 100°C, 110°C and 120°C.

To investigate the influence of E-field on the performance of the devices, the J-V curves were plotted at the same temperature for each case. The results obtained for OLEDs treated with applying an electric field during the annealing process revealed that there was a significant reduction in the threshold voltage and a considerable current enhancement compared to the samples treated with only annealing without any electric field as can be seen in Fig. 4.17.

The threshold voltages and maximum current densities of the devices thermally annealed with and without an electric field are presented in Table 4.7. Moreover, the table shows the values obtained for the fabricated devices without any treatment. It should be pointed out that the maximum current density was recorded just before the device damage.

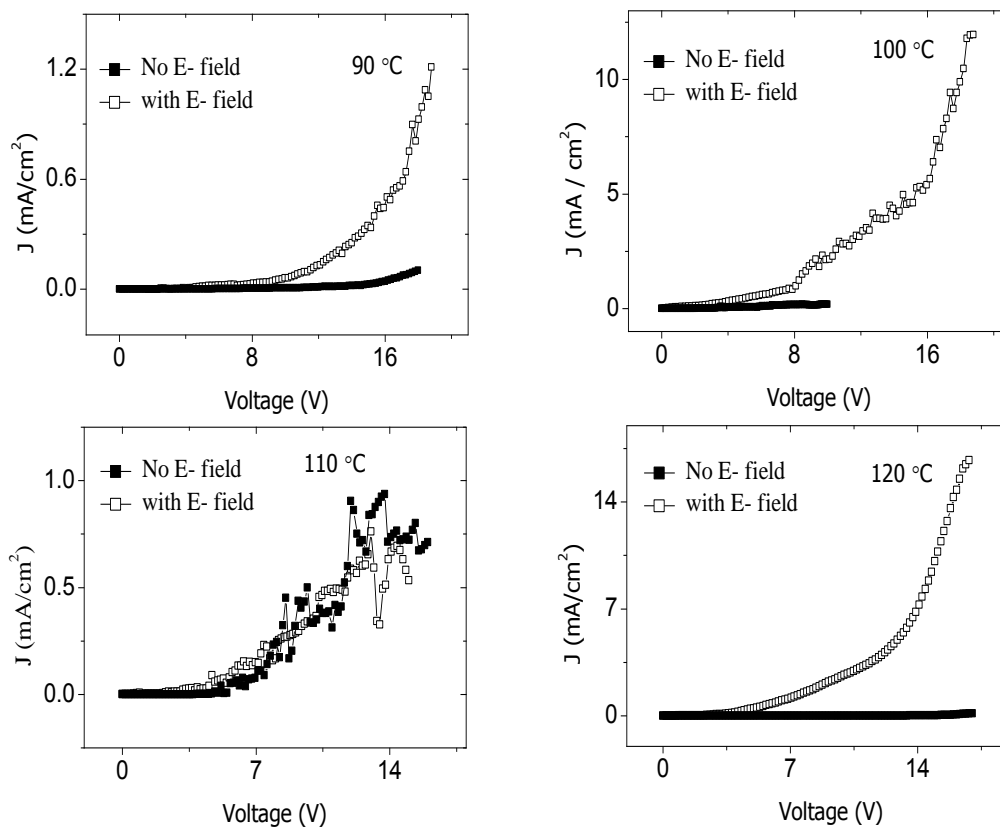


Fig. 4. 17. Current density-voltage characteristic curves of the OLEDs thermally treated with and without an electric field.

Table 4. 7. Threshold voltages and maximum current densities for OLEDs treated by heating with and without an electric field.

Temperature	Heat treatment				Heat-external E-field treatment				Control device
	90°C	100°C	110°C	120°C	90°C	100°C	110°C	120°C	
V_{th} (Volt)	14.26	2.53	5.53	13.60	11.87	6.26	5.38	4.73	7.80
J_{max} (mA/cm ²)	0.10	0.23	0.93	0.15	1.20	11.94	0.76	16.74	39.92

CHAPTER 5

IMPEDANCE SPECTROSCOPY OF OLEDs

5.1 INTRODUCTION

Current density-Voltage-Electroluminescence (J-V-EL) measurements can be used to determine threshold voltage (V_{th}), maximum current density, and the turn-on voltage (V_{on}) at which an OLED emits light. Impedance spectroscopy (IS) measurements can be used to present useful information about OLEDs, like capacitance-voltage (C-V) of the device for different applied bias voltages V_{DC} whereas the C-V curves give more information about the physical processes in OLEDs like the voltages at which holes and electrons start injection into organic OLED layers from the electrodes, moreover the voltage V_{on} which OLEDs start to emit light, equivalent circuit models, and Bode Plots.

5.2 IMPEDANCE SPECTROSCOPY

Impedance spectroscopy (IS) is a powerful method for studying the electrical properties of materials and their interfaces. It can be employed to investigate the dynamics of bound or mobile charges in the bulk or the interfacial regions, with the great advantage of being a non-destructive method. In literature, IS has also been successfully applied to a variety of issues for organic electronic devices [28].

In an IS experiment, a small, alternating electrical signal $V_{AC}(t) = V_{AC} \cos(2\pi f \cdot t)$ with small amplitude V_{AC} and frequency f is applied to the sample in addition to a constant bias voltage V_{DC} , resulting in a total applied voltage of

$$V(t) = V_{DC} + V_{AC}(t) = V_{DC} + V_{AC} \cos(2\pi f \cdot t) \quad (5.1)$$

The response of the sample, the current $I(t)$ is also a result of the combined DC (I_{DC}) and AC (I_{AC}) response, where

$$I_{AC}(t) = I_{AC} \cos(2\pi f \cdot t + \varphi) \quad , \quad (5.2)$$

where φ is the phase shift between voltage and current. V_{DC} serves as a handle to change the working point on the current-voltage characteristics of the sample. The complex impedance $\hat{Z}(f)$ is defined as the ratio of applied alternating voltage and the current response. In complex notation

$$V = V_{AC} \exp(i \cdot 2\pi f \cdot t), \quad (5.3)$$

$$\hat{I} = I_{AC} \exp(i \cdot (2\pi f \cdot t + \varphi)), \quad (5.4)$$

$$\hat{Z} = \frac{V}{\hat{I}} = \frac{V_{AC}}{I_{AC}} \exp(-i \varphi) = \text{Re}(\hat{Z}) + i \text{Im}(\hat{Z}). \quad (5.5)$$

The modulus $|\hat{Z}|$ and the phase shift are therefore given by

$$|\hat{Z}| = \sqrt{(\text{Re}(\hat{Z}))^2 + (\text{Im}(\hat{Z}))^2} \quad , \quad (5.6)$$

$$\varphi = \arctan\left(\frac{\text{Im}(\hat{Z})}{\text{Re}(\hat{Z})}\right). \quad (5.7)$$

There are different equivalent representations of the complex impedance, however, the most intuitive one for semiconductor devices is the capacitance C , defined as

$$C(f) = \frac{1}{2\pi f} \frac{-\text{Im}(\hat{Z})}{(\text{Re}(\hat{Z}))^2 + (\text{Im}(\hat{Z}))^2} \quad , \quad (5.8)$$

In this work, different curves were measured using IS technique such as, modulus-frequency ($Z-f$) and capacitance-voltage (C-V) curves. Equivalent circuits of the devices were used to explain charge injection / transport and an interfacial charge in the fabricated OLEDs.

5.3 CAPACITANCE-VOLTAGE CHARACTERIZATION

The capacitance-voltage characteristics of OLEDs can be used to know and determine the onset of majority and minority charge carrier injection into the active organic layer from the electrodes. Fig. 5.1 shows a typical C-V curve for an OLED and four distinct regions are marked in the figure corresponding to neutral regime, dark current regime, majority charge-injection regime, and charge recombination regime.

The voltage V_1 is the bias voltage at which the majority charge injection into the organic starts in forward bias and sometime called transition voltage (V_T) [29]. Below this voltage the organic is neutral with a very small amount of charge trapped in the defect sites near the interface. The organic layer can be thought of as composed of small charge regions near the interface and large neutral region elsewhere [29].

Above V_1 , a sharp capacitance increase is observed corresponding to the majority charge injection. The voltage V_2 corresponds to the device turn-on voltage, at which the light emission from the organic begins and marks a sharp decline in the value of the measured capacitance of the device [29]. The voltage V_2 or sometime called built-in voltage (V_{bi}) is the bias voltage at which the minority charge starts injection into the organic layer.

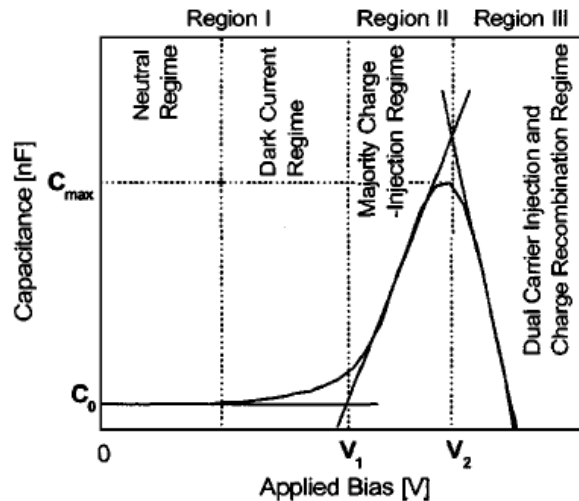


Fig. 5. 1. A typical C-V curve for an OLED device under forward applied bias [29].

5.3.1 Influence of CuPc thin layer on C-V curves

The CuPc layer as hole transport layer was deposited on the ITO substrate using thermal vacuum evaporation technique to form ITO/CuPc/PVK/Rhodamine B dye/Pb device. Four different CuPc layer thicknesses were used with each PVK/Rhodamine B dye/Pb device. The effect of the CuPc layer was studied and the transition voltage at which holes are injected to the device and built-in voltage at which electrons are injected to the device were investigated in details with CuPc layer thickness.

Figure 5.2 shows the capacitance-voltage curve for the control device with the structure of ITO/~44.88nm PVK/30nm Rhodamine B dye/35nm Pb. It is clear that the C-V characteristic curve shows minor and major peaks which refers to the injection of charges into the device. At the minor peak, the capacitance increases at transition voltage V_{T1} which approximately at 7.0 V due to the injection of holes, where at voltage of about 7.7 V which called the built-in voltage V_{bi1} some electrons can be injected, then decreases until the transition voltage of the major peak. For a major peak, holes are injected into the PVK layer at transition voltage $V_{T2}= 8.6$ V.

At $V_{bi2} = 9.7$ V, electrons are injected from the cathode into the device. As a result, electrons and holes recombine to generate the light and the charge is annihilated.

Figure 5.3 illustrates the C-V curves for devices with the structure of ITO/different thickness of CuPc/ \sim 44.88nm PVK/30nm Rhodamine B dye/35nm Pb. For a thickness of 5nm of the CuPc layer the transition voltages V_{T1} and V_{T2} at which holes are injected to the CuPc layer are 10.4 V, 12.2 V, respectively.

On the other hand, the built-in voltages V_{bi1} , V_{bi2} at which electrons are injected into the device are 11.0 V and 13.0 V, respectively. For a thickness of 10 nm of CuPc the V_{T1} , and V_{T2} are 1.3 V and 4.2 V, respectively, the V_{bi1} , and V_{bi2} are 1.9 V and 6.8 V respectively. In the case of 30nm CuPc, the voltage at which holes can be injected with increasing the potential V_{T1} , and V_{T2} are at 5.5 V, 12.0 V, respectively. On the other hand, at $V_{bi1} = 7.5$ V and $V_{bi2} = 13.4$ V the electrons can be injected into the device. Finally, for a thickness of 50nm of the CuPc layer the transition voltages V_{T1} and V_{T2} are 11.5 V, 14.5 V, respectively, and the built-in voltages V_{bi1} , V_{bi2} are 13.6 V and 15.4 V, respectively. As the thickness of CuPc decreases the V_T and V_{bi} decrease as shown in Table 5.1, except for a thickness 5 nm which shows negative differential resistance (NDR).

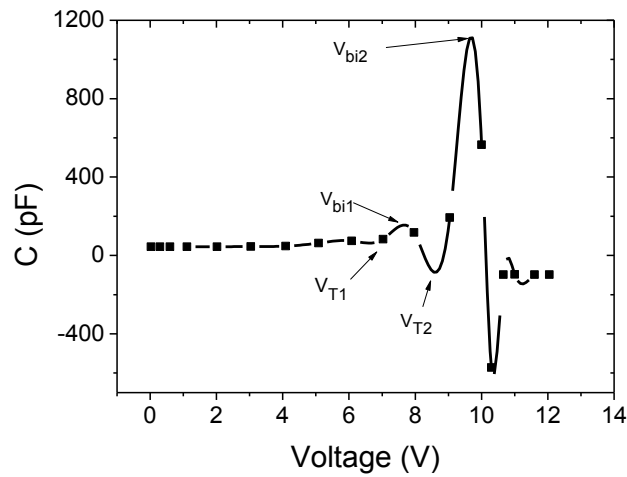


Fig. 5. 2. Capacitance- voltage characteristic curve of the standard device consisting of ITO/ ~44.88nm PVK/ 30nm Rhodamine B/ 35nm Pb.

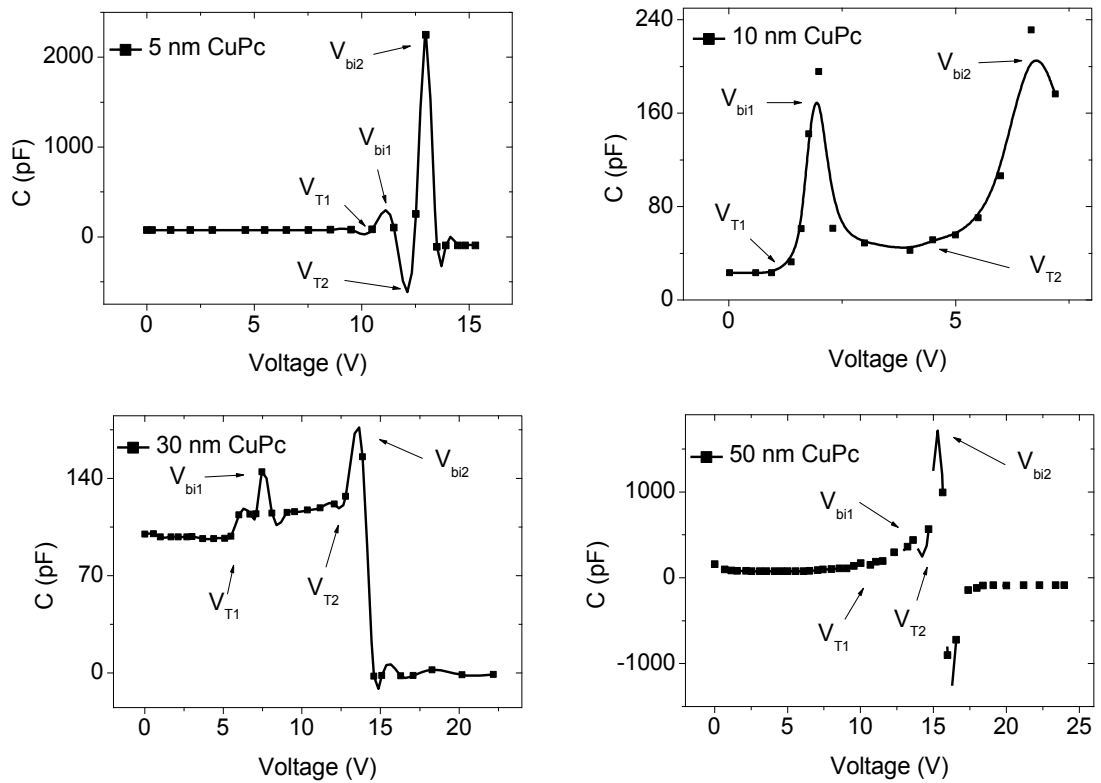


Fig. 5. 3. Capacitance- voltage characteristic curves of the device consisting of ITO/(5, 10, 30, and 50 nm) CuPc/ ~44.88nm PVK/ 30nm Rhodamine B / 35nm Pb.

Table 5. 1. The transition and built-in voltages for different CuPc layer thickness.

Thickness of CuPc (nm)	0	5	10	30	50
V_{T1}	7.0	10.4	1.3	5.5	11.5
V_{T2}	8.6	12.2	4.2	12.0	14.5
V_{bi1}	7.7	11.0	1.9	7.5	13.6
V_{bi2}	9.7	13.0	6.8	13.4	15.4

5.3.2 Heat treatment

In heat treatment process, the PVK/Rhodamine B layers were heated at different temperatures. In this subsection, the influence of heat treatment on transition and built-in voltages are studied.

Figure 5.4. shows the C-V curves for the devices treated at different temperatures. As can be seen from the figure, minor and major peaks appear in the C-V curves which indicates that the flow of charges through the devices occurs in several stages. If the bias becomes larger than a transition voltages V_{T1} , V_{T2} holes are injected into the device, raising the capacitance. Increasing the bias voltage further resulted in increasing the capacitance due to accumulation of charges at the barriers until it reaches the built-in voltages V_{bi1} , V_{bi2} which indicate the beginning of bipolar charge carrier injection, for even higher bias the capacitance decreases because holes and electrons are recombined. As the temperature increases, the transition and built-in voltages increase as shown in Table 5.2 except at temperature 100°C.

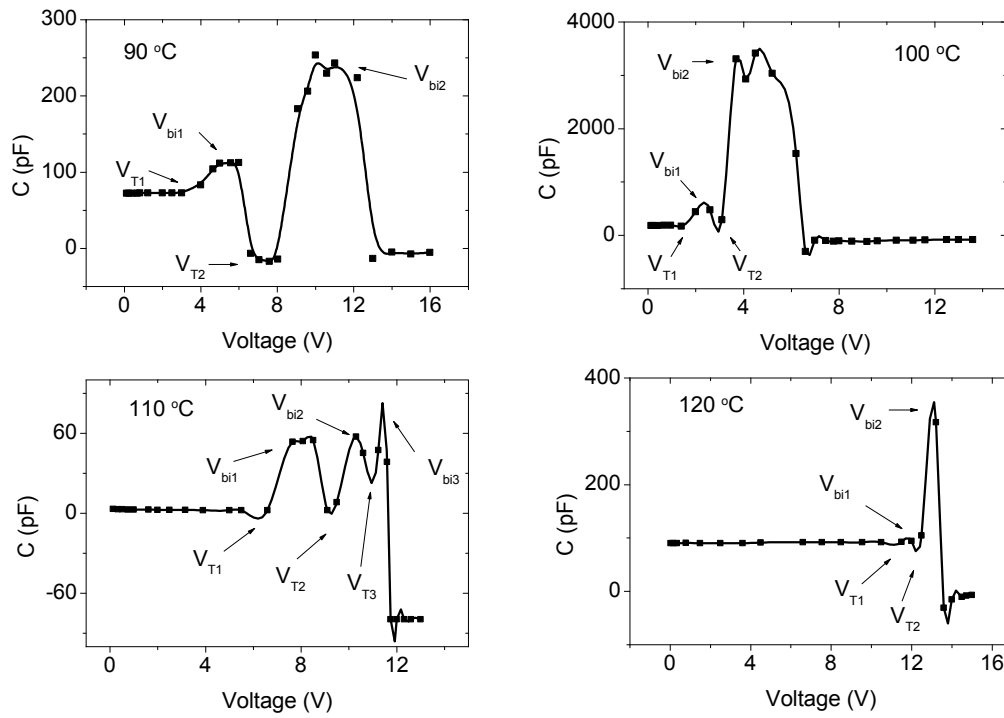


Fig. 5. 4. Capacitance-voltage curves for the devices consisting of ITO/ \sim 44.88nm PVK/30nm Rhodamine B dye/35nm Pb at different annealing temperatures.

Table 5. 2. The transition and built-in voltages for different annealing temperature.

Temperature	90°C	100°C	110°C	120°C
V_{T1}	3.0	1.5	6.6	11.5
V_{T2}	8.0	3.0	9.3	12.3
V_{T3}	11.0
V_{bi1}	5.5	2.3	8.0	11.7
V_{bi2}	11.0	4.6	10.3	13.0
V_{bi3}	11.5

5.3.3 External electric field-heat treatment

Some samples were exposed to an external electric field during thermal treatment as described in chapter 4. The voltage V_T and V_{bi} for each sample were determined. Figure 5.5 shows the capacitance-voltage curves for the devices exposed to the electric field during thermal annealing. It is clear that the C-V curves show minor and major peaks, which indicate the injection of charges into the device. Table 5.3. presents the values of transition and build-in voltages for all devices.

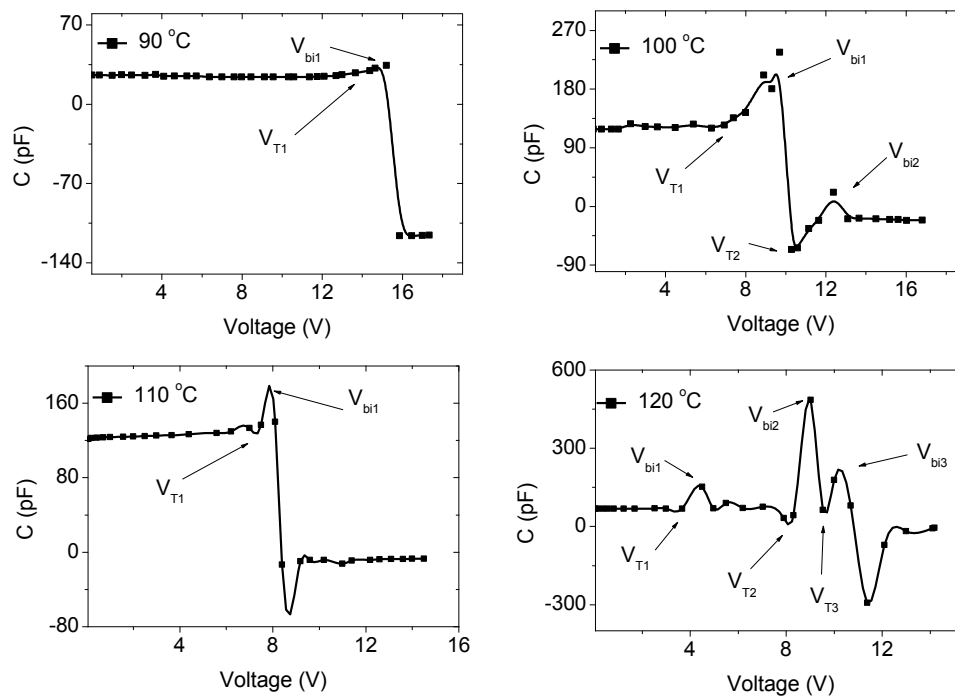


Fig. 5. 5. Capacitance-voltage curves for the devices consisting of ITO /~44.88nm PVK /30nm Rhodamine B dye/35nm Pb which were treated by external electric field at different temperatures.

Table 5. 3.The transition and build-in voltages for the devices treated by an external electric field during thermal annealing.

Temperature	90°C	100°C	110°C	120°C
V _{T1}	13.2	7.0	7.3	3.7
V _{T2}	10.5	8.2
V _{T3}	9.6
V _{bi1}	14.8	9.4	7.8	4.3
V _{bi2}	12.5	8.9
V _{bi3}	10.2

5.3.4 Comparison between heat treatment with and without an electric field

In Fig. 5.6 values of the capacitance of the devices treated by an E-field at temperatures of 90°C and 100°C were smaller than those of the devices treated by thermal annealing only at the same temperatures. But devices treated by an E-field at temperatures of 110°C and 120°C are found to have capacitance larger than that of the devices treated by thermal annealing only at the same temperatures as shown in Fig. 5.6.

It is expected that the electric field at temperatures of 110°C and 120°C attracts the dye from the edges of the device to the center, then the thickness was increases at the center as shown in Figs. 4.15 and 5.7. Figure 5.7 shows the reflected beam received from the sample center and the two edges which was treated at temperature 110°C as a function of wavelength.

It is well know that when the device thickness increases, the capacitance decreases according to

$$C = \epsilon_k A/d, \quad (5.9)$$

where ϵ_k is the permittivity of the material, A is the area of capacitor plate and d the is distance between the two plates.

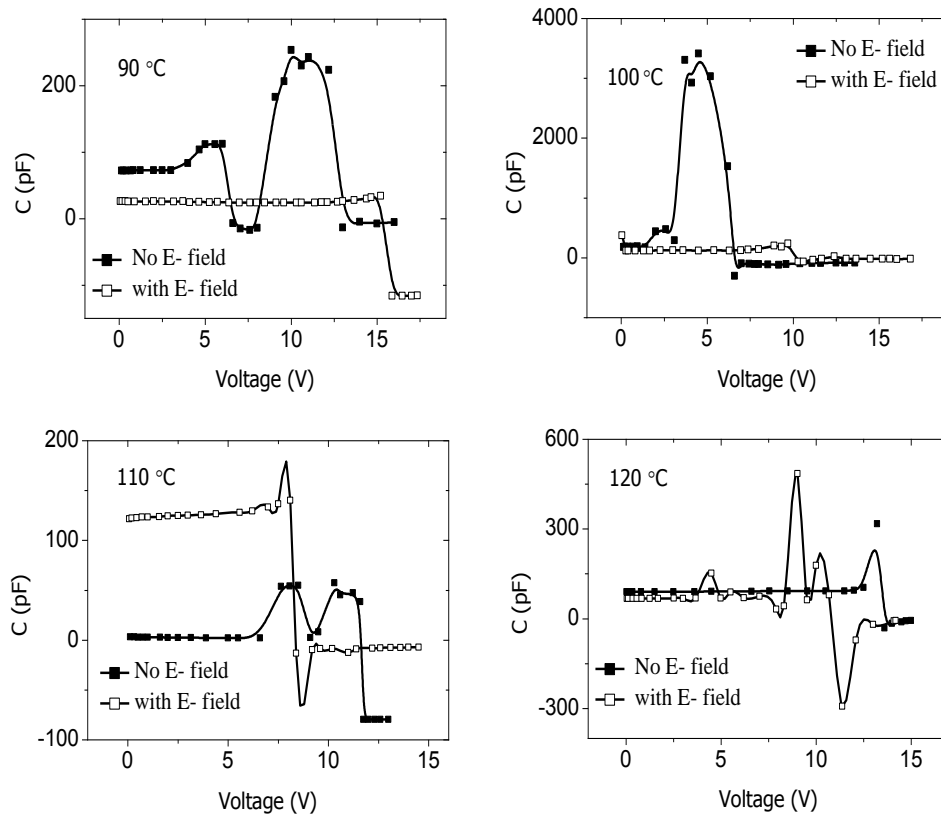


Fig. 5. 6. Capacitance-voltage curves for devices consisting of ITO/ \sim 44.88nm PVK/30nm Rhodamine B dye/Pb treated by heat and electric field.

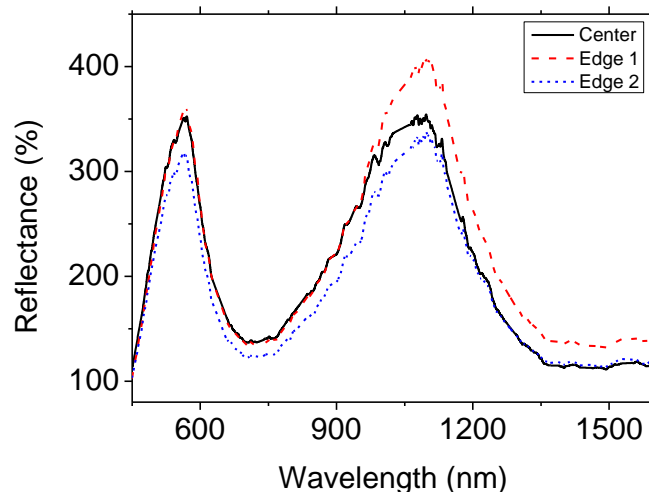


Fig. 5. 7. The reflected beam received from the sample center and the two edges which was treated at temperature 110°C as a function of wavelength.

5.3.5 Comparison between (J-V) and (C-V)

The J-V curves usually provide very limited information about the physical processes in OLEDs whereas the C-V curves give more information about the physical processes in OLEDs like the transition, built-in voltage, and the turn-on voltage (V_{on}), which OLEDs start to emit light.

Figure 5.8 show the current density-capacitance curve (a) and relative light intensity-capacitance curve (b) as a function of the applied forward bias for the control device without any treatment or addition CuPc layer. At a positive bias of approximately $V_{bi}= 7.7$ V, the current density drastically increases. This increment in current density is due to injection holes and electrons into the device. On the other hand, the light emission is observed at the same value of the applied potential at which the capacitance starts decreasing due to the recombination of holes and electrons, annihilating charges. Sometime the experimental quantities for V_{on} voltage can be changed to the V_{th} and V_{bi} voltages by some tenths of a volt as clearly in Fig. 5.8 (a) and (b), similar to the results of [28].

Figures 5.9 through 5.12 show the devices having the structure ITO/(5nm, 10nm, 30nm, and 50nm) CuPc/ PVK/ Rhodamine B/Pb, respectively. As it can be seen in the figures, when the current density begins to increase in J-V curves, the capacitance also increases in C-V curves at the same voltage approximately. On the other hand, when the thickness of CuPc decreases the V_T and V_{bi} decrease.

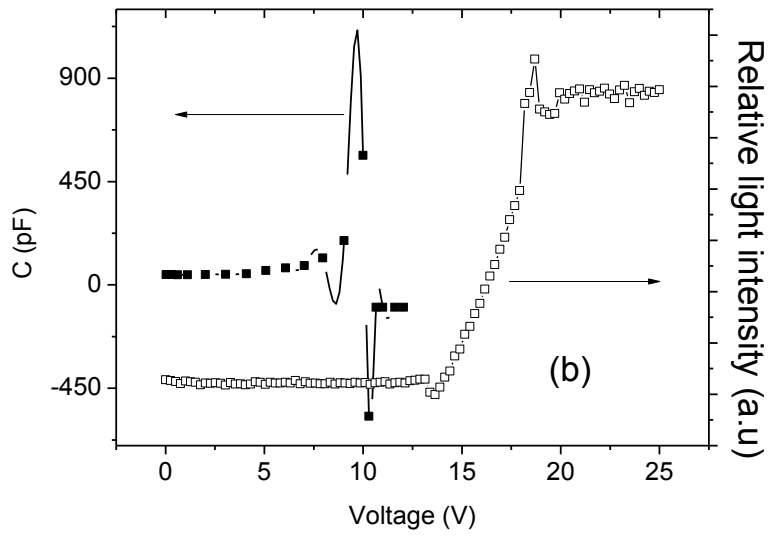
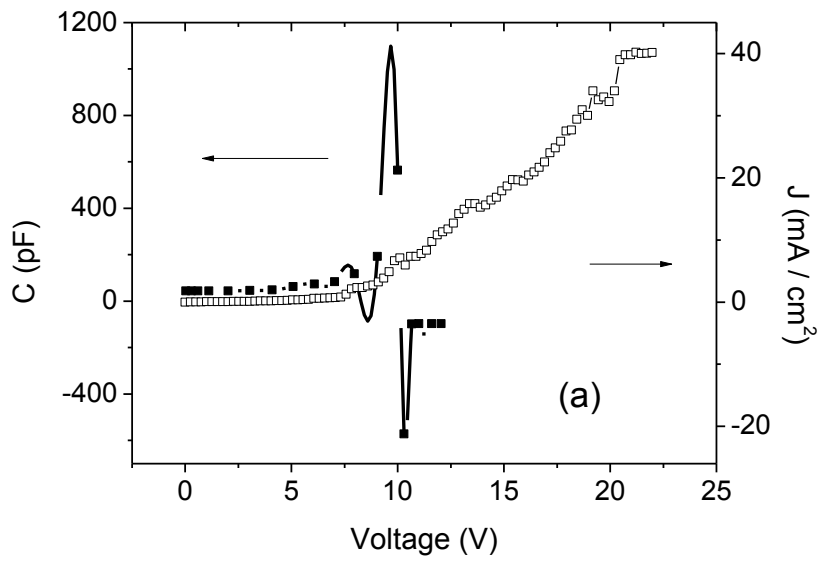


Fig. 5. 8. Current density-capacitance curve (a) and relative light intensity-capacitance curve (b) as a function of the applied forward bias for ITO/ \sim 44.88nm PVK/30nm Rhodamine B/35nm Pb device.

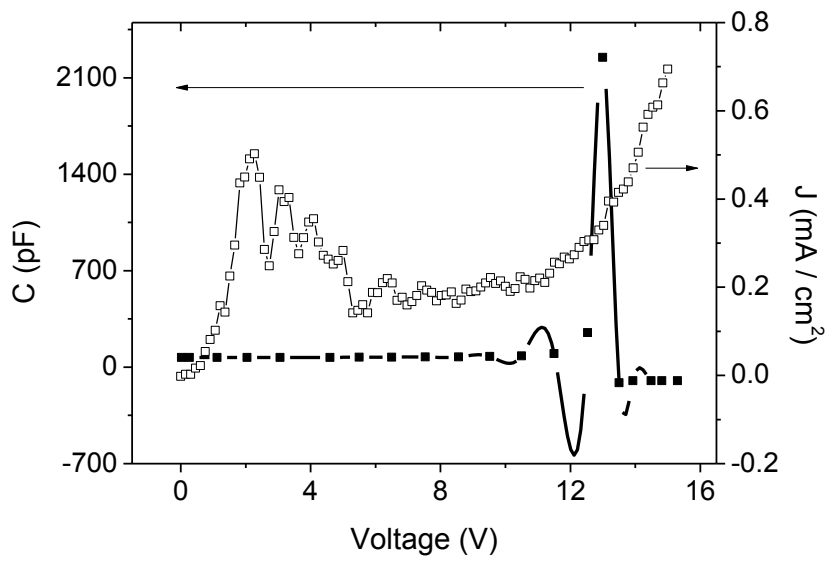


Fig. 5. 9. Current density-capacitance curves as a function of the applied forward bias for the device consisting of ITO/ 5nm CuPc/ ~44.88nm PVK/ 30nm Rhodamine B dye/ 35nm Pb.

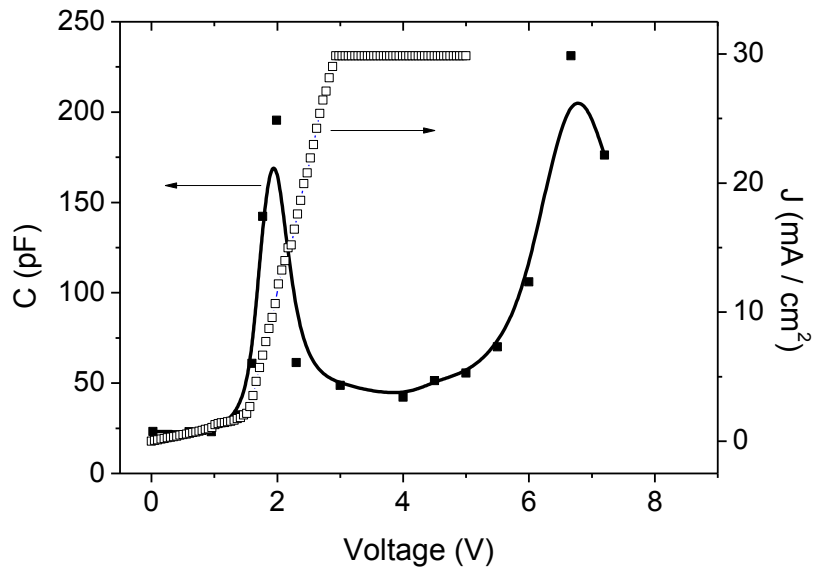


Fig. 5. 10. Current density-capacitance curves as a function of the applied forward bias for the device consisting of ITO/ 10nm CuPc/ ~44.88nm PVK/ 30nm Rhodamine B dye/ 35nm Pb.

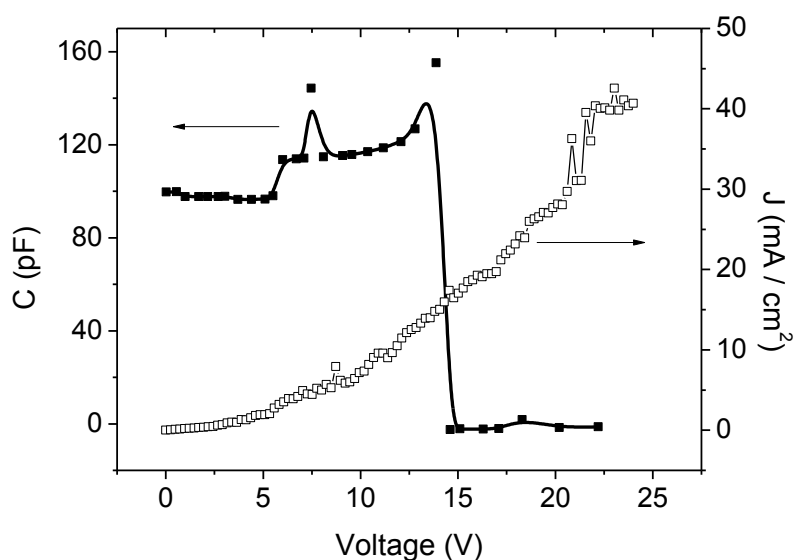


Fig. 5. 11. Current density-capacitance curves as a function of the applied forward bias for the device consisting of ITO/ 30nm CuPc/ ~44.88nm PVK/ 30nm Rhodamine B dye/ 35nm Pb.

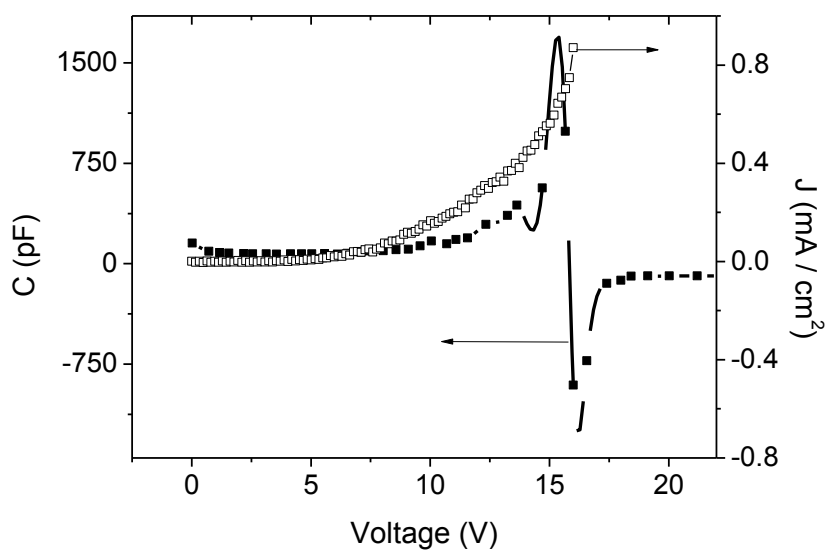


Fig. 5. 12. Current density-capacitance curves as a function of the applied forward bias for the device consisting of ITO/ 50nm CuPc/ ~44.88nm PVK/ 30nm Rhodamine B/ 35nm Pb.

Figures 5.13 through 5.16 show the current density-capacitance curves as a function of the applied forward bias for the devices treated at different temperatures with the structure of ITO/PVK/Rhodamine B/Pb.

Figures 5.17 through 5.20 show the current density-capacitance curves as a function of the applied forward bias for the devices exposed to the electric field during thermal annealing. As shown in the figures from 5.8 through 5.20, at V_T in C-V curves at which the major charges are injected into the devices, the current density begins to increase in the J-V curves. At built-in voltage in C-V curves the minor charges injected from the electrode into the device. With increasing the potential, the capacitance of the devices decreases rapidly as holes and electrons recombine to each other.

On the other hand, the current density drastically increases because more holes and electrons are injected into the devices from the two electrodes.

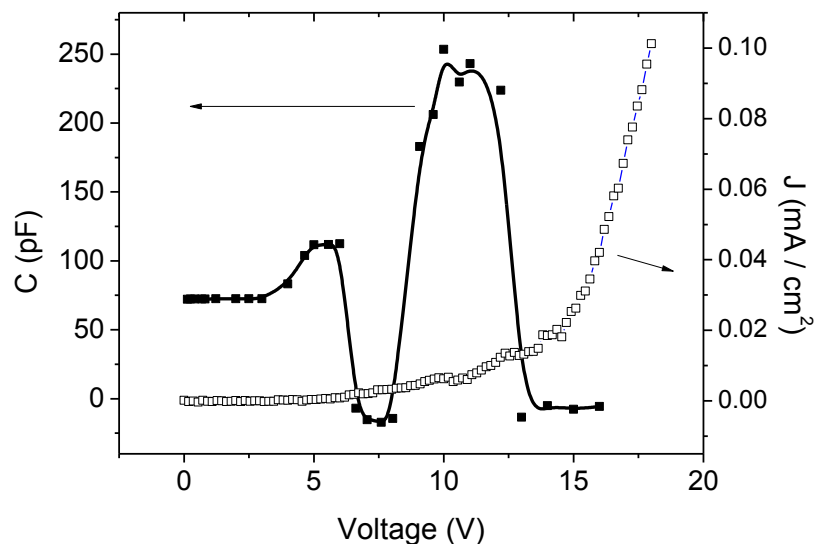


Fig. 5. 13. Current density-capacitance curves as a function of the applied forward bias for the device consisting of ITO/ ~44.88nm PVK/ 30nm Rhodamine B dye/35nm Pb, was treated at 90 °C.

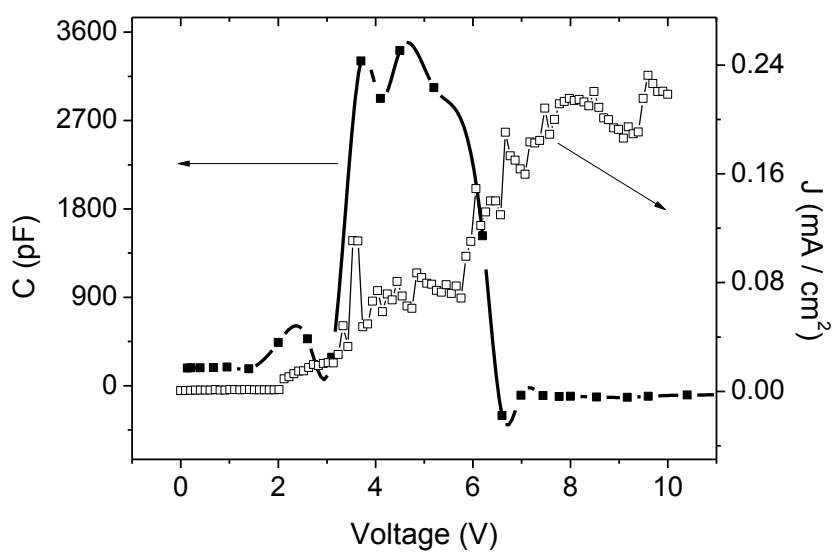


Fig. 5. 14. Current density-capacitance curves as a function of the applied forward bias for the device consisting of ITO/ ~44.88nm PVK/ 30nm Rhodamine B dye/35nm Pb was treated at 100 °C.

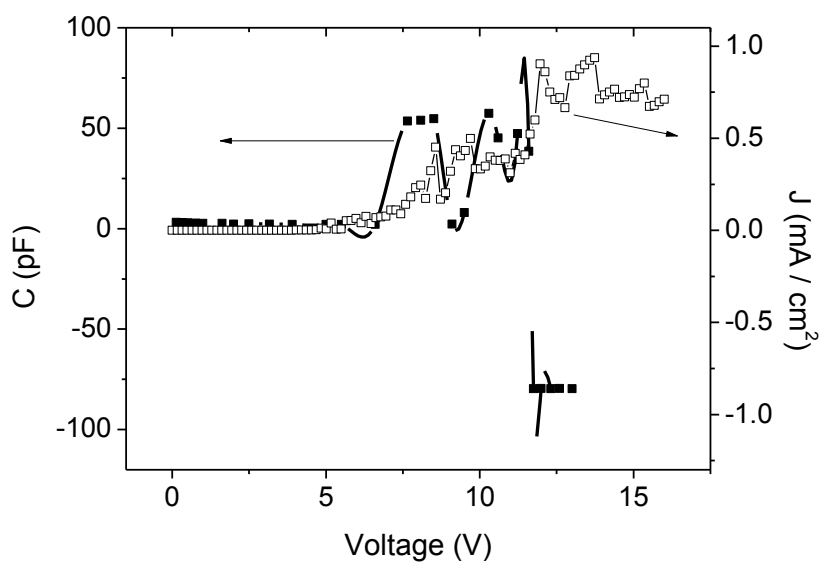


Fig. 5. 15. Current density-capacitance curves as a function of the applied forward bias for the device consisting of ITO/ ~44.88nm PVK/ 30nm Rhodamine B dye/35nm Pb was treated at 110°C.

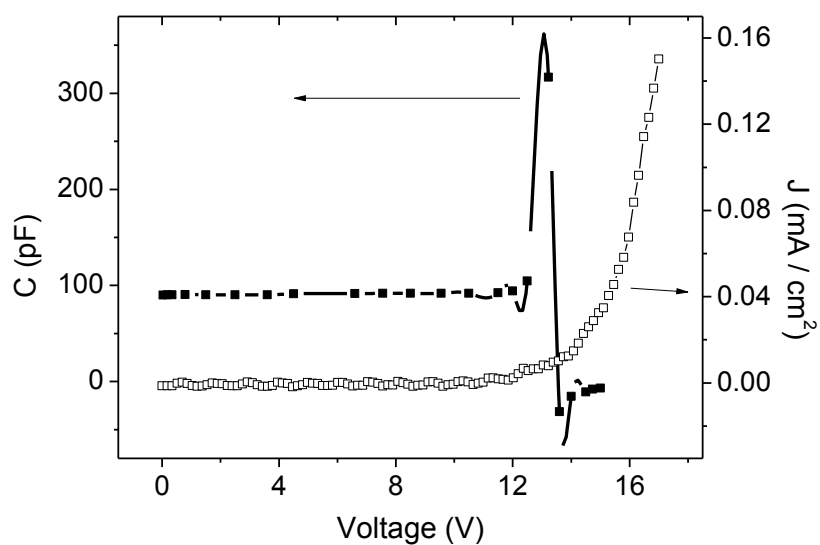


Fig. 5. 16. Current density-capacitance curves as a function of the applied forward bias for the device consisting of ITO/ ~44.88nm PVK/ 30nm Rhodamine B dye/35nm Pb was treated at 120°C.

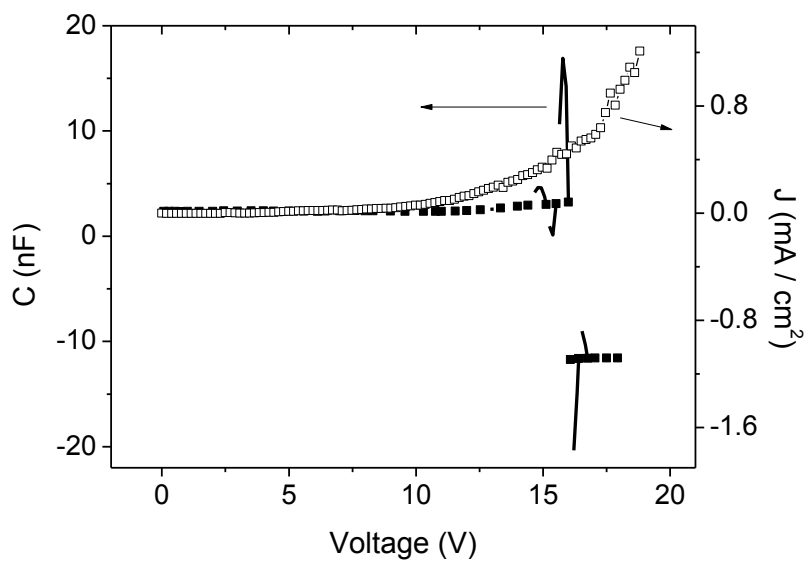


Fig. 5. 17. Current density-capacitance curves as a function of the applied forward bias for the device consisting of ITO/ ~44.88nm PVK/ 30nm Rhodamine B dye/35nm Pb which was treated by external electric field at 90°C.

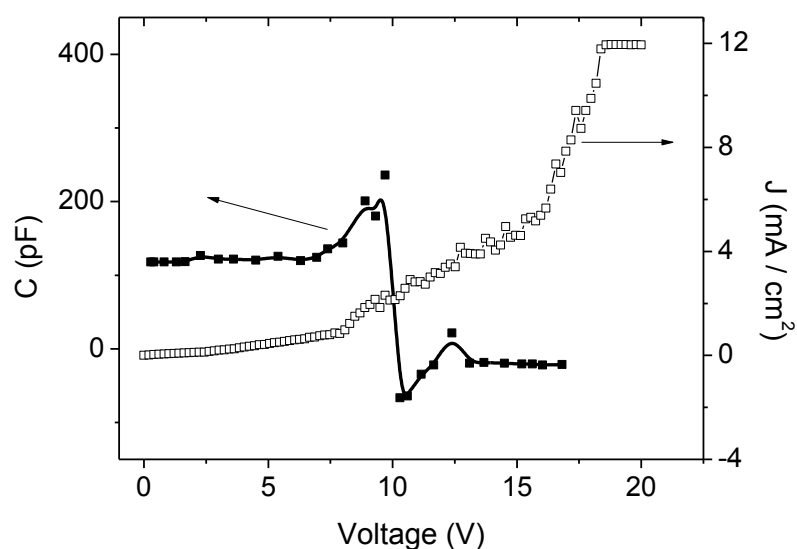


Fig. 5. 18. Current density-capacitance curves as a function of the applied forward bias for the device consisting of ITO/ ~44.88nm PVK/ 30nm Rhodamine B dye/35nm Pb which was treated by external electric field at 100°C.

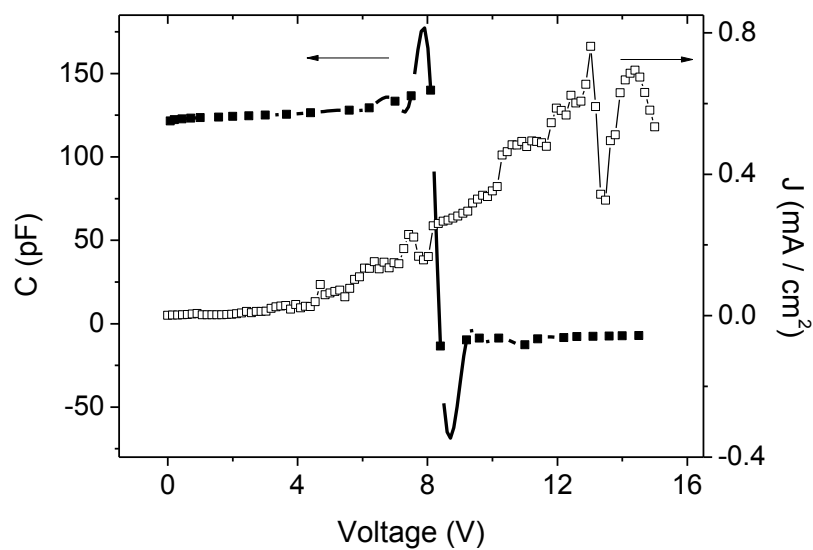


Fig. 5. 19. Current density-capacitance curves as a function of the applied forward bias for the device consisting of ITO/ ~44.88nm PVK/ 30nm Rhodamine B dye/35nm Pb which was treated by external electric field at 110°C.

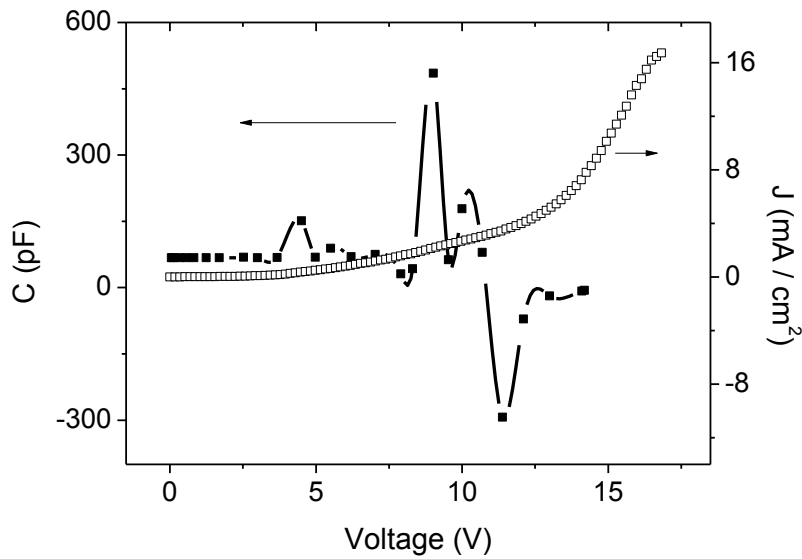


Fig. 5. 20. Current density-capacitance curves as a function of the applied forward bias for the device consisting of ITO/ ~44.88nm PVK/ 30nm Rhodamine B dye/35nm Pb which was treated by external electric field at 120°C.

5.4 BODE PLOTS

Generally, the impedance spectrum of an OLED system can be presented in Bode plots, which are representations of the impedance Z as a function of frequency f .

A Bode plot is an alternative representation of the impedance. There are two types of Bode diagram, $\text{Log } Z\text{-Log } f$ (or $Z - \text{Log } f$) and $\theta - \text{Log } f$, describing the frequency dependencies of the modulus f and phase θ , respectively. Both plots usually start at a high frequency and end at a low frequency, which enables the initial resistor to be found more quickly [30].

The equivalent circuit of OLED devices fabricated at this research consists of a series resistance with parallel combination of resistance and capacitance as shown in Fig. 5.21. The series and parallel resistances can be computed by fixing

the points of series resistance and parallel resistance from Bode plot [31] as shown in Fig. 5.22.

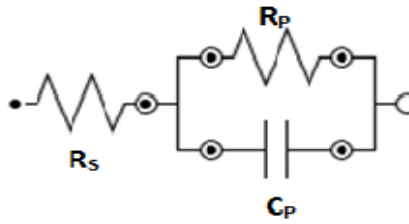


Fig. 5. 21. Equivalent Circuit of OLED devices.

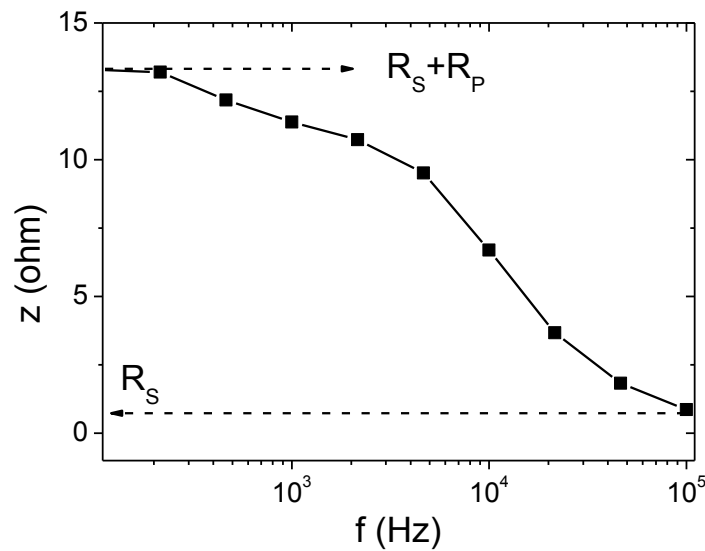


Fig. 5. 22. Deducing equivalent circuit from impedance plots.

5.4.1 Bode modulus for OLEDs with CuPc layer

The Bode plot contains an impedance magnitude plot and a phase angle plot. It is shown in Fig. 5.23 the Bode plot of the control device without CuPc layer. In Figs. 5.24 through Fig. 5.27 the Bode diagrams of the OLED devices consisting of ITO/different thicknesses CuPc/PVK/Rhodamine B/Pb.

At a thickness of 5nm of the CuPc layer, the values of R_s and R_p are 0.08 k Ω , and -0.05 k Ω , respectively. For the devices have a thicknesses of CuPc 10nm, 30nm, and 50nm the series resistances are 0.45 k Ω , 58.17 $\times 10^4$

$k\Omega$, and $1261.0 k\Omega$, respectively, where the values of parallel resistances are $6.10 k\Omega$, $36.39 \times 10^4 k\Omega$, and $7936.0 k\Omega$, respectively. Figure 5.28 shows the impedance resistance as a function of the frequency for devices consisting of ITO/different thicknesses CuPc/PVK/Rhodamine B/Pb. At a thickness of 30nm CuPc layer, the device has a large value of R_S and R_P .

On the other hand, the parallel resistance have negative value at a thickness of 5nm which may refer to negative differential resistance NDR phenomenon. The mechanism proposed to explain the NDR behavior for the generation of guest hopping side (GHS) and phonon scattering phenomenon.

Table 5.4 presents the values of R_S and R_P for different CuPc layer thicknesses. The phase modulus as a function of the frequency for devices consisting of ITO/different thicknesses CuPc/PVK/Rhodamine B dye/Pb is shown in Fig. 5.29.

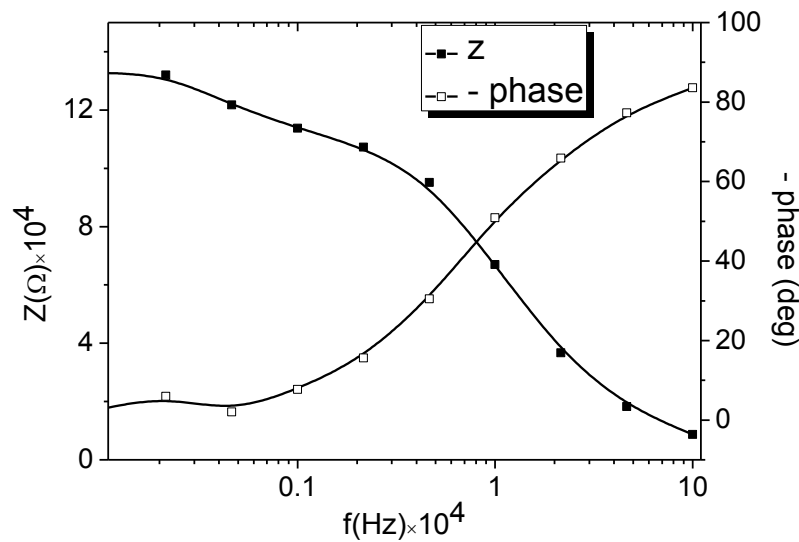


Fig. 5. 23. Bode modulus and phase for the OLED device consisting of ITO/PVK/Rhodamine B dye/Pb.

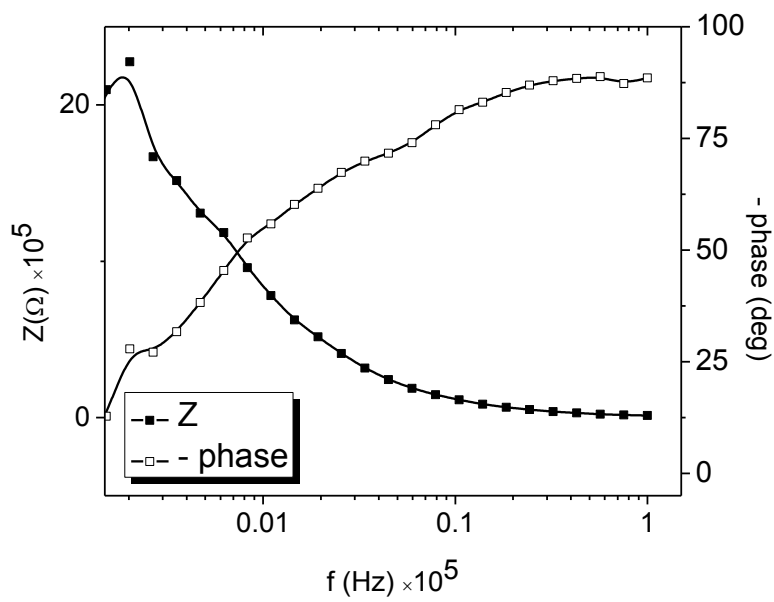


Fig. 5. 24. Bode modulus and phase for the OLED device consisting of ITO/50nmCuPc/PVK/Rhodamine B dye/Pb

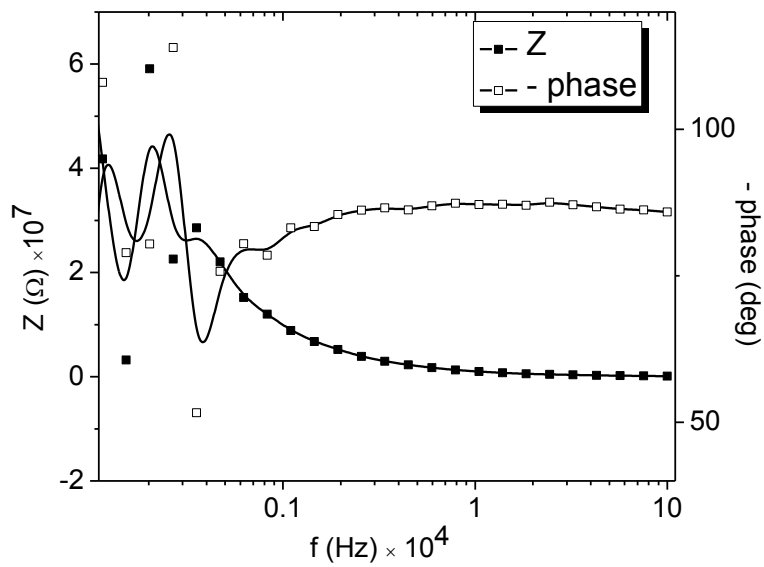


Fig. 5. 25. Bode modulus and phase for the OLED device consisting of ITO/30nmCuPc/PVK/Rhodamine B dye/Pb.

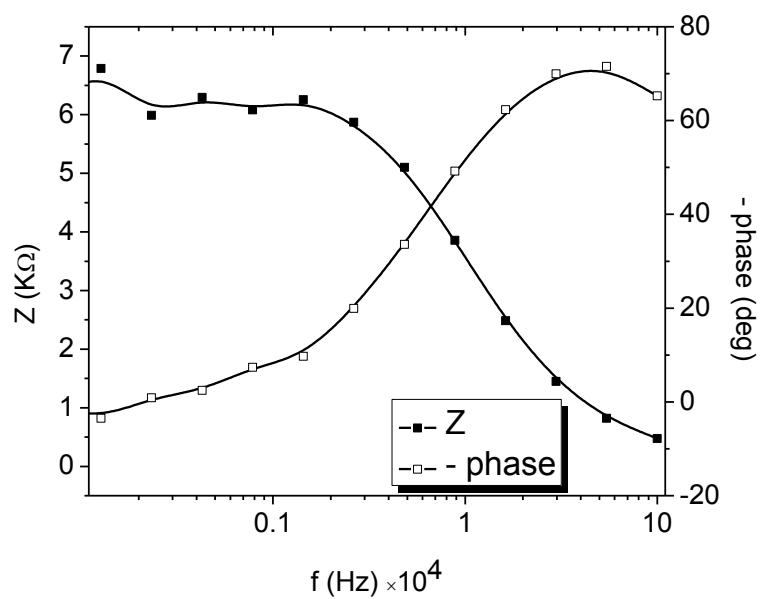


Fig. 5. 26. Bode modulus and phase for the OLED device consisting of ITO/10nmCuPc/PVK/Rhodamine B dye/Pb.

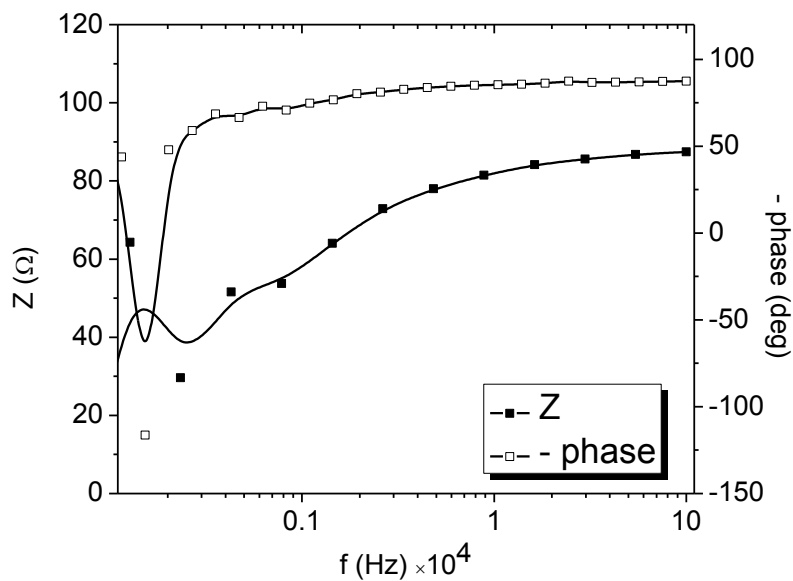


Fig. 5. 27. Bode modulus and phase for the OLED device consisting of ITO/5nmCuPc/PVK/Rhodamine B dye/Pb.

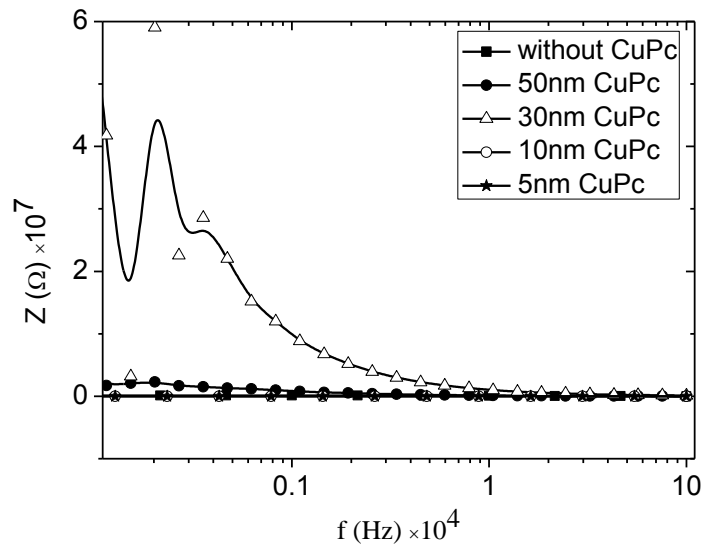


Fig. 5. 28. Bode modulus for the OLED devices consisting of ITO/CuPc/PVK/Rhodamine B dye with different thicknesses of CuPc layer.

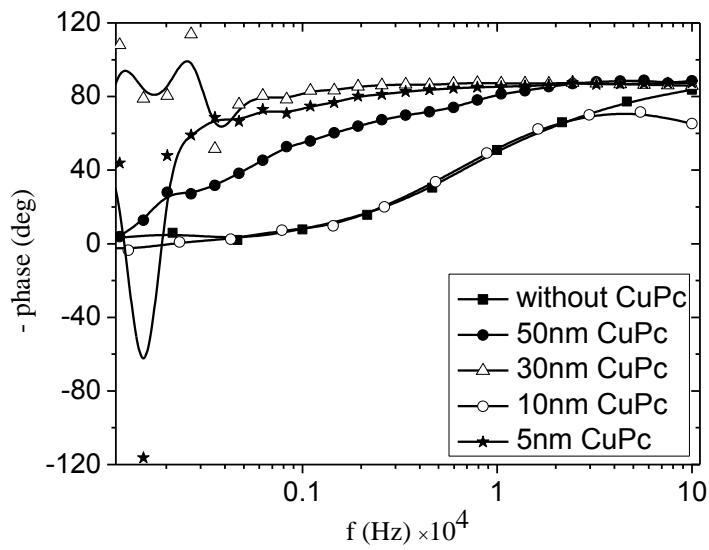


Fig. 5. 29. Phase modulus for the OLED devices consisting of ITO/CuPc/PVK/Rhodamine B dye with different thicknesses of CuPc layer.

Table 5. 4. Values of series and parallel resistances.

Thickness (nm)	0	5	10	30	50
R_S (K Ω)	8.99	0.08	0.45	581750.0	1261.0
R_P (K Ω)	123.40	-0.05	6.10	363950.0	7936.0

5.4.2 Bode modulus for OLEDs treated by heat

Bode plots for the OLEDs treated by thermal annealing of PVK/Rhodamine B dye before deposited Pb electrode are shown in Fig. 5.30 through Fig. 5.33.

For devices treated at temperatures 26°C, 90°C, 100°C, 110°C, and 120°C the series resistances are 8.99 k Ω , 14.51 k Ω , 126.08 k Ω , 59.48 k Ω , and 20.60 k Ω , respectively. and the parallel resistances are 123.4 k Ω , 7.07 k Ω , 461.41 k Ω , 10.88 k Ω , and 4.97 k Ω respectively. The parallel resistance have a large value at 110°C. Table 5.5. presents the values of R_S and R_P at different temperatures.

Figure 5.34 shows the resistance impedance of the treated devices as a function in frequency. The phase angle as a function of the frequency for devices thermally treated are shown in Fig. 5.35.

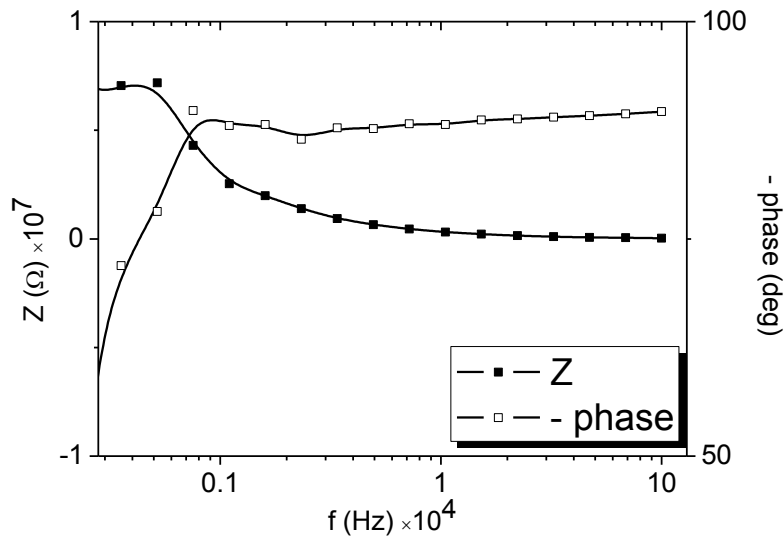


Fig. 5. 30. Bode modulus and phase for the OLED device consisting of ITO /PVK/Rhodamine B dye/Pb which was treated at 90°C.

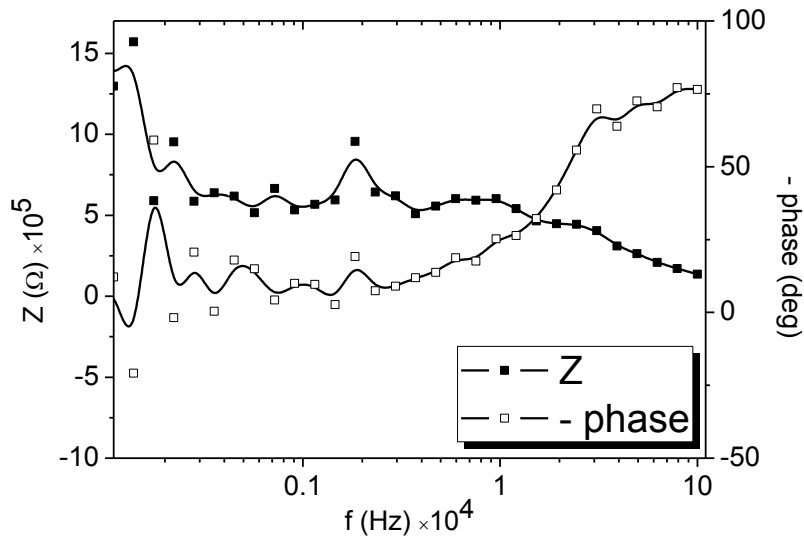


Fig. 5. 31. Bode modulus and phase for the OLED device consisting of ITO /PVK/Rhodamine B dye/Pb which was treated at 100°C.

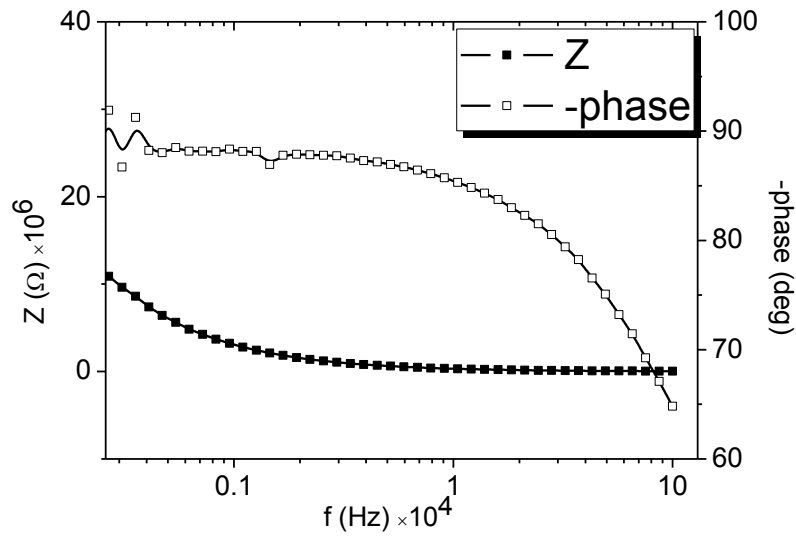


Fig. 5. 32. Bode modulus and phase for the OLED device consisting of ITO /PVK/Rhodamine B dye/Pb which was treated at 110°C.

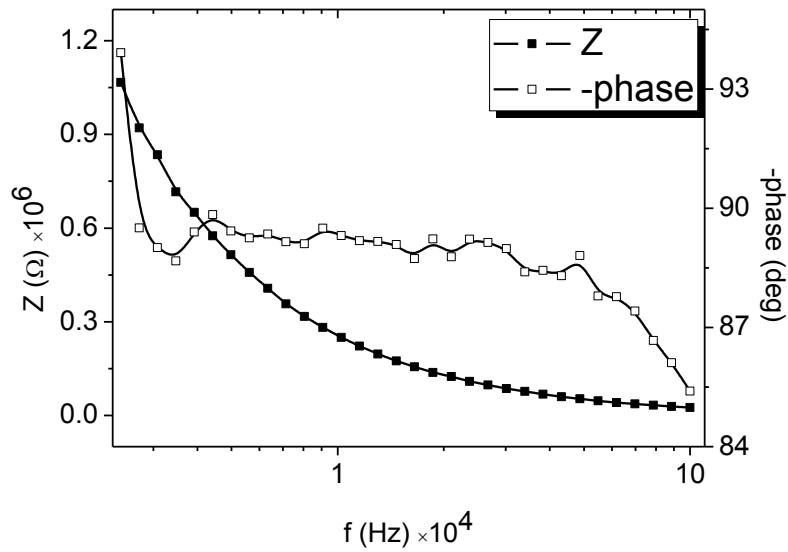


Fig. 5. 33. Bode modulus and phase for the OLED device consisting of ITO /PVK/Rhodamine B dye/Pb which was treated at 120°C.

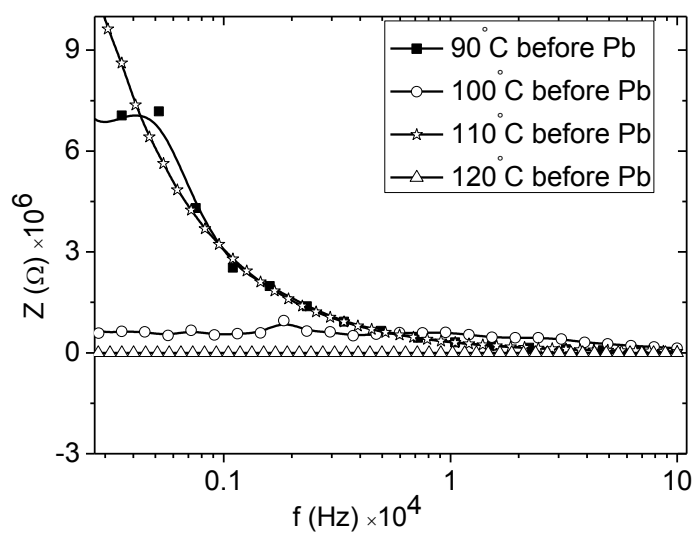


Fig. 5. 34. Bode modulus of OLEDs devices treated by heating at different temperatures.

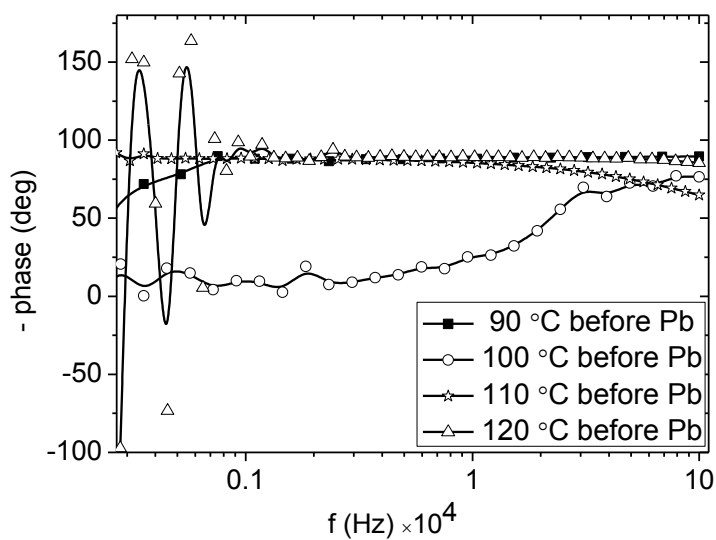


Fig. 5. 35. Phase modulus of OLEDs devices treated by heating at different temperatures.

Table 5. 5. Values of series and parallel resistances for devices treated by heating at different temperatures.

Temperature	26 °C	90 °C	100 °C	110 °C	120 °C
R _S (kΩ)	8.99	14.51	126.08	59.48	20.60
R _P (kΩ)	123.4	7.07×10 ³	461.41	10.88×10 ³	4.97×10 ³

5.4.3 Bode modulus for OLEDs treated by an electric field during heating

The Bode plots for OLEDs treated by an electric field during heating are shown in Fig. 5.36 through Fig. 5.39. The series resistances are 8.99 kΩ, 0.79 kΩ, 0.04 kΩ, 3.02 kΩ, and 37.89 kΩ for devices treated at 26 °C, 90 °C, 100 °C, 110 °C, and 120 °C, respectively. whereas the parallel resistances are 123.40 kΩ, 4.76 kΩ, 0.16 kΩ, 43.48 kΩ, 399.08 kΩ, respectively. The values of series and parallel resistances are listed in Table 5.6. As can be seen in the table, the device treated at 120 °C has a large values of R_S and R_P.

The phase angle as a function of the frequency for devices thermally treated are shown in Fig. 5.40. Fig. 5.41 show the resistance impedance of the treated devices as a function of frequency.

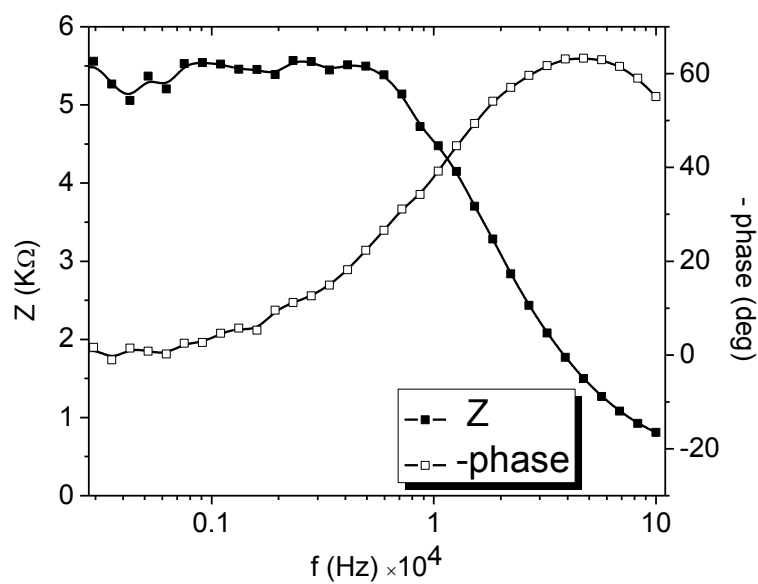


Fig. 5. 36. Bode modulus and phase for the OLED device consisting of ITO /PVK/Rhodamine B dye/Pb which was treated by an E-field at 90°C.

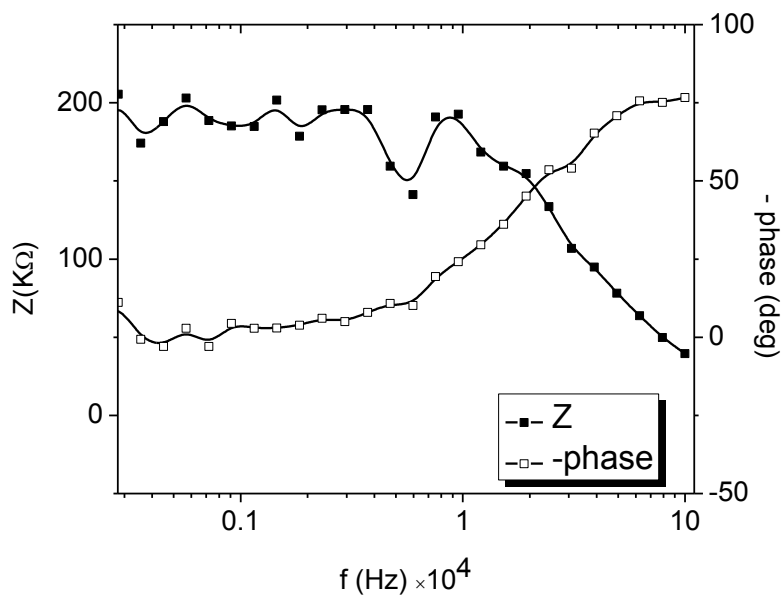


Fig. 5. 37. Bode modulus and phase for the OLED device consisting of ITO /PVK/Rhodamine B dye/Pb which was treated by an E-field at 100°C.

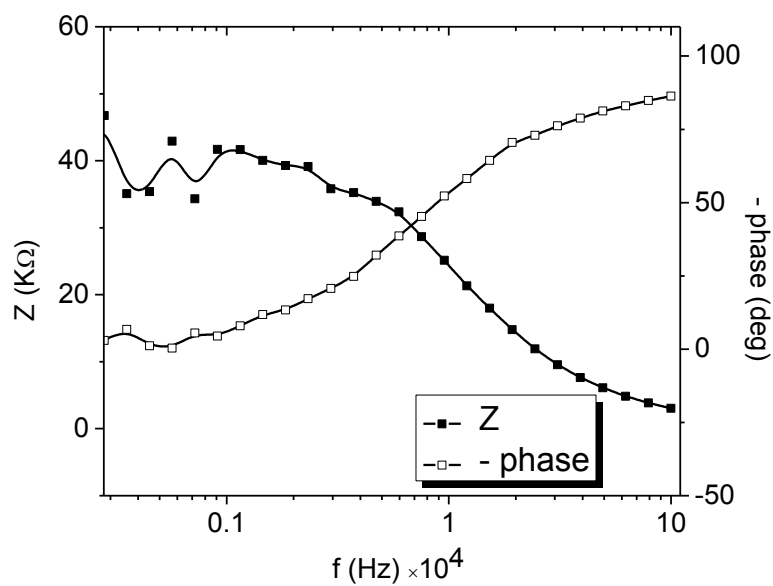


Fig. 5. 38. Bode modulus and phase for the OLED device consisting of ITO /PVK/Rhodamine B dye/Pb which was treated by an E-field at 110°C.

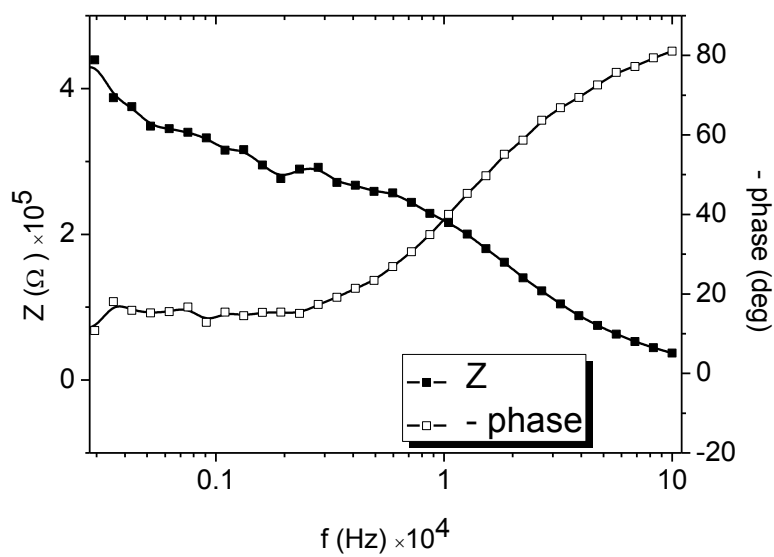


Fig. 5. 39. Bode modulus and phase for the OLED device consisting of ITO /PVK/Rhodamine B dye/Pb which was treated by E-field at 120°C.

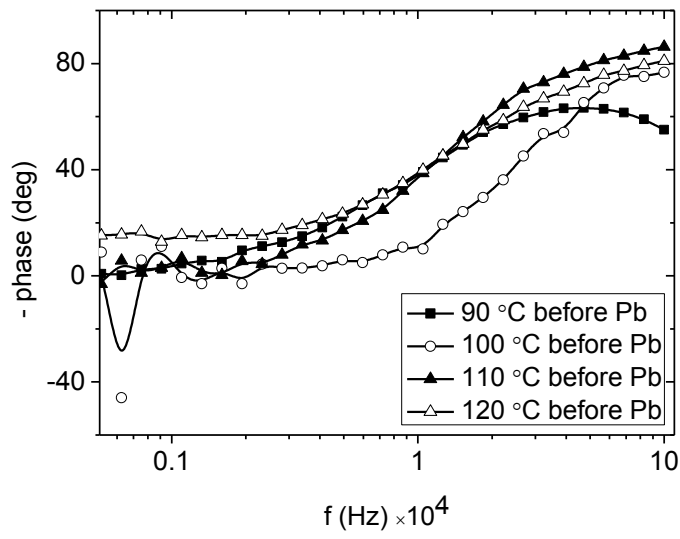


Fig. 5. 40. Phase modulus of OLEDs devices treated by E-field at different temperatures.

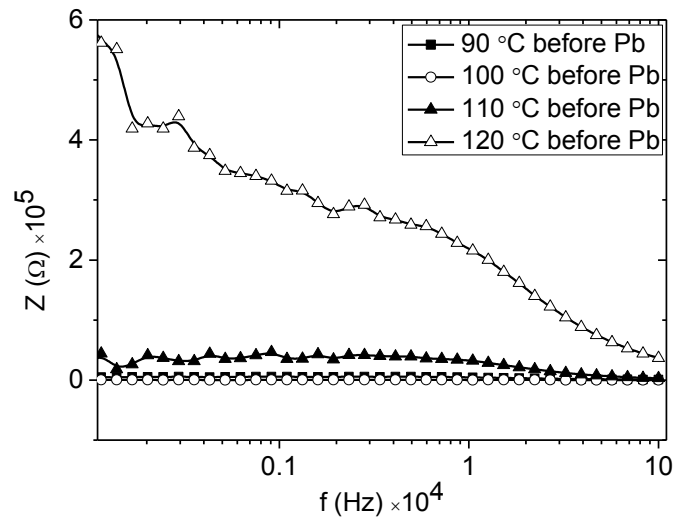


Fig. 5. 41. Bode modulus of OLEDs devices treated by E-field at different temperatures.

Table 5. 6. Values of series and parallel resistances for devices treated by E-field at different temperatures.

Temperature	26 °C	90 °C	100 °C	110 °C	120 °C
R_S (k Ω)	8.99	0.79	0.04	3.02	37.89
R_P (k Ω)	123.4	4.76	0.16	43.48	399.08

CONCLUSION

In this work, two types of OLED devices were fabricated. The first one was a double layer with the structure ITO/PVK/ Rhodamine B dye/Pb, and the second device was a multilayer with the structure ITO/CuPc/PVK/Rhodamine B dye/Pb.

The J-V characteristics and electroluminescence-voltage curves of the control OLED device with the structure of ITO/~44.88nm PVK/30nm Rhodamine B dye/35nm Pb was examined and the threshold voltage V_{th} was determined to be 7.8 volt, but the turn-on voltage V_{on} at which the light was detected was ~14 volt due to recombination of electrons and holes.

In addition, the double layer device was treated by two methods, post-fabrication heat treatment and a combined external electric field and heat treatments. The effects of the heat treatment and heat treatment associated with an applied electric field treatment on the J-V characteristic curves of OLED devices were investigated. OLEDs with the structure ITO/PVK/Rhodamine B dye/Pb were fabricated under ambient atmosphere without taking any preventive measures against exposure to oxygen and water vapors. Heat treatment of PVK/Rhodamine B dye layers significantly increased the threshold voltage as the annealing temperature increased except at 90°C. The best annealing temperature was 110°C which corresponds to the highest current density.

By applying an external electric field to the PVK/Rhodamine B dye layers during annealing, it was observed that when the annealing temperature increased, the threshold voltage decreased and the current dramatically increased expect at 110°C. The improved threshold voltage of OLEDs with organic layers annealed at elevated temperature could be attributed to the reduced defects and improved the interface structures of organic and organic/ITO interfaces.

The best annealing temperature in the presence of an electric field was 120°C which corresponds to the highest current density.

We may conclude that thermal treatment in the presence of an electric field is much better than thermal treatment only. On the other hand, all devices treated by heating with and without applying an electric field didn't emit light compared to the controlled device without any annealing. This can be attributed to the dye aggregation.

The second group was a multilayer device with the structure ITO/CuPc with different thicknesses/PVK/ Rhodamine B/Pb. The effect of CuPc hole-injection layer on the J-V characteristics and the electroluminescence were investigated. The results showed that the threshold voltage of the devices can be dramatically lowered by inserting the CuPc layer. The reduction in threshold voltage can be attributed to a decrease in the hole-injection barriers between CuPc and anode. This is because the HOMO level of CuPc is near to the work function of the ITO anode. On the other hand, no luminescence was detected in these devices. This may suggest that there is an easier route for electron injection other than that for the LUMO level of Rhodamine B dye. It is expected that using a polymer, with a low-lying LUMO, instead of the organic material could cause light emission because the threshold voltage of such a polymer light emitting diode should be smaller than that of OLED device.

In addition, impedance spectroscopy measurements were used to study charge injected in two types of OLED devices. The first was a double layer with the structure ITO/PVK/ Rhodamine B dye/Pb treated by heating with and without an electric field, and the second device was an OLED consisting of ITO/CuPc/ PVK/Rhodamine B dye/Pb, with different CuPc layer thicknesses. The effect of this layer in the transition voltage V_T and built-in voltage V_{bi} , was as follows: when the thickness of the CuPc

layer decreases V_T and V_{bi} were found to decrease, except at a thickness of 5 nm due to negative differential resistance (NDR).

Finally, it was found that capacitance-voltage analysis is a sensitive tool to monitor charge injection, where current density-voltage measurements are not sensitive.

REFERENCES

- [1] Han-Yua. Cheng, "Electrode Modifications of Molecular Light Emitting Diode", National Sun Yat-sen University, July, (2003).
- [2] J. Friedl, "Preparation Characterization and Application of Organic Light Emitting Diodes", master thesis, Iowa State University, (1999).
- [3] B. Choudhury, "Organic Light Emitting Devices (OLEDs) and Structurally integrated Photoluminescence Based Chemical and Biological Sensors Excited by OLEDs", PhD Thesis, Iowa State University, (2005).
- [4] Wesley C. Pirkle, "Nontraditional Architectures and Spin Processes in Organic Light Emitting Device", PhD Thesis, The OHIO State University, (2005).
- [5] Alexandros Ioannis Dimopoulos, "Characterization of Poly (3-HEXYLTHIO PHENE) Based Schottky Diodes", Master Thesis, The University of British Columbia, April, (2012).
- [6] H. Musleh, "Investigation of the Effect of Various Dyes on OLEDs Electroluminescence", Master of Science Thesis, Islamic University of Gaza, Gaza, (2009).
- [7] W. Tabaza, "Some Electrical Properties of Doped Poly(9-vinylcarbazole)", Master of Science Thesis, Islamic Universtiy of Gaza, Gaza, (2005).
- [8] M. Tuttle, "A brief Introduction to Polymeric Materials", University of Washington, Seattle, (1999).
- [9] K. Chi Kao, "Dielectric Phenomena in Solids", Elsevier (2004).
- [10] Thomas L. Floyd, "Electronic Devices", Seventh Edition, Pearson Education International (2005).

- [11] A. Buckley, "Light-Emitting Diodes (OLEDs) Materials Devices and Applications", Woodhad Publishing, (2013).
- [12] A. El-Afghani," Electrical and Optical Properties of Organic Diodes", Master of Science Thesis, Islamic Universtiy of Gaza, Gaza, Aug, (2012).
- [13] S. M. Sze and Kwok K.Ng,"Physics of Semiconductor Devices"Third Edition, John Wiley and Sons, Hoboken, New Jersey (2007).
- [14] S. Nowy,"Understanding Losses in OLEDs: optical device simulation and electrical characterization using impedance spectroscopy", PhD Thesis, April (2010)
- [15] www.filmetrics.com
- [16] B. Norris, "Characterization of Organic Light-Emitting Devices", Master of Science Thesis, Oregon State University, June, (2000).
- [17] P. C. Kao, S. Y. Chu, S. J. Liu, Z. X. You, and C. A. Chuang, "Improved Performance of Organic Light-Emitting Diodes Using a Metal-Phthalocyanine Hole-Injection Layer", Electrochemical Society 153(6), H122-H126 (2006).
- [18] V. Shrotriya and Y. Yang, "Capacitance-voltage characterization of polymer light-emitting diodes", Applied Physics, 97, 054504 (2005).
- [19] J. Chen, M. A. Reed, A. M. Rawlett and J. M. Tour, "Large On-Off Ratios and Negative Differential Resistance in a Molecular Electronic Device", Science, 286, 1550, (1999).
- [20] J. Cornil and J. L. Bredas, J. Am. Chem Soc., 2001, 123, 10076.
- [21] J. Chen, W. Wang, M. A. Reed, A. M. Rawlett, D. W. Price and J. M. Tour, "Room-temperature negative differential resistance in nanoscale molecular junction", Appl. Phys. Lett., 77(8), 1224-1226, (2000).
- [22] J. Seminario, A. G. Zacarias and J. M. Tour, J. Am, "Theoretical study of a molecular resonant tunneling diode", Chem. Soc., 122, 3015-3020, (2000).

- [23] E. G. Emberly and G. Kirczenow, "Current-Driven Conformational Changes, Charging and Negative Differential Resistance in Molecular Wires", *Phys. Rev. B* 64, 125318 pp.1-5 (2001).
- [24] M. Mohd Sarjidan, S. Basri, N. Za'aba, M. Zaini, W. Abd Majid, "Electroluminescence and negative differential resistance studies of TPD:PBD:Alq₃ blend organic-light emitting diodes, low Dimensional Materials Research centre, Department of physics, university of Malaya, 50603 Kuala lumpur, Malaysia.
- [25] Z. Chunlin, Z. Yong, L. Haixia, W. Fangcong, Z. Guobing, C. Da, J. Xiaoyun and L. Su, "Enhancing the Performance of the Organic Light-Emitting Device (OLED) by Thermal Treatment", *Chinese Journal of Electronics*, Vol. 20, No.1, Jan.2011.
- [26] S. Jang, H. Chae, D. Jung, H. Kim, Ch. Kim, "Simultaneous Oxygen Plasma and Thermal Treatments of an ITO Surface to Improve the Electrical Characteristics of Organic Light-Emitting Diodes", *Journal of the Korean Physical Society*, Vol. 51, No. 3, September 2007, pp. 956_962.
- [27] B. Chen, X. Sun and K. Sarma, "Phosphorescent organic light-emitting devices with in situ post-growth annealed organic layers", *Material Science and Engineering B*, 139(2007), 192-196.
- [28] S. Nowy, W. Ren, J. Wagner, J. Weber, and W. Brutting, "Impedance spectroscopy of organic hetro-layer OLEDs as a probe for charge carrier injection and device degradation", *Proc. of SPIE* Vol. 7415 74150G-1 (2009).
- [29] V. Shrotriya, Y. Yang, "Capacitance-voltage characterization of polymer light-emitting diodes", *Physics* 97, 054504 (2005).
- [30] X. Yuan, C. Song, H. Wang, and J. Zhang, "Electrochemical Impedance Spectroscopy in PEM Fuel Cells Fundamentals and Application", Springer (2010).

[31] T. Shahul Hameed, P. Predeep, and M, Baiju, "Organic Light Emitting Diodes:Device Physics and Effect of Ambience on Performance Parameters", Optoelectronics-Devices and Applications, ISBN 978-953-307-576-1, October, (2011).

